

Magma Plumbing Systems: A Geophysical Perspective

Craig Magee^{1*}, Carl T. E. Stevenson², Susanna K. Ebmeier³,
Derek Keir^{4,5}, James O. S. Hammond⁶, Joachim H. Gottsmann⁷,
Kathryn A. Whaler⁸, Nick Schofield⁹, Christopher A-L. Jackson¹,
Michael S. Petronis¹⁰, Brian O'Driscoll¹¹, Joanna Morgan¹,
Alexander Cruden¹², Stefan A. Vollgger¹², Greg Dering¹³,
Steven Micklethwaite¹² and Matthew D. Jackson¹

¹Department of Earth Science and Engineering, Imperial College London, London SW7 2BP, UK; ²School of Geography, Earth and Environmental Sciences, University of Birmingham, Birmingham B15 2TT, UK; ³School of Earth Science and Environment, University of Leeds, Leeds LS2 9JT, UK; ⁴Ocean and Earth Science, University of Southampton, Southampton SO14 3ZH, UK; ⁵Dipartimento di Scienze della Terra, Università degli Studi di Firenze, Florence 50121, Italy; ⁶Department of Earth and Planetary Sciences, Birkbeck, University of London, London WC1E 7HX, UK; ⁷School of Earth Sciences, University of Bristol, Bristol BS8 1RJ, UK; ⁸School of GeoSciences, University of Edinburgh, Grant Institute, Edinburgh EH9 3FE, UK; ⁹Geology and Petroleum Geology, School of Geosciences, University of Aberdeen, Aberdeen AB24 3UE, UK; ¹⁰Environmental Geology, Natural Resource Management Department, New Mexico Highlands University, PO Box 9000, Las Vegas, NM 87701, USA; ¹¹School of Earth and Environmental Sciences, University of Manchester, Manchester M13 9PL, UK; ¹²School of Earth, Atmosphere and Environment, Monash University, Melbourne, Victoria 3800, Australia; ¹³School of Earth Sciences, University of Western Australia, Perth 6009, Australia

*Corresponding author. Department of Earth Science and Engineering, Imperial College London, London SW7 2BP, UK. Telephone: +44 (0)20 7594 6510. E-mail: c.magee@imperial.ac.uk

Received June 1, 2017; Accepted June 11, 2018

ABSTRACT

Over the last few decades, significant advances in using geophysical techniques to image the structure of magma plumbing systems have enabled the identification of zones of melt accumulation, crystal mush development, and magma migration. Combining advanced geophysical observations with petrological and geochemical data has arguably revolutionised our understanding of, and afforded exciting new insights into, the development of entire magma plumbing systems. However, divisions between the scales and physical settings over which these geophysical, petrological, and geochemical methods are applied still remain. To characterise some of these differences and promote the benefits of further integration between these methodologies, we provide a review of geophysical techniques and discuss how they can be utilised to provide a structural context for and place physical limits on the chemical evolution of magma plumbing systems. For example, we examine how Interferometric Synthetic Aperture Radar (InSAR), coupled with Global Positioning System (GPS) and Global Navigation Satellite System (GNSS) data, and seismicity may be used to track magma migration in near real-time. We also discuss how seismic imaging, gravimetry and electromagnetic data can identify contemporary melt zones, magma reservoirs and/or crystal mushes. These techniques complement seismic reflection data and rock magnetic analyses that delimit the structure and emplacement of ancient magma plumbing systems. For each of these techniques, with the addition of full-waveform inversion (FWI), the use of Unmanned Aerial Vehicles (UAVs) and the integration of geophysics with numerical modelling, we discuss potential future directions. We show that approaching problems concerning magma plumbing systems from an integrated petrological, geochemical, and geophysical perspective will undoubtedly yield

important scientific advances, providing exciting future opportunities for the volcanological community.

Key words: magma plumbing systems; geophysical methods; magma flow; melt; mush

INTRODUCTION

Igneous petrology and geochemistry are concerned with the chemical and physical mechanisms governing melt genesis, mobilisation, and segregation, as well as the transport/ascent, storage, evolution, and eruption of magma. The reasons for studying these fundamental processes include understanding volcanic eruptions, modelling the mechanical development of magma conduits and reservoirs, finding magma-related economic ore deposits, exploring for active geothermal energy sources, and determining the impact of magmatism in different plate tectonic settings on the evolution of the lithosphere and crustal growth. However, whilst petrological and geochemical studies over the last century have shaped our understanding of the physical and chemical evolution of magma plumbing systems, assessing the distribution, movement, and accumulation of magma in the Earth's crust from these data remains challenging. A key frontier in igneous petrological and geochemical research thus involves deciphering how and where magma forms, the routes it takes toward the Earth's surface, and where exactly it is stored.

This contribution will demonstrate how geophysical data can be used to determine the architecture of magma plumbing systems, providing a structural framework for the interpretation of petrological and geochemical data. To aid the alignment of petrological, geochemical, and geophysical disciplines it is first important to delineate what we mean by 'magma'. We follow [Glazner *et al.* \(2016\)](#) and define magma as, 'naturally occurring, fully or partially molten rock material generated within a planetary body, consisting of melt with or without crystals and gas bubbles and containing a high enough proportion of melt to be capable of intrusion and extrusion'. Importantly, this definition specifically considers that magma: (i) forms through the migration and accumulation of partial melt that is initially distributed throughout pore spaces in a rock volume; and (ii) is a suspension of particles (i.e. crystals, xenoliths, and/or bubbles) within melt (see [Cashman *et al.*, 2017](#)). As magma starts to solidify, the proportion of suspended crystals and thus the relative viscosity of the magma increases until a relatively immobile, continuous network of crystals and interstitial melt develops; we term this a 'crystal mush' (e.g. [Hildreth, 2004](#); [Glazner *et al.*, 2016](#); [Cashman *et al.*, 2017](#)). The rheological transition from a magma to a crystal mush is partly dependent on its chemistry, but typically occurs abruptly when the particle volume increases above the 50–65% range ([Cashman *et al.*, 2017](#)). Crystal mushes

thus exist at or above the solidus and generally cannot be erupted, although they may be partly entrained in eruptible magma as glomerocrysts, cumulate nodules, or restite ([Cashman *et al.*, 2017](#)). Migration of interstitial melt within a crystal mush can lead to its accumulation and, thus, formation of a magma. A magma plumbing system, therefore, consists of interconnected magma conduits and reservoirs, which store magma as it evolves into a crystal mush, ultimately fed from a zone of partial melting (e.g. [Fig. 1](#)). These definitions are supported by geophysical imaging and analyses of contemporary magma reservoirs, which show that melt volumes in the mid- to upper crust are typically low (<10%) and likely exist within a crystal mush (e.g. [Paulatto *et al.*, 2010](#); [Koulakov *et al.*, 2013](#); [Hammond, 2014](#); [Ward *et al.*, 2014](#); [Comeau *et al.*, 2015, 2016](#); [Delph *et al.*, 2017](#)). These definitions and geophysical data question the traditional view that magma resides in long-lived, liquid-rich, and volumetrically significant magma chambers. Following this, the emerging paradigm for igneous systems is thus that liquid-rich magma chambers are short-lived, transient phenomena with: (i) melt typically residing in mushes that develop through the incremental injection of small, distinct magma batches; and (ii) magma accumulating in thin lenses (e.g. [Hildreth, 2004](#); [Annen *et al.*, 2006, 2015](#); [Annen, 2011](#); [Miller *et al.*, 2011](#); [Solano *et al.*, 2012](#); [Cashman & Sparks, 2013](#); [Cashman *et al.*, 2017](#)). We are now starting to view magmatic systems as vertically extensive, transcrustal, interconnected networks of magma conduits and magma/mush reservoirs ([Fig. 1](#)) (e.g. [Cashman *et al.*, 2017](#)).

The current use of geophysical techniques within the igneous community can be separated into two distinct areas focused on either characterising active volcanic domains or investigating the structure and emplacement of ancient magma plumbing systems. For example, in areas of active volcanism, our understanding of magma plumbing system structure principally comes from the application of geophysical techniques that detect sites of magma movement or accumulation (e.g. [Sparks *et al.*, 2012](#); [Cashman & Sparks, 2013](#)). Such geophysical techniques include Interferometric Synthetic Aperture Radar (InSAR; e.g. [Biggs *et al.*, 2014](#)), seismicity (e.g. recording of earthquakes associated with magma movement; e.g. [White & McCausland, 2016](#)), various seismic imaging methods (e.g. [Paulatto *et al.*, 2010](#); [Hammond, 2014](#)), gravimetry (e.g. [Battaglia *et al.*, 1999](#); [Rymer *et al.*, 2005](#)), and electromagnetic techniques (e.g. [Desissa *et al.*, 2013](#); [Comeau *et al.*, 2015](#)). These techniques allow examination of: (i) the

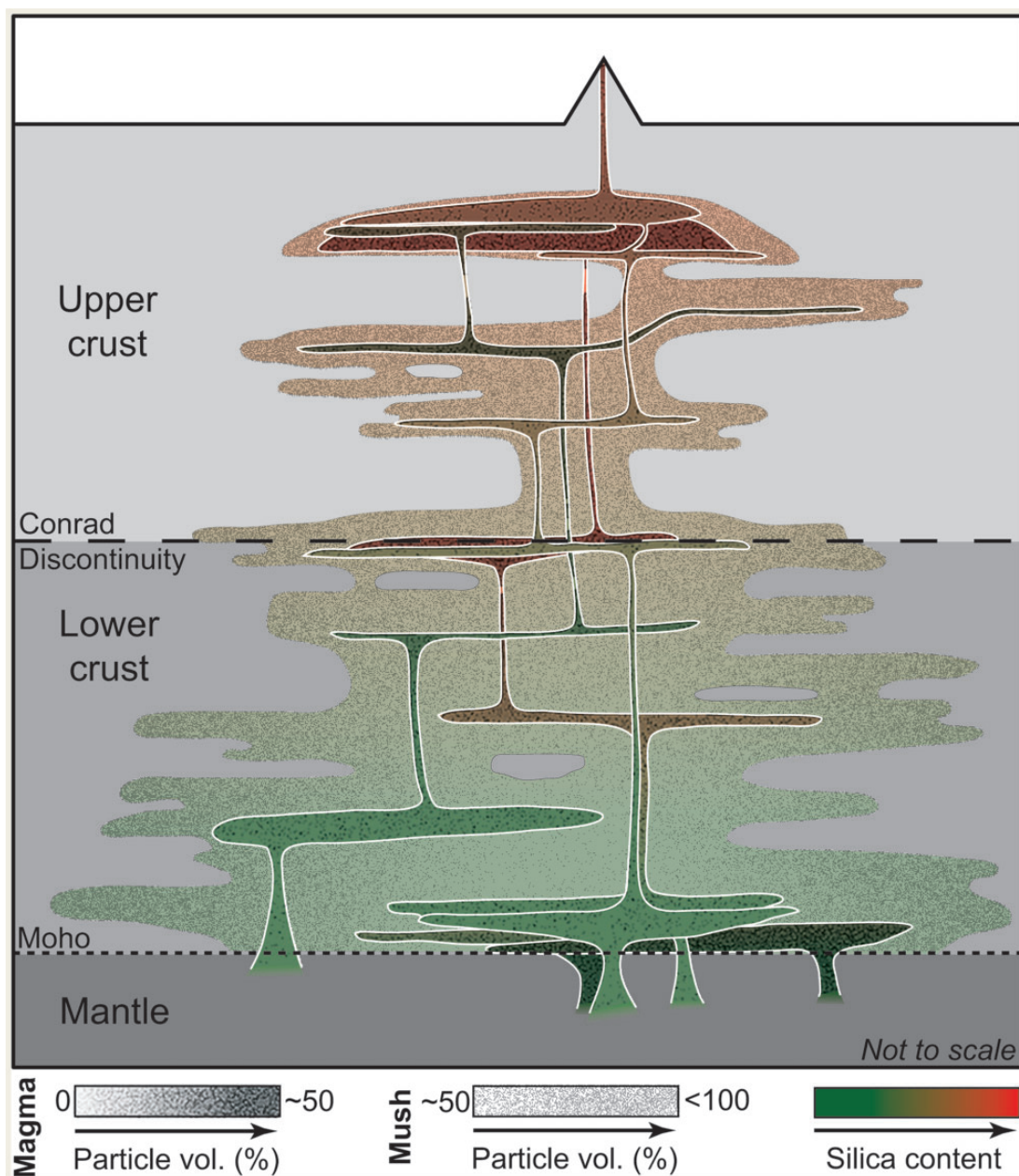


Fig. 1. Schematic of a vertically extensive, transcrustal magma plumbing system involving transient, interconnected, relatively low-volume tabular magma intrusions (e.g. dykes, sills, and laccoliths) within a crystal mush (based on [Cashman *et al.*, 2017](#); [Cruden & Weinberg, 2018](#)).

temporal development of magma plumbing systems (e.g. [Pritchard & Simons, 2004](#); [Sigmundsson *et al.*, 2010](#)); (ii) vertical and lateral movements of magma (e.g. [Keir *et al.*, 2009](#); [Jay *et al.*, 2014](#)); (iii) the relationship between eruption dynamics, volcano deformation, and intrusion (e.g. [Sigmundsson *et al.*, 2010, 2015](#)); and (iv) estimates of melt sources and melt fractions (e.g. [Desissa *et al.*, 2013](#); [Johnson *et al.*, 2016](#)). However, inversion of these geophysical data typically results in non-unique, relatively low-resolution models of subsurface structures. Furthermore, some methods only capture active processes, which may be short-lived or even

instantaneous, potentially providing information on only a small fraction of the magma plumbing system.

In contrast to the study of active volcanic domains, the analysis of ancient plumbing systems through field observations, geophysical imaging techniques (e.g. reflection seismology, gravity, and magnetic data) and/or rock magnetic experiments can provide critical insights into magma emplacement, mush evolution, and allow the geometry of entire plumbing systems to be reconstructed (e.g. [Cartwright & Hansen, 2006](#); [Stevenson *et al.*, 2007a](#); [Petronis *et al.*, 2013](#); [Muirhead *et al.*, 2014](#); [O'Driscoll *et al.*, 2015](#); [Magee *et al.*, 2016](#)). Whilst such

studies of ancient plumbing systems provide a framework for interpreting the structure of active intrusion networks, capturing a snapshot of how magma moved and melt was distributed through the system at any one time is difficult because magmatism has long since ceased.

All the techniques employed to define active and ancient plumbing systems, including petrological and chemical analyses, provide information at different spatial and/or temporal resolutions. Answering the major outstanding questions in studies of magma plumbing systems, therefore, requires the integration of complementary petrological, geochemical, geophysical, geochronological, and structural techniques. Here, we examine active plumbing systems using InSAR, seismicity, seismic imaging, gravimetry, and electromagnetic techniques. To provide a context for the interpretation of data pertaining to the active systems, we also discuss how seismic reflection data and rock magnetic techniques can be used to derive the structure and evolution of ancient intrusion networks. The potential of emerging techniques involving seismic full-waveform inversion (FWI) and unmanned aerial vehicles (UAVs) are also considered, as is the role of numerical modelling in bringing together outputs from different datasets. For each technique described, we briefly discuss the methodology and limitations and provide a summary of the key findings and potential uses, with a focus on integration with petrological and geochemical data. The aim of this review is to facilitate and promote integration between petrologists, geochemists, geochronologists, structural geologists, and geophysicists interested in addressing outstanding problems in studies of magma plumbing systems.

UNDERSTANDING MAGMA PLUMBING SYSTEM STRUCTURE

Here, we discuss a range of techniques that can be utilised to define different aspects of magma plumbing system structure and evolution. In particular, we describe how InSAR, seismicity, seismic imaging (e.g. seismic tomography), gravity, and electromagnetic data are used to determine melt fractions and distribution, track movement of magma in near real-time and/or locate sites and examine the evolution of magma or mush storage. Overall, these geophysical techniques allow the structure of active plumbing systems and their transient evolution to be assessed. We also discuss how seismic reflection data can provide unprecedented images of ancient plumbing systems and associated host rock deformation in three-dimensions at resolutions of tens of metres. Finally, we examine the application of rock magnetic techniques to assess magma flow and crystallisation processes at a range of scales.

Although beyond the scope of this review, it is critical to highlight that interpreting the geophysical response of a rock, magma, or mush relies on understanding its physical and chemical properties (e.g. density, temperature and melt fraction). Laboratory

experiments testing how rock or magma properties influence geophysically measured parameters (e.g. seismic velocities and resistivity) thus provide context for interpreting magma plumbing system structure and evolution from geophysical data (e.g. Gaillard, 2004; Pommier *et al.*, 2010; Pommier, 2014).

Insights into magma plumbing systems from ground deformation data

Techniques

Changes in volume within magma plumbing systems can deform the host rock, potentially resulting in displacement of the Earth's surface. Such displacements are a unique source of information for volcanologists and can be modelled to estimate geodetic source depth and, to varying extents, the source geometry and volume change (e.g. Segall, 2010). Measuring the deformation of the Earth's surface can thus provide information about the characteristics and timing of magma movement and accumulation, as well as variations in internal reservoir conditions. Traditionally, deformation measurements are made using levelling, electronic distance meters, tiltmeters, and Global Positioning System (GPS), all of which have proven to be reliable methods and thus are widely used in volcano monitoring (e.g. Dzurisin, 2006). For example, GPS measurements retrieve the relative positions of receivers on the Earth's surface from dual frequency carrier phase signals transmitted from GPS or Global Navigation Satellite System (GNSS) satellites with precisely known orbits. Distances between satellites and receivers are assessed from the travel-time, i.e. the measured difference between the transmitted and received times of a unique ranging code, allowing movement of the Earth's surface over time to be monitored (see review by Dixon, 1991). Permanently installed receivers record position data continuously, but receivers can also be deployed for a limited time during GPS campaigns to provide additional measurements, normally made relative to a standard benchmark location (e.g. Dvorak & Dzurisin, 1997). Whilst tiltmeters and GPS can provide continuous measurements, their spatial resolution is limited by logistical constraints such as cost and accessibility, which may be restricted at active volcanoes.

The geographic reach of volcano geodesy has been greatly expanded over the past two decades by the application of Interferometric Synthetic Aperture Radar (InSAR), an active remote sensing technique that uses microwave electromagnetic radiation to image the Earth's surface (e.g. Simons & Rosen, 2007; Pinel *et al.*, 2014). Surface displacements can be measured by constructing interferograms, where the difference in phase between radar echoes from time-separated images appear as 'fringes' of variation in the line of sight distance to the satellite (Fig. 2). The patterns of fringes in individual interferograms are distinctive for different deformation source geometries, such as for horizontal (sill-like) or vertical (dyke-like) opening of intrusions, or the

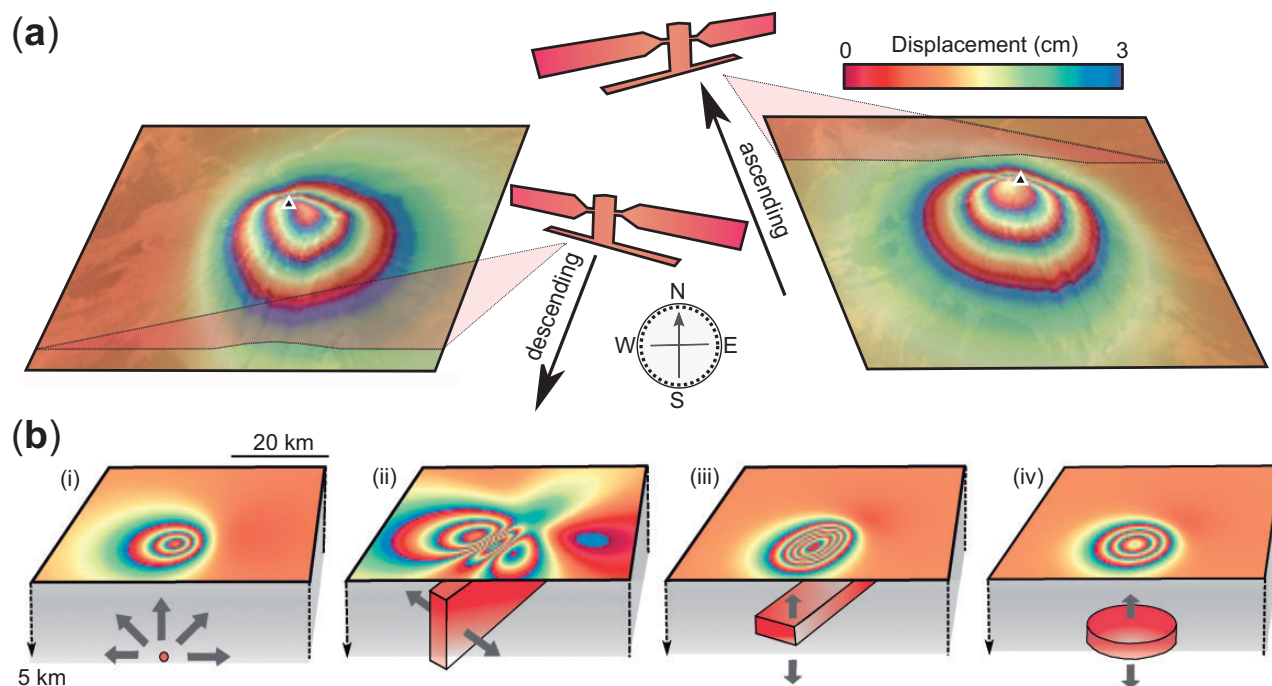


Fig. 2. (a) Interferograms showing fringes caused by the pressurisation of a point source directly beneath a stratovolcano from both ascending and descending satellite lines of sight. Note that the centre of the fringes are slightly offset from the summit of the volcano (marked by a black triangle). (b) Typical fringe patterns for analytical deformation sources in an elastic half space from ascending satellite geometry: (i) Mogi source at 5 km depth; (ii) dyke extending between depths of 3 and 9 km; (iii) rectangular sill; and (iv) a penny-shaped horizontal crack both at 5 km depth.

pressurisation of a spheroidal reservoir (i.e. a Mogi source) (e.g. Fig. 2b). However, magma intrusion processes can rarely be uniquely identified from geodetic source geometry alone and distinguishing between magmatic, hydrothermal, structural (e.g. faulting and compaction), and combinations of elastic and inelastic sources is particularly challenging (e.g. Galland, 2012; Holohan *et al.*, 2017).

Whilst a single interferogram only provides displacements in satellite line-of-sight, a pseudo-3D displacement field can be estimated by combining multiple images from polar orbits that are ascending (i.e. satellite moves roughly northward, looking east) and descending (i.e. satellite moves roughly southward, looking west) (Fig. 2a), especially where GNSS measurements can also be incorporated. The lateral spatial resolution of most InSAR data is on the order of metres to tens of metres, whilst vertical movements can be resolved on the order of centimetres and sometimes millimetres. Temporal resolution depends on the satellite revisit time and ranges between days to months depending upon the sensor type and satellite orbit. This means that InSAR can be used to regularly assess ground deformation at virtually any volcano worldwide situated above sea level, with a higher spatial density of measurements than achieved using from ground-based instrumentation.

Magmatic processes are only observable by InSAR when either magma movement or internal reservoir processes (e.g. cooling and contraction, phase changes) cause changes in pressure and thereby instigate deformation of the host rock and free surface. The best-fit

parameters of a deformation source (e.g. an intruding magma body) are most often assessed by inverting measured displacements using analytical elastic-half space models of simple source geometries, although there are often trade-offs between parameters such as source depth and volume change (e.g. Pritchard & Simons, 2004). Complex and more realistic deformation source geometries may be retrieved using finite element-based linear inversion of displacement fields (e.g. Ronchin *et al.*, 2017). A proportion of any pressure change may be accommodated by magma compressibility, leading to underestimation of volume changes (e.g. Rivalta & Segall, 2008; McCormick Kilbride *et al.*, 2016). Assessing both volume changes and especially the total volume of a magma reservoir from geodetic data, therefore, remains challenging. Furthermore, host rocks in areas of repeated intrusion that have been heated above the brittle–ductile transition are better described by a viscoelastic rheology (e.g. Newman *et al.*, 2006; Yamasaki *et al.*, 2018), while ductile accommodation of volume changes may occur at greater depth. Where some constraints are available for the structure and rheology of Earth's crust, finite or boundary element models may achieve a more realistic model of the deformation source (e.g. Masterlark, 2007; Gottsmann *et al.*, 2017; Hickey *et al.*, 2017).

Observations

Measurements of volcano deformation preceding and, or, accompanying eruption have provided insights into

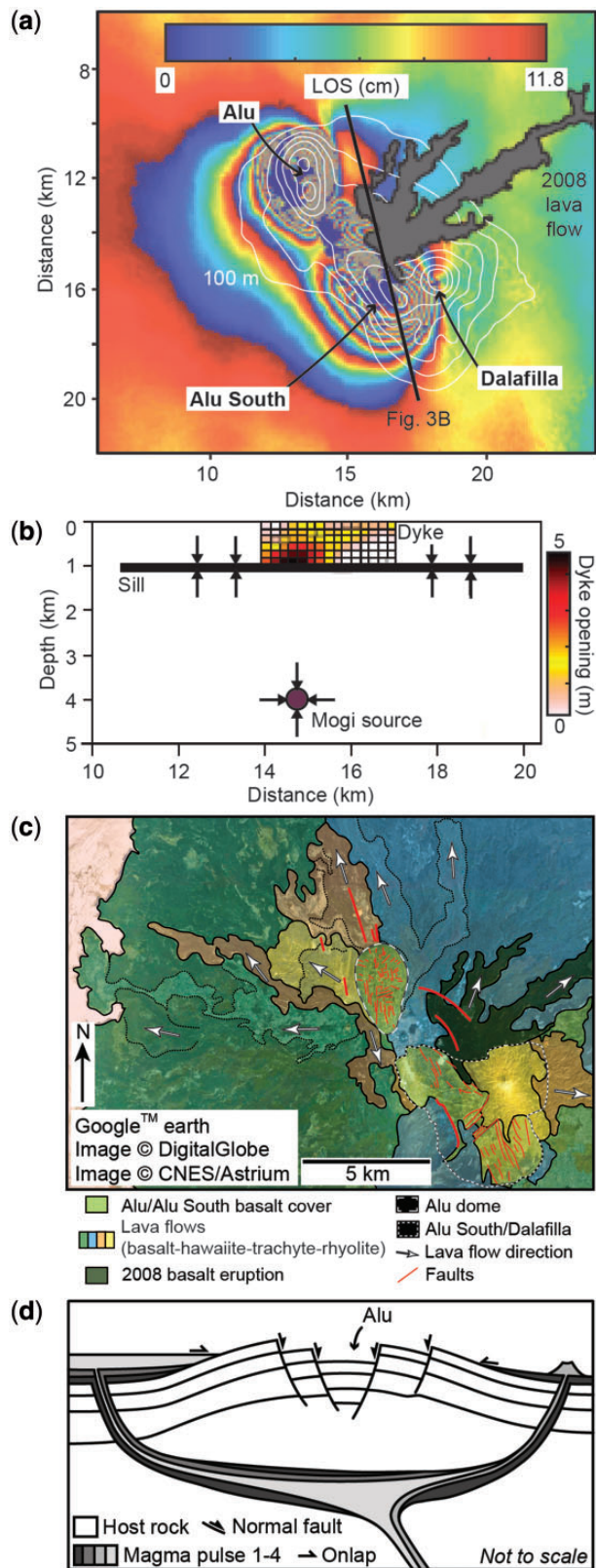


Fig. 3. (a) Ascending line of sight (LOS) co-eruptive interferogram from the 2008 basalt lava extrusion between the Alu and Alu South domes and the Dalafilla stratovolcano (modified from Pagli *et al.*, 2012). (b) Inversion of uplift and subsidence patterns, recorded by InSAR during the 2008 basalt lava eruption at the Alu dome in the Danakil Depression, suggested ground deformation could be attributed to a combination of:

the extent and structure of magma plumbing systems and, in some instances, the dynamics of magma movement. For example, InSAR-based observations at Eyjafjallajökull, Iceland, have recognised the intrusion of multiple, distinct sills over a decade and their subsequent extraction when tapped during an explosive eruption (e.g. Pedersen & Sigmundsson, 2006; Sigmundsson *et al.*, 2010). Extensive lateral connections via dykes and sills between reservoirs and/or volcanoes have been illuminated by eruptions or unrest accompanied by ground deformation tens of kilometres away and by the existence of multiple deformation sources (e.g. Alu-Dalafilla shown in Fig. 3a and b, Pagli *et al.*, 2012; Korovin, Lu & Dzurisin, 2014; Cordon-Caille, Jay *et al.*, 2014; Kenyan volcanoes, Biggs *et al.*, 2014; global synthesis, Ebmeier *et al.*, 2018). Interruptive deformation at calderas is especially complex and seems to be particularly frequent and high magnitude (e.g. Laguna del Maule: Fournier *et al.*, 2010; Singer *et al.*, 2014; Le Mével *et al.*, 2015), with the location of the deformation sources inferred to vary over time (e.g. Campi Flegrei, Trasatti *et al.*, 2008; Yellowstone, Wicks *et al.*, 2006). The geometries of dykes and sills inferred from InSAR data inform our understanding of changing subsurface stress fields (e.g. Afar, Hamling *et al.*, 2010; Fernandina, Bagnardi *et al.*, 2013), as do measurements of displacements caused by moderate earthquakes in close proximity to magma plumbing systems (e.g. Kilauea, Wauthier *et al.*, 2013; Chiles-Cerro Negro, Ebmeier *et al.*, 2016).

At a transcrustal scale, deformation measurements have contributed to evidence for temporal variations in magma supply rates (e.g. in Hawaii, Poland *et al.*, 2012). Volume increases in the mid- to lower-crust, notably in the Central Andes, have provided the first observations of deep pluton growth (Pritchard & Simons, 2004). Furthermore, uplift during episodes of unrest that have not (yet) resulted in eruption have been detected at a broad range of volcanoes (e.g. Westdahl, Mount Peulik, Lu & Dzurisin, 2014; Alutu & Corbetti, Biggs *et al.*, 2011) and, in some cases, have been interpreted as evidence for the 'pulsed' accumulation of potentially eruptible magma (e.g. Santorini, Parks *et al.*, 2012). In addition to magma movement, volume changes associated with internal reservoir processes can also cause deformation of the host rock and free surface. For example, InSAR measurements have recorded subsidence linked to cooling and crystallisation of sills (Medicine Lake,

(i) deflation of a reservoir, modelled as a Mogi source, at ~4 km depth; (ii) inflation and deflation of a tabular sill at ~1 km depth; and (iii) opening of a dyke beneath the eruptive fissure (Fig. 3a and b) (Pagli *et al.*, 2012). See Fig. 3a for location. (c) Geological map showing that lava flows radiate out from Alu and originate from the periphery of the dome, which is cross-cut by an array of randomly oriented faults (modified from Magee *et al.*, 2017a). (d) Magee *et al.*, (2017a) inferred Alu is underlain by a saucer-shaped sill plumbing system, based on field observations and comparison to seismic reflection data, not a tabular sill (b).

Parker, 2016; Taupo Volcanic Zone, Hamling *et al.*, 2015). Transient periods of subsidence during inter-eruptive uplift have been attributed to phase transitions in response to the addition of more juvenile magma (e.g. Okmok, Caricchi *et al.*, 2014).

Implications and integration

InSAR has increased the number of volcanoes at which measurements of ground deformation have been made, from less than 50 in the late 1990s to over 200 today (Biggs & Pritchard, 2017; Ebmeier *et al.*, 2018). This increase in coverage has been particularly influential in the developing world where monitoring infrastructure is typically poor (Chaussard & Amelung, 2013; Ebmeier *et al.*, 2013), with InSAR often providing the first evidence of magmatic activity at many volcanoes previously considered to be inactive (e.g. Pritchard & Simons, 2004; Biggs *et al.*, 2009, 2011; Lu & Dzurisin, 2014). A continued increase in the number and range of satellite- and large-scale UAV-based SAR instruments, as well as enhancements to their spatial and temporal resolution, will allow the detection of a greater range of volcanic ground deformation (e.g. Salzer *et al.*, 2014; Schaefer *et al.*, 2015; Stephens *et al.*, 2017). Overall, improved InSAR coverage will also increase the number of volcanoes where deformation measurements have been made across multiple cycles of eruption and deformation, increasing its usefulness for both hazard assessment and for characterising the extent, geometry, and changes in magma plumbing systems.

Geodetic measurements provide information only about the parts of a plumbing system that are currently active, and do not necessarily reflect the full extent and character of the intrusion network (e.g. Sigmundsson, 2016). However, geodetic analyses of ground deformation provide critical insight into the spatial and temporal development of active plumbing systems. Comparing observations of ancient plumbing systems (e.g. Magee *et al.*, 2013a; Schofield *et al.*, 2014), integration of ground deformation measurements with petrological observations (e.g. Caricchi *et al.*, 2014; Jay *et al.*, 2014) or thermal models (Parker *et al.*, 2016), as well as tomographic geophysical imaging, will increase the sophistication of models of magmatic systems. Integrating InSAR with gravity or electromagnetic measurements is particularly powerful, as it can allow discrimination between melt, volatiles, and hydrothermal fluids for which deformation signals are similar (see below) (e.g. Tizzani *et al.*, 2009).

Seismicity and magma plumbing systems

Technique

Seismicity (i.e. earthquakes) at volcanoes is primarily caused by the dynamic interaction of magma and hydrothermal fluids with the solid host rock (e.g. Chouet & Matoza, 2013), as well as by fracturing and fragmentation of silicic magma (e.g. Tuffen *et al.*, 2008). There are a number of primary physical mechanisms

for causing volcano seismicity (e.g. faulting), each of which typically produces seismic signals of specific frequency content (Chouet & Matoza, 2013). Recording and isolating different volcano seismicity signals, therefore, allows a variety of plumbing system processes to be assessed. The majority of volcano monitoring agencies have now deployed or aim to use a network of distributed seismic sensors, including broadband seismometers, to monitor volcano activity (Neuberg *et al.*, 1998; Sparks *et al.*, 2012). Furthermore, an increase in computing power and reduction in cost of seismic sensors means that researchers are now developing fast, fully automated detection and real-time location techniques that can locate seismicity to sub-decimetre precision (e.g. Drew *et al.*, 2013; Sigmundsson *et al.*, 2015).

Observations

Volcano-tectonic (VT) seismicity generally produces relatively high frequency (1–20 Hz), short period signals, involving clear primary (P), secondary (S) and surface waves, which are caused by displacement on new or existing faults in the host rock in response to fluid-induced stress changes (e.g. Rubin & Gillard, 1998; Roman & Cashman, 2006; Tolstoy *et al.*, 2008). These earthquakes commonly occur near the propagating edge of intrusions, meaning the space-time evolution of VT earthquake locations can be used to track the horizontal and vertical growth of sills and dykes (e.g. Keir *et al.*, 2009; Sigmundsson *et al.*, 2010, 2015). Inflation of a magma or mush body can also induce VT seismicity on any preferentially oriented faults surrounding the intrusion, thereby recording the delivery time and locus of new magma injected into a reservoir (e.g. Roman & Cashman, 2006; Vargas-Bracamontes & Neuberg, 2012).

Earthquakes with longer period seismic signals and low-frequencies (0.5–2 Hz) are thought to be generated near the interface between magma and solid rock (Chouet & Matoza, 2013). The earthquake source proximity to the magma causes the seismic signal to resonate in parts of the plumbing system (e.g. conduits, dykes, and cracks), leading to a reduction in its frequency content (Chouet & Matoza, 2013). These earthquakes can potentially be caused by stick-slip motion between the magma and wall-rock or fracturing of cooling magma near the conduit wall (Neuberg *et al.*, 2006; Tuffen *et al.*, 2008). Such earthquakes typically occur at restricted portions of conduits where the magma flow and shear strain rate are highest (Neuberg *et al.*, 2006; Tuffen *et al.*, 2008).

Very long period seismicity (VLP) of 10 s of seconds to several minutes period are typically attributed to inertial forces associated with perturbations in the flow of magma and gases through conduits (Chouet & Matoza, 2013). These signals can record the response of the host rock to reservoir inflation and deflation and may be used to model conduit shape and size (Chouet *et al.*, 2008). To do this requires a better understanding of the links between flow processes and resultant pressure/

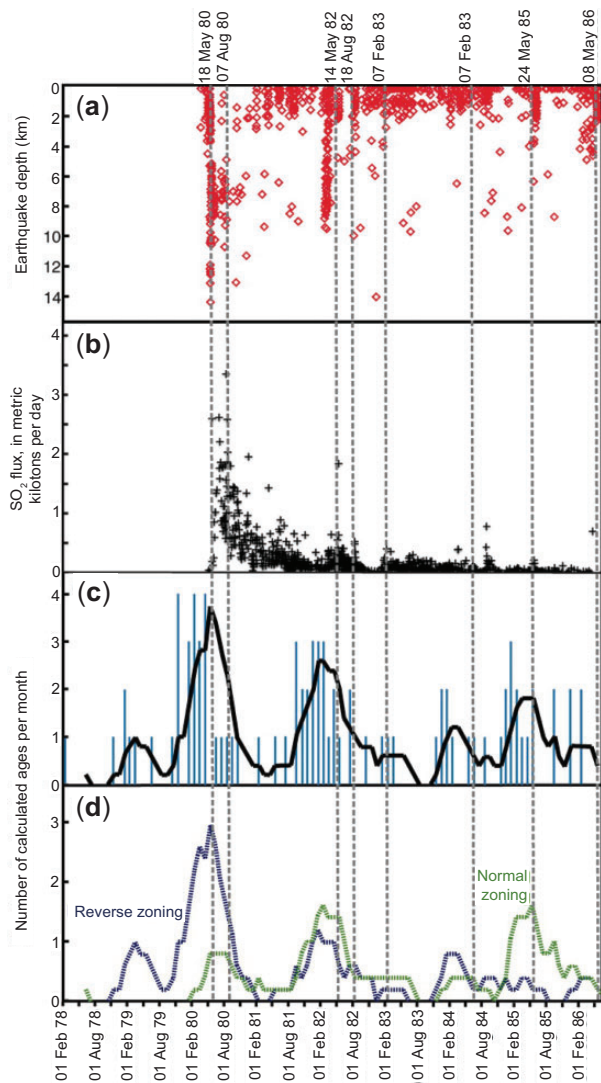


Fig. 4. Example of integrating seismology and petrology to constrain time-scales of magma storage and recharge (from Saunders *et al.*, 2012). Calculated Fe–Mg diffusion time scales of orthopyroxene crystals compared to monitoring data for the same eruptive period for Mount St. Helens. (a) The seismic record of depth against time of the 1980–1986 eruption sequence. (b) Measured flux of SO₂ gas. (c) Calculated age of orthopyroxene rim growth binned by month for the entire population. The age recorded is the month in which the orthopyroxene rim growth was triggered by magmatic perturbation. The black line displays the running average (over five points, equivalent to the average calculated uncertainty in calculated time scales) of all the data. The peaks in the diffusion time series correspond to episodes of deep seismicity in 1980 and 1982 and to elevated SO₂ flux in 1980 and possibly 1982. (d) Running average of the orthopyroxene rim time scales, displaying reverse zonation (Mg-rich rims) in blue and normal zonation (Fe-rich rims) in green. There are reverse zonation peaks in early 1980, probably due to rejuvenation of the magma system by hotter pulses, whereas Fe-rich rims are more dominant from 1982 on. Vertical dashed grey lines represent the volcanic eruptions.

momentum changes using laboratory experiments and numerical models that include the elastic response to magma flow across multiple signal frequency bands (e.g. Thomas & Neuberg, 2012).

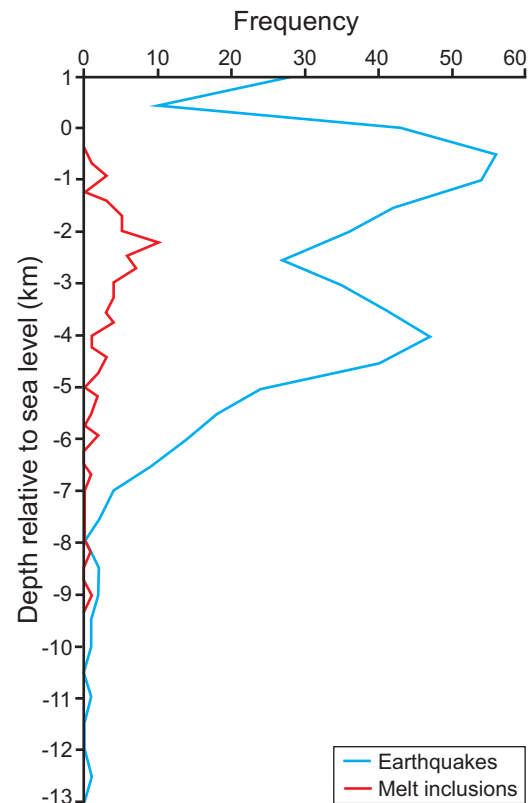


Fig. 5. Plot of melt inclusion saturation and earthquake hypocentre depths, which suggest magma storage occurred at 1–5 km depth beneath the Dabbahu volcanic system in Afar, Ethiopia (modified from Field *et al.*, 2012). Melt inclusion data obtained from analyses of alkali feldspar, clinopyroxene, and olivine phenocrysts within Dabbahu lavas <8 Kyr (Field *et al.*, 2012). Earthquake data recorded during the 2005 dyke event (Ebinger *et al.*, 2008).

Implications and integration

Studies of evolving reservoirs now aim to link episodes of seismicity related to new magma injection to petrological evidence for timing of reservoir recharge events, thereby providing independent constraints on day to year-long time-scales of magma residence and input prior to eruptions. For example, Fe–Mg diffusion chronometry modelling of orthopyroxene crystals from the 1980–1986 eruption of Mount St. Helens indicates that compositionally distinct rims grew within 12 months prior to eruption (Fig. 4) (Saunders *et al.*, 2012). Peaks in crystal growth correlated extremely well with increased seismicity and SO₂ flux (Fig. 4), confirming the relationship between seismicity and magma movement, as well as demonstrating how a combination of seismicity and petrological information can be used to detect magma injections (Saunders *et al.*, 2012).

Petrology and seismicity can also be integrated with other methods, such as GPS and InSAR. Field *et al.* (2012) analysed volatiles in melt inclusions trapped in phenocrysts within peralkaline lavas from historic eruptions at the Dabbahu Volcano in Afar, Ethiopia. Volatile saturation pressures at typical magmatic temperatures were constrained to be in the range 43–207 MPa,

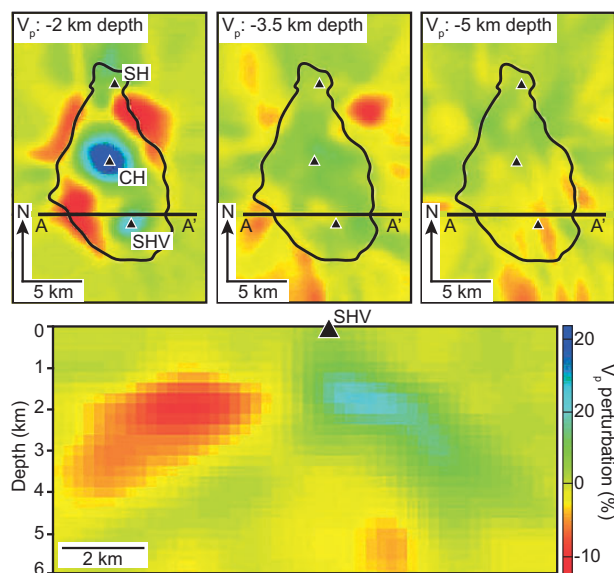


Fig. 6. P-wave (V_p) tomography beneath Montserrat (black outline), highlighting the location of fast and slow seismic velocity anomalies (i.e. $>6\%$ faster or slower than average) relative to the location of the Silver Hills (SH), Central Hills (CH), and Soufrière Hills (SHV) volcanoes (modified from Shalev *et al.*, 2010). The fast velocity anomalies, interpreted to represent solidified andesitic intrusions underlie the volcanoes (Shalev *et al.*, 2010).

consistent with the phenocryst assemblage being stable at 100–150 MPa. The interpreted magma/mush storage depths for these historic eruptions are ~ 1 –5 km, consistent with the depths of earthquakes associated with reservoir inflation following dyke intrusion in 2005–2006 (Fig. 5) (Ebinger *et al.*, 2008; Field *et al.*, 2012). Additionally, the best-fit result for modelling of uplift patterns recorded by InSAR data, which were collected over the same time period as seismicity measurements, suggests the magma/mush reservoir comprises a series of stacked sills over a ~ 1 –5 km depth range (Fig. 5) (Ebinger *et al.*, 2008). The consistency of depth estimates based on petrological study of ancient eruptions, along with the seismicity and inflation of the Dabbahu Volcano following axial dyke intrusion in 2005–2006, implies a vertically extensive and potentially long-lived magma/mush storage region. Such multidisciplinary studies demonstrate that joint observations and modelling of seismic signals, petrological data, and other techniques (e.g. geodesy and gas emissions) significantly strengthen interpretation of the physical structure, emplacement, and evolution of magma plumbing systems.

Identifying melt in plumbing systems using seismic imaging

Techniques

Both active and passive source seismological techniques, which utilise man-made seismic events and natural earthquakes respectively, can be used to identify areas where the presence of partial melt or magma

causes a local reduction in seismic wavespeed, an increase in anisotropy, or an increase in attenuation (e.g. Berryman, 1980; Hammond & Humphreys, 2000a, 2000b). With the recent availability of dense seismic networks, resolution of the crust and mantle seismic velocity structure has improved to the degree that active source seismic experiments can: (i) use tomographic techniques to image likely storage regions in the upper crust beneath ocean island volcanoes (e.g. Soufrière Hills Volcano, Montserrat; Fig. 6) (Paulatto *et al.*, 2010; Shalev *et al.*, 2010) and, occasionally, onshore volcanoes (e.g. Mt Erebus, Antarctica, Zandomenighi *et al.*, 2013; Mt. St. Helens, Kiser *et al.*, 2014); and (ii) utilise reflected data to image individual sills beneath mid-ocean ridges (e.g. Kent *et al.*, 2000; Marjanovic *et al.*, 2014). A further example from Katla volcano Iceland, demonstrates how active source seismic experiments can be used to identify S-wave shadow zones (i.e. S-waves cannot travel through fluids) and delays in P-waves, which may be used to infer the location and geometry of shallow-level magma reservoirs (Gudmundsson *et al.*, 1994). However, recent modelling approaches suggest that the upper crust likely represents only a small portion of magma plumbing systems and long-term storage is dominated by mushy zones throughout the lower crust (e.g. Annen *et al.*, 2006). Active source seismic experiments, particularly on land where the crust is thick and coverage less uniform, cannot penetrate to these depths efficiently. Furthermore, whilst seismic tomographic methods using local earthquakes offer 3D images of crustal velocity beneath many volcanoes (e.g. Mt. St. Helens, Waite & Moran, 2009; Askja, Iceland, Mitchell *et al.*, 2013), they can only resolve areas directly above the deepest earthquakes. Non-uniform coverage thus makes interpreting tomographic images difficult as resolution varies across the model (see review by Lees, 2007).

To illuminate lower crustal regions, seismologists rely on passive seismology. Extending seismic tomographic images of magma plumbing systems to lower crustal depths requires the use of teleseismic body-wave and surface wave data, which emanate far (>1000 km) from the measurement site. However, these data are dominated by longer period signals, meaning their resolution is relatively low. For example, the Fresnel zone (i.e. the region within $1/4$ seismic wavelength and an estimate of the minimum resolvable structure) for active source data at 10 Hz is on the order of 3 km in the upper crust compared to 10–15 km for 1 Hz teleseismic data used in receiver function or tomography studies.

Observations

Active and passive seismological techniques provide crucial insight into transcrustal melt and magma distribution. For example, P-wave seismic travel-time tomography across Montserrat and the Soufrière Hills Volcano

images a series of relatively fast seismic velocity zones, which are interpreted as solidified andesitic intrusions, surrounded by regions of slow seismic velocities likely related to either areas of hydrothermal alteration or buried volcanoclastic deposits (Fig. 6) (Paulatto *et al.*, 2010; Shalev *et al.*, 2010). Within the lower crust, inversions using surface wave data generated by ambient seismic noise and receiver function data, which isolates P-wave to S-wave conversions at major discontinuities in the Earth, have identified low shear-wave velocities probably related to melt presence beneath several volcanic settings (e.g. New Zealand, Bannister *et al.*, 2007; Toba, Sumatra, Stankiewicz *et al.*, 2010; Ethiopia, Hammond *et al.*, 2011; Jaxybulatov *et al.*, 2014; Costa Rica, Harmon & Rychert, 2015).

When trying to determine how much melt or magma is present, numerous studies have shown that seismic velocities are more sensitive to the shapes of melt/magma-filled spaces on a range of scales compared to the melt fraction (e.g. Hammond & Humphreys, 2000a, 2000b; Miller & Savage, 2001; Johnson & Poland, 2013; Hammond & Kendall, 2016). On the grain-scale, melt commonly wets grain boundaries, forming planar pockets (e.g. Takei, 2002; Garapic *et al.*, 2013; Miller *et al.*, 2014), whereas on the larger scale magma may form planar intrusions of either mush (e.g. Annen *et al.*, 2006), or liquid-rich dykes or sills. If these features are preferentially aligned, they will appear as a distributed region of melt to seismic waves and the analyses described will not be able to discriminate between a melt-poor region dominated by aligned melt-pockets on grain boundaries and an elongate melt-rich body such as an intrusion (e.g. Hammond & Kendall, 2016). A further problem is that seismic velocities are affected by variations in temperature (Jackson *et al.*, 2002), composition (Karato & Jung, 1998), and attenuation (Goes *et al.*, 2012). Therefore, relating seismic velocity anomalies to melt fraction is difficult without some prior knowledge of melt distribution (Hammond & Kendall, 2016).

One possible approach to investigate melt distributions further is through measuring seismic anisotropy. If melt has some preferential distribution on a length-scale smaller than the seismic wavelength, such as a stacked network of sills or an anisotropic permeability on the grain scale, then the seismic wavespeed will vary with direction of propagation, i.e. be anisotropic. As a result, measuring the effects of seismic anisotropy allows inferences about sub-seismic wavelength structures, leading to estimates of the preferential orientation of melt distribution. It is common to observe strong anisotropy beneath volcanoes and this has been used to place constraints on melt distribution. For example, high degrees of shear-wave splitting from volcanic earthquakes can either directly map out regions of significant quantities of melt aligned in pockets (Keir *et al.*, 2011), or map out stress changes related to overpressure from injections of magma into the upper crust (Gerst & Savage, 2004; Roman *et al.*, 2011). To image the deeper crustal magmatic system, azimuthal

variations in the ratio of P-wave to S-wave speeds (i.e. V_p/V_s) from receiver functions led to the interpretation that a stacked network of sills is present in the lower crust beneath the Afar Depression, Ethiopia (Hammond, 2014). Differences in the velocity of Rayleigh Waves and Love Waves, which are vertically polarised shear waves and horizontally polarised shear waves, respectively, suggest a similar anisotropic melt distribution is present beneath the Toba Caldera, Sumatra (Jaxybulatov *et al.*, 2014) and Costa Rica (Harmon & Rychert, 2015).

Implications and integration

Due to the interference of signals denoting the geometry of melt-filled pockets and the volumetric proportion of that melt, estimating melt fraction remains difficult using seismology alone. Some attempt has been made to directly infer magma/mush reservoir properties from seismic velocities. For example, Paulatto *et al.*, (2012) used thermal modelling to test the range of melt fractions that could account for the low velocity zones imaged in the upper crust beneath Soufrière Hills Volcano (Fig. 6), Montserrat, and concluded the melt fraction is between 3 and 10%. However, accounting for resolution of the tomography, together with uncertainties in the distribution and geometry of melt, means >30% melt may be present more locally in the low velocity zones defined beneath Soufrière Hills Volcano (Paulatto *et al.*, 2012). Possible ways forward involve integrating seismological data with: (i) petrological data that can place limits on likely melt fractions and/or emplacement depths (e.g. McKenzie & O'Nions, 1991; Comeau *et al.*, 2016); (ii) geochemical techniques that can help determine timescales of melt and magma evolution (e.g. Hawkesworth *et al.*, 2000); and (iii) geodetic or other monitoring data, which helps determine magma movement (Sturkell *et al.*, 2006). Recent efforts applying industry software, such as full waveform inversions (FWI; Warner *et al.*, 2013), which is discussed below, are also pushing the potential application of seismological data further and mean that it may be possible to resolve features to sub-kilometre levels, particularly in the upper crust. Together, these techniques may allow us to directly relate seismic velocity anomalies to melt fractions and distributions in the whole crust.

Studying magma plumbing systems using gravimetry

Techniques

Gravimetry measures the gravitational field and its changes over space and time, which can be related to variations in the subsurface distribution and redistribution of mass (e.g. magma). A variety of gravimeter instruments (e.g. free-fall, superconducting, and spring-based) and techniques (e.g. ground-based, sea-floor, ship-borne, and air-borne instrumentations) are available. Spring gravimeters, where a test mass is suspended on a spring, are mostly used to study magmatic and volcanic processes in ground-based surveys (e.g.

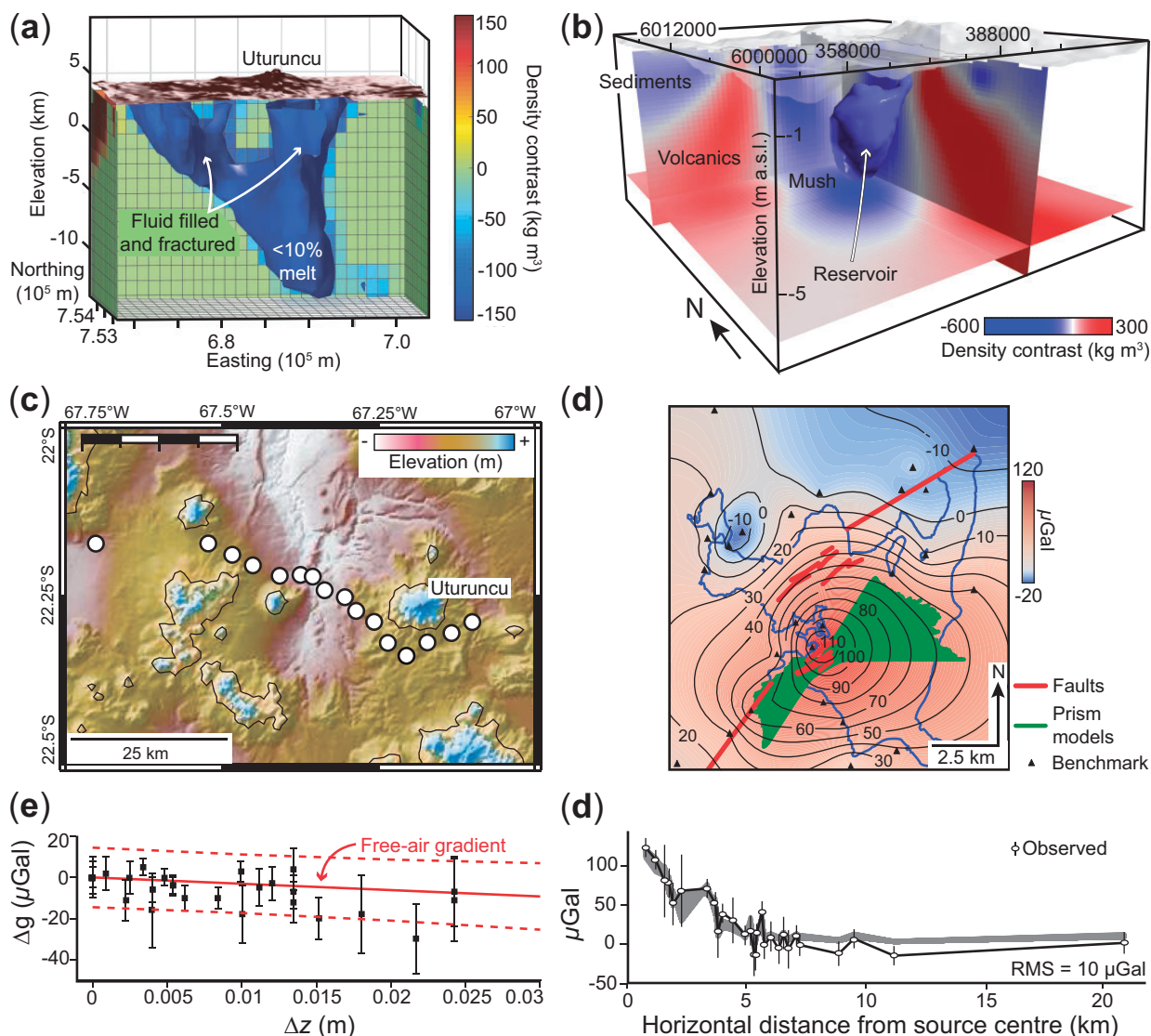


Fig. 7. Static and dynamic gravimetric investigations of two active silicic magmatic systems in the Andes: Uturuncu volcano (Bolivia; a, c, e) and the Laguna del Maule volcanic field (Chile; b, d, f). (a) 3D view of the isosurface corresponding to the -120 kg m^{-3} density contrast beneath Uturuncu volcano, derived from Bouguer gravity data, interpreted to reflect a large ($\sim 750 \text{ km}^3$) plumbing system composed of a lower ($< -10 \text{ km}$) partially molten reservoir and upper, fractured and fluid-filled solidified intrusions above sea level (after del Potro *et al.*, 2013). (b) 3D view of the -600 kg m^{-3} density contrast isosurface beneath the Laguna del Maule, which is interpreted to define a magma reservoir ($> 50\%$ melt) within a larger region of a crystal mush system; the 2D planes show slices through the dataset (Miller *et al.*, 2017). Elevation above sea level (a.s.l.) shown. See (d) for area of data coverage. (c) Map of the 55 km long, dynamic gravity network (white circles) installed to track changes in gravity over time and space at Uturuncu volcano between 2010 and 2013 (modified from Gottsmann *et al.*, 2017). (d) Spatio-temporal residual gravity changes at Laguna del Maule recorded from 2013–2014, after correcting for deformation effects (modified from Miller *et al.*, 2017). (e) Gravity and deformation data, recorded from Uturuncu from 2010–2013, plotted against the measured free-air gravity gradient (solid red line) and associated errors (broken red lines) (modified from Gottsmann *et al.*, 2017). The data follow the gradient and are indicative of a subsurface density change as a cause of the uplift, possibly reflecting the release of fluids from a large deep-seated magma reservoir (i.e. the Altiplano-Puna Magmatic Body; Chmielowski *et al.*, 1999) through the vertically extensive crystal mush system shown in (A) (Gottsmann *et al.*, 2017). (f) Plot of gravity against horizontal distance for the source centre at Laguna del Maule (modified from Miller *et al.*, 2017). The increase in gravity of up to $120 \mu\text{Gal}$ is explained by a hydrothermal fluid injection focused along a fault system, shown in (d), at 1.5–2 km depth as a result of a deeper seated magma injection, and is best modelled by a vertical rectangular prism source.

Carbone *et al.*, 2017; Van Camp *et al.*, 2017). Changes in the gravitational acceleration across a survey area shorten or lengthen the spring, which is recorded electronically and converted to gravity units. These changes are evaluated across a survey network in relation to a reference and are hence termed 'relative

measurements'. Absolute gravimetry can also be measured, i.e. the value of gravitational acceleration, and serves primarily to create a reference frame into which other geodetic methods (e.g. InSAR, GNSS, levelling, relative gravimetry) can be integrated for joint data evaluation. Recent reviews by Carbone *et al.*, (2017) and

Van Camp *et al.*, (2017) provide a broad account of gravimetric instruments, measurement protocols, and data processing relevant for the study of magmatic systems.

Static gravimetric techniques obtain a single snapshot of the subsurface mass distribution. For example, Bouguer anomaly maps are perhaps the best-known products of static gravity surveys and capture spatial variations in gravity over an area of interest, providing insight into anomalous mass distribution in the subsurface. Within magmatic studies, computational modelling and inversion of Bouguer anomaly data allows identification of shallow intrusions (e.g. dykes and sills; Rocchi *et al.*, 2007), magma-related ore bodies (Hammer, 1945; Bersi *et al.*, 2016), and plutons (e.g. Fig. 7a and b) (e.g. Vigneresse, 1995; Vigneresse *et al.*, 1999; Petford *et al.*, 2000) exhibiting a density contrast with their host rocks.

In contrast to static surveys, dynamic gravimetric observations allow spatio-temporal mass changes to be tracked. Dynamic gravimetric studies investigate how the subsurface architecture changes over time and is usually performed by measuring variations in gravity

across a network of survey points (e.g. Fig. 7c) or, in a few exceptional cases, by installing a network of continuously operating gravimeters. Dynamic observations demand one-to-two orders of magnitude higher data precision (i.e. to a few μGal where $1 \mu\text{Gal} = 10^{-8} \text{m/s}^2$) compared to static surveys, making them an elaborate and time-consuming exercise. However, dynamic gravity data yields important insights into the source processes behind non-tectonic volcano and crustal deformation, particularly if combined with surface deformation data (e.g. InSAR and GNSS) as subsurface mass and volume changes can be employed to characterise the density of the material behind the stress changes (Figs 7c–f and 8) (e.g. Jachens & Roberts, 1985; Battaglia & Segall, 2004; Poland & Carbone, 2016). There are also cases where volcano unrest, due either to magma intrusion into a ductile host rock or to volatile migration at shallow depths, does not result in resolvable surface deformation; in these scenarios, gravity data have provided vital clues about subsurface processes otherwise hidden from conventional monitoring techniques (e.g. Gottsmann *et al.*, 2006, 2007; Miller *et al.*, 2017).

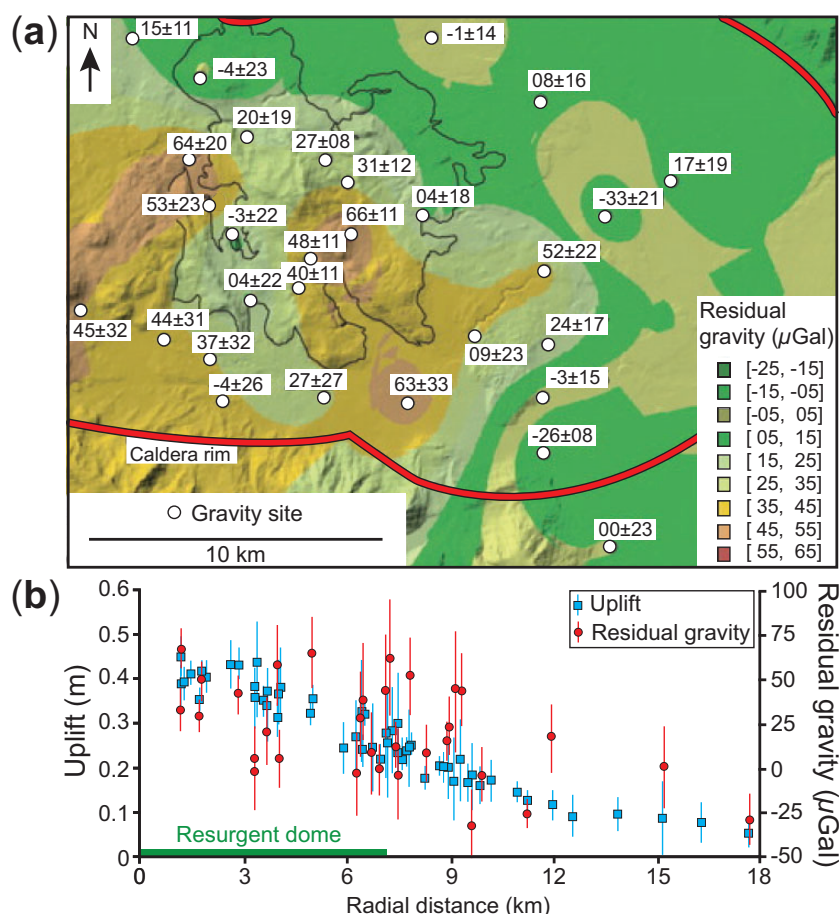


Fig. 8. Gravity changes and deformation at the restless Long Valley caldera, California, USA, which hosts a resurgent dome (black outline), to highlight changes in residual gravity between 1982 and 1999 (modified from Tizzani *et al.*, 2009). (b) Plot of ground uplift and residual gravity changes with radial distance from the centre of the resurgent dome in (a) (modified from Tizzani *et al.*, 2009). The correlation between uplift and positive gravity residuals across the resurgent dome indicates ground deformation was instigated by intrusion of magma (Tizzani *et al.*, 2009).

Whilst static and dynamic gravimetric observations offer considerable insight into the structure and dynamics of magma plumbing systems, care must be exercised when collecting and interpreting gravity data from active magmatic areas where seasonal variations in hydrothermal systems, aquifers, or the vadose zone can influence subsurface mass distribution (e.g. Hemmings *et al.*, 2016). These seasonal changes can, in some cases, result in data aliasing artefacts and inhibit the quantification of deeper-seated magmatic processes (e.g. Gottsmann *et al.*, 2005, 2007).

Observations

Gravimetric investigations have been at the heart of studies into the subsurface structure of active and ancient magma plumbing systems for more than 80 years (e.g. Carbone *et al.*, 2017; Van Camp *et al.*, 2017). Using techniques initially designed for imaging salt domes, silicic plutons were the first components of magma plumbing systems to be examined using gravimetry because their low density relative to surrounding rocks produces clear, negative gravity anomalies of ~ 10 to ~ 40 mGal amplitude (e.g. Reich, 1932; Bucher, 1944; Bott, 1953). Gravity data have been instrumental in the investigation of upper-crustal, silicic magma plumbing systems, helping to reveal: (i) the 3D geometry of plutons by allowing floor morphologies (e.g. flat-floored or wedge-shaped) to be determined (e.g. Vigneresse *et al.*, 1999; Petford *et al.*, 2000); and (ii) how plutons are constructed, for example, by the amalgamation of multiple intrusions fed from depth by dykes (e.g. Vigneresse, 1995). Furthermore, recent high-precision static surveys over active silicic volcanoes have enabled detailed modelling of the sub-volcanic magma plumbing system, commonly demonstrating the occurrence of vertically extensive, transcrustal magma bodies (Fig. 7a and b) (e.g. Gottsmann *et al.*, 2008; del Potro *et al.*, 2013; Saxby *et al.*, 2016; Miller *et al.*, 2017). In addition to examining silicic magma plumbing systems, negative gravity anomalies with typical amplitudes of up to 60 mGal and up to 100 km wavelength can be associated with, and provide insight into, the geometry and size of silicic ash-flow calderas (e.g. Eaton *et al.*, 1975; Masturyono *et al.*, 2001). Positive gravity anomalies with amplitudes of up to 30 mGal and wavelengths of up to 20 km are commonly identified at mafic volcanoes and likely result from dense intrusive complexes (e.g. Rymer & Brown, 1986).

Dynamic gravity observations have provided unprecedented insight into the evolution of magma plumbing systems over timescales of seconds to decades, including: (i) the characterisation of multi-year lava lake dynamics (e.g. Poland & Carbone, 2016); (ii) mass budgets of magma intrusions (e.g. Fig. 8) (e.g. Battaglia *et al.*, 1999; Jousset *et al.*, 2000; Rymer *et al.*, 2005; Bonforte *et al.*, 2007; Tizzani *et al.*, 2009); (iii) shallow hydrothermal fluid flow processes induced by deeper magmatic

unrest (e.g. Battaglia *et al.*, 2006; Gottsmann *et al.*, 2007; Miller *et al.*, 2017); and (iv) parameters of magmatic geothermal reservoirs (e.g. Hunt & Bowyer, 2007; Sofyan *et al.*, 2011). For example, using data from a network of continuously recording gravimeters, Carbone *et al.*, (2013) calculated the density of the Kilauea lava lake as $950 \pm 300 \text{ kg m}^{-3}$, i.e. similar to and potentially less than that of water, suggesting that the magma column within the upper portions of the volcanic edifice is gas-rich. Because density and volatile content are critical controls on magma rheology, identification of a gas-rich magma column and lava lake at Kilauea is crucial to modelling and understanding convection and eruption dynamics (Carbone *et al.*, 2013).

Implications and integration

The advent of data-rich geodetic observations from satellite-remote sensing (e.g. InSAR), in conjunction with spatio-temporal gravity studies, provides unprecedented opportunities to characterise magma plumbing system dynamics and the driving mechanisms behind volcano deformation. At Long Valley caldera, for example, a residual gravity increase of more than 60 μGal between 1982 and 1999 indicates a mass addition at depth (Battaglia *et al.*, 1999). Joint inversion of InSAR and gravity data from Long Valley derives a best-fit source density of 2509 kg m^{-3} and is indicative of a magmatic intrusion (Fig. 8) (Tizzani *et al.*, 2009). At the deforming Laguna del Maule volcanic centre, Chile, multi-year InSAR and dynamic gravity records demonstrate that uplift and extension above an inflating sill-like reservoir at ~ 5 km depth promoted migration of hydrothermal fluids along a fault to shallow (1–2 km) depths (Miller *et al.*, 2017). Alternatively, although no ground deformation is observed at Tenerife, Canary Islands, Spain, deconvolution of dynamic gravity into a shallow and deep gravity field provides evidence of unrest (Prutkin *et al.*, 2014). The gravity data suggest hybrid processes have generated the unrest, whereby fluids were released and migrated upward along deep-rooted faults from an intrusion at ~ 9 km beneath the summit of Teide Volcano (Prutkin *et al.*, 2014). Overall, combining ground deformation and gravimetric observations has highlighted complex processes both within magma reservoirs (e.g. mass addition by magma input, density decrease by volatile exsolution, or density increase by crystallisation; Fig. 7c–f) and in the surrounding host rock (e.g. migration of magmatic fluids, phase changes in hydrothermal systems). Key to a better understanding of the processes governing these magma plumbing system and volcano deformation dynamics is the integration of gravimetric and geodetic data with other geophysical data (e.g. seismicity or magnetotellurics) and petrological data. Coupled with advanced numerical modelling, such multi-parameter studies promise exciting new insights into the inner workings of sub-volcanic magma plumbing systems

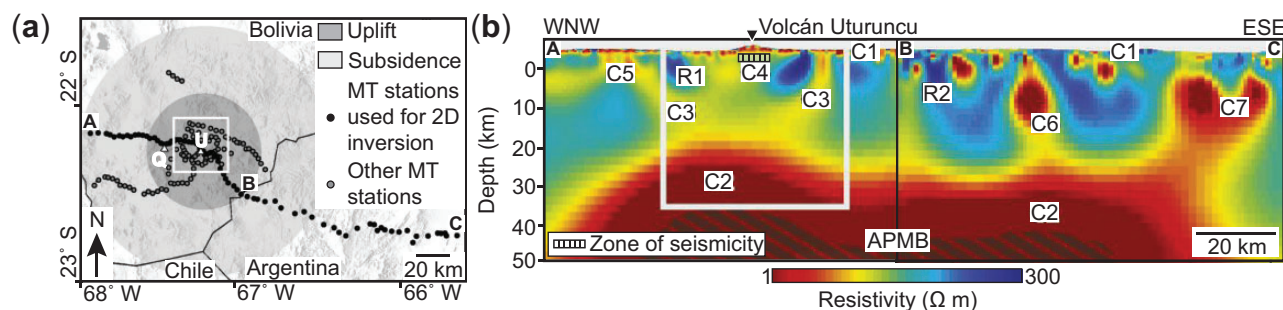


Fig. 9. (a) Map showing MT stations deployed around Volcán Uturuncu (U) and Volcán Quetena (O), relative to areas of uplift and subsidence (modified from [Comeau et al., 2015](#)). The white box shows area of modelled 3D MT data ([Comeau et al., 2015](#)). (b) Regional 2D magnetotelluric line through the Altiplano-Puna magma body (APMB) highlighting the position of Volcán Uturuncu (modified from [Comeau et al., 2015](#)). The APMB corresponds to a large, conductive (i.e. low-resistivity) body ([Comeau et al., 2015, 2016](#)). Above the APMB are other areas of low-resistivity (e.g. C4) that are likely upper crustal magma reservoirs and dykes ([Comeau et al., 2016](#)). C1–C7 and R1–R2 identify discrete zones of marked conductivity or resistivity, respectively (see [Comeau et al., 2015, 2016](#) for details). The white box shows area of modelled 3D MT data ([Comeau et al., 2015](#)). See (a) for location.

(e.g. [Currenti et al., 2007](#); [Hickey et al., 2016](#); [Currenti et al., 2017](#); [Gottsmann et al., 2017](#); [Miller et al., 2017](#)).

Resolving magma plumbing system structure with electromagnetic methods

Techniques

Electromagnetic (EM) methods probe subsurface electrical resistivity or its inverse, i.e. electrical conductivity. Spatial variations in resistivity control the position, strength, and geometry of local electrical eddy currents and the magnetic fields they produce. These electrical eddy currents are induced by time-varying, naturally occurring magnetic fields external to Earth, which forms the basis of the magnetotelluric (MT) technique, or by controlled sources. Monitoring these decaying electrical and magnetic fields, therefore, allows the subsurface resistivity distribution to be inferred. Controlled source methods generally probe only the shallow subsurface, but MT has a greater depth range as it uses longer-period signals to penetrate deeper. The signals propagate diffusively, which means EM methods typically have a lower resolution than seismic techniques. However, melt, magma, and magmatic hydrothermal fluids are generally considerably less resistive than solid rock and can thus easily be detected by EM methods, which are sensitive to conductive materials (e.g. [Whaler & Hautot, 2006](#); [Wannamaker et al., 2008](#); [Desissa et al., 2013](#); [Comeau et al., 2015](#)). Therefore, EM methods, particularly MT, have been used extensively to study magmatic systems in various tectonic settings.

MT equipment, data acquisition and processing are described by [Simpson & Bahr \(2005\)](#) and [Ferguson \(2012\)](#). Measured field variations have very low amplitudes, meaning equipment needs to be positioned and installed carefully to reduce vibrational (e.g. from wind, vegetation, or vehicles) and electrical (e.g. from power lines) noise. If data are recorded synchronously at a second, less noisy site, remote reference methods can be

used to improve the data quality (e.g. [Gamble et al., 1979](#)). One further problem is that small-scale resistivity anomalies in the shallow subsurface generate galvanic (non-inductive) effects that distort MT data. The distortion is identified and corrected for, which may involve using controlled source transient electromagnetic data to ensure complete removal (e.g. [Sternberg et al., 1988](#)), at the same time as assessing whether the data can be modelled with a one-, two- or three-dimensional resistivity structure (e.g. [Jones, 2012](#)). Failure to remove galvanic distortion can result in models having resistivity features at the wrong depth. For example, there has been controversy as to whether a conductor beneath Vesuvius Volcano, Italy is caused by a deep (~8–10 km depth) magma reservoir ([Di Maio et al., 1998](#)) or a shallow brine layer ([Manzella et al., 2004](#)). These and other factors can be a significant problem when using MT to study magmatic systems, especially on volcanic islands.

The relationship between MT data and subsurface resistivity is strongly non-linear meaning that inversion is fundamentally non-unique and computationally expensive (e.g. [Bailey, 1970](#); [Parker, 1980](#); [Weaver, 1994](#)). Most practical algorithms for inverting MT data obtain a unique result by minimising a combination of misfit to the data and a measure of model roughness (e.g. [Constable et al., 1987](#)). This approach poorly delimits how magma is distributed in the subsurface, whether it is in sills, dykes, or larger reservoirs ([Johnson et al., 2016](#)). Whilst MT data are sensitive to the top surface of a conductor, its base may not be detected because conductive material reduces the penetration depth of the signal. Sensitivity analysis is used to ascertain the model features required to fit the MT data, which allows a conductor to be confined to a certain depth range and thereby constrains its base (e.g. [Desissa et al., 2013](#)). Furthermore, if the resistivity of a conductor can be inferred, its conductance (i.e. a product of thickness and conductivity) can be used to determine its thickness (e.g. [Comeau et al., 2016](#)).

Observations

EM induction surveys have been conducted on most major sub-aerial volcanoes and magmatic systems; only a few will be mentioned here to illustrate the type of information on magma plumbing systems that has been obtained. MT data have been used to image several low resistivity features in the central Andes, particularly beneath the uplifting (10–15 mm/yr) Volcán Uturuncu, Bolivia (Fig. 9a) (Comeau *et al.*, 2015, 2016). The deepest of these bodies has resistivities of $<3 \Omega \text{ m}$, has a top contact at $\sim 15\text{--}20 \text{ km}$ depth (beneath Uturuncu), likely has a thickness of $>6 \text{ km}$, and extends E–W for $\sim 170 \text{ km}$ (Fig. 9) (Comeau *et al.*, 2015, 2016). This large-scale structure is interpreted to be the Altiplano-Puna magma body (APMB), which has been identified in other geophysical datasets (e.g. Fig. 7a) (e.g. gravimetry, del Potro *et al.*, 2013), with its low resistivity attributed to the presence of at least 20% andesitic melt and/or magma. Extending from the top of the APMB towards the surface are several vertical, narrow ($<10 \text{ km}$ wide), low resistivity ($<10 \Omega \text{ m}$) zones that coincide with areas of seismicity and negative gravity anomalies (Fig. 9). These zones likely reflect a network of dykes and upper crustal magma reservoirs (Jay *et al.*, 2012; del Potro *et al.*, 2013; Comeau *et al.*, 2015, 2016).

Monitoring of magmatic systems can also be undertaken by both time-lapse and continuous EM measurement. For example, MT data collected immediately after the 1977–1978 eruption at Usu volcano, Japan revealed a conductive zone ($<100 \Omega \text{ m}$) beneath the summit that probably corresponded to intruded magma. By 2000, MT data revealed that this conductive body had become resistive ($500\text{--}1000 \Omega \text{ m}$) as the intrusion cooled, from 800°C to 50°C , and crystallised (Matsushima *et al.*, 2001). Continuous MT monitoring of Sakurajima volcano, Japan between May 2008 and July 2009 revealed temporal changes in resistivity in the data, some of which were correlated to periods of surface deformation and were inferred to reflect mixing between groundwater and volatiles exsolved from an underlying magma body (Aizawa *et al.*, 2011). Continuous MT monitoring at La Fournaise, Réunion Island recorded apparent resistivity decreases associated with the large 1998 eruption, which were attributed to the injection of a N–S striking dyke (Wawrzyniak *et al.*, 2017).

Several EM studies have focussed on magma plumbing systems at divergent margins, including mid-ocean ridges and continental rifts. For example, at the fast-spreading East Pacific Rise, a $\sim 10 \text{ km}$ wide, sub-vertical conductor, slightly displaced from the ridge axis and connected to a deep, broad conductive zone was interpreted as a channel efficiently transporting melt to the base of the crust (Baba *et al.*, 2006; Key *et al.*, 2013). Imaging of a crustal conductor for the first time beneath a slow-spreading ridge, i.e. the Reykjanes Ridge in the Atlantic Ocean, suggests that magma injection into crustal reservoirs is intermittent but

rapid (MacGregor *et al.*, 1998; Heinson *et al.*, 2000). Conversely, slow-spreading continental rifting in the Dabbahu magma segment, Afar, Ethiopia, appears to be underlain by a large conductor, either at the top of the mantle or straddling the Moho, containing more melt ($>300 \text{ km}^3$) than is intruded during a typical rifting episode (Desissa *et al.*, 2013). The volume of this large conductor implies it is a long-lived feature that could source magmatic activity for tens of thousands of years (Desissa *et al.*, 2013).

Implications and integration

It is clear from MT studies of the APMB that other geophysical techniques aid and/or corroborate data interpretation (Fig. 9) (e.g. Comeau *et al.*, 2015, 2016). Over the last two decades, numerous geophysical studies have been applied to examine magma and melt distribution beneath various portions of the East African Rift, providing an excellent opportunity to test how different techniques and data can be integrated. For example, extensive zones of melt beneath the Afar region in Ethiopia inferred from MT data by Desissa *et al.*, (2013) are supported by: (i) the occurrence of coincident, low P-wave velocity (down to 7.2 km s^{-1}) zones identified from analysis of seismic Pn waves that propagate along the Moho (Stork *et al.*, 2013); (ii) surface wave studies that reveal lower crustal areas in magmatic domains with low S-wave velocities ($\sim 3.2 \text{ km s}^{-1}$) (Guidarelli *et al.*, 2011); and (iii) high V_p/V_s ratios and low amplitude receiver functions, which are indicative of the presence of melt (Hammond *et al.*, 2011; Hammond, 2014). Similarly, crustal conductors along the northern flanks of the Main Ethiopian Rift, interpreted to represent melt or magma (Whaler & Hautot, 2006; Samrock *et al.*, 2015), coincide with locations where receiver functions either have amplitudes too low to interpret or indicate high V_p/V_s values (Dugda *et al.*, 2005; Stuart *et al.*, 2006). Electrical anisotropy can be inferred directly from MT data consistent with a two-dimensional subsurface resistivity distribution (Padilha *et al.*, 2006; Hamilton *et al.*, 2006). Large amounts of electrical anisotropy were found in the lower crust beneath Quaternary magmatic segments in Afar, Ethiopia, where there is also significant crustal seismic anisotropy (see figure 11 of Ebinger *et al.*, 2017); oriented melt-filled pockets are the probable cause of both.

Although EM methods can image subsurface conductors that are interpreted to represent magma bodies or zones of partial melt (i.e. crystal mushes), additional information is required to determine their composition, volume, and/or melt fraction. However, there are several challenges in inverting measured bulk resistivities to recover this information. Two-phase mixing laws predict bulk resistivity is primarily a function of melt resistivity and geometry in the rock matrix when the fluid phase has low resistivity, as in the case of partial melt. Well-connected melt gives a lower bulk

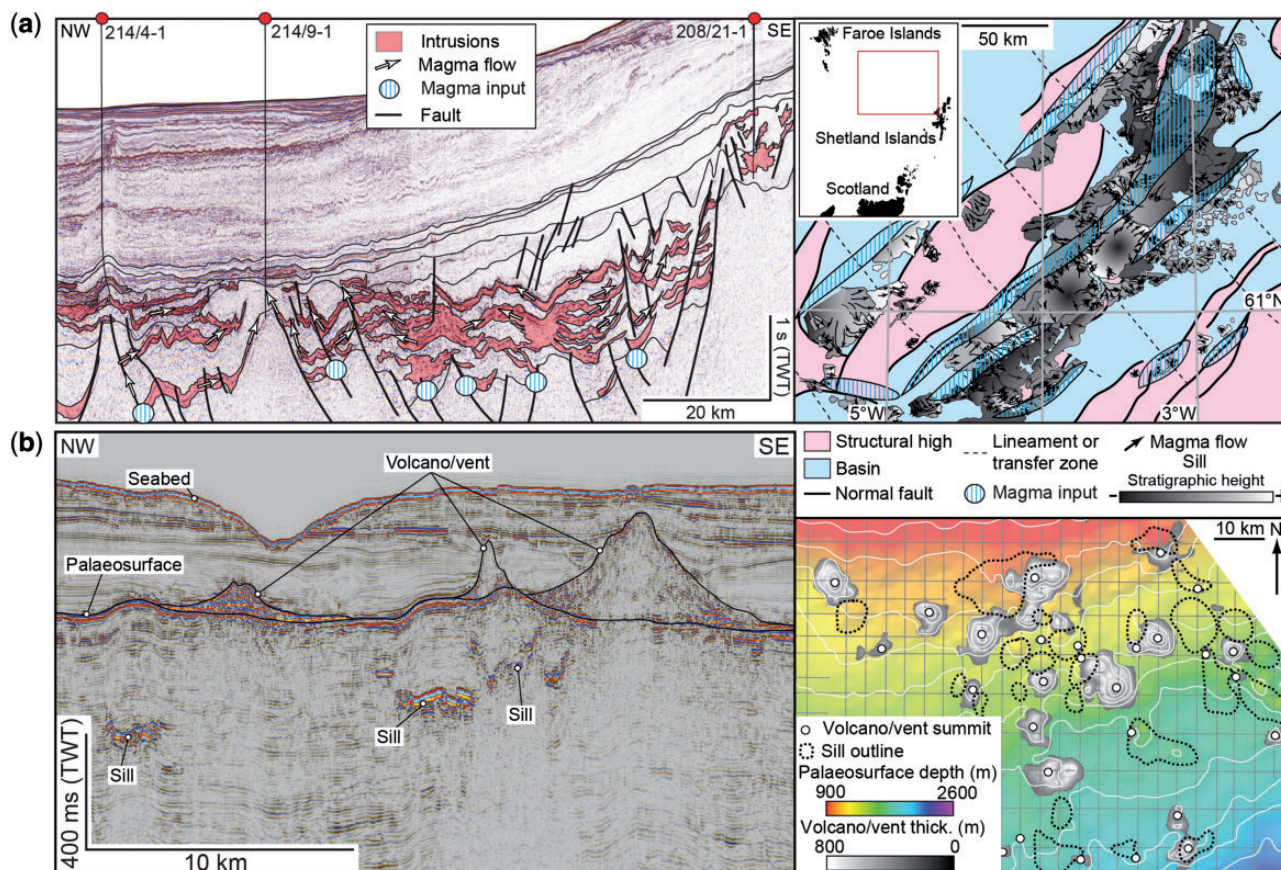


Fig. 10. (a) Interpreted seismic section and geological map showing the distribution of, and connectivity between, sills within the Faroe-Shetland Basin (modified from Schofield *et al.*, 2017). Mapping of magma flow patterns within individual sills reveals that the sill-complex facilitates extensive vertical and lateral magma transport. Magma was fed into the sedimentary basin via basement-involved faults. TWT, two-way travel time. (b) Interpreted seismic section and geological map describing the spatial relationship between volcanoes/vents and sills, inferred to represent the magma plumbing system, emplaced at ~42 Ma (modified from Jackson *et al.*, 2013; Magee *et al.*, 2013b). Sills are laterally offset from the volcanoes/vents summits. No 'magma chambers' are observed in the seismic data, which images down to ~8 s TWT (i.e. ~10 km) (Magee *et al.*, 2013b).

resistivity than isolated melt pockets, for the same melt fraction and resistivity (e.g. Hashin & Shtrikman, 1962; Roberts & Tyburczy, 1999; Schmeling, 1986). Whilst resistivities of basaltic and rhyolitic melts have been measured in laboratory experiments (e.g. Laumonier *et al.*, 2015; Guo *et al.*, 2016), they are strongly dependent on temperature, pressure, silica, sodium and water content, making extrapolation uncertain. The web-based SIGMELTS tool can, however, be used to predict melt and bulk resistivities for a wide range of compositions and conditions (Pommier & Le Trong, 2011). Importantly, petrological and geochemical characterisation of eruptive products can help inform interpretations of associated, subsurface conductors, but it is difficult to ascertain either whether their composition reflects the current magma/melt present in the plumbing system or whether melt pockets are interconnected. These large uncertainties in the resistivity of the melt and the requirement to make assumptions about its geometry mean direct inference of melt fraction is difficult. Nonetheless, information from laboratory studies, petrology and geochemistry aids interpreting resistivity

anomalies in magmatic regions (see review by Pommier, 2014).

Imaging ancient magma plumbing systems in seismic reflection data

Techniques

Over the last two decades, major advances have been made in imaging deep crustal melt beneath active volcanic terrains using P- and S-wave tomographic data (e.g. Yellowstone, Husen *et al.*, 2004; Mt. St. Helens, Lees, 2007; Hawaii, Okubo *et al.*, 1997). These data image deep (>7 km), often laterally extensive (up to 20 km), sill-like magma reservoirs (e.g. Paulatto *et al.*, 2012). However, like many geophysical and geodetic techniques applied to study active magma plumbing systems, these data typically lack the spatial resolution to resolve the detailed geometry of pathways transporting magma to the Earth's surface. Active source seismic reflection data, which have a spatial resolution of metres-to-decimetres down to depths of ~5 km, can provide unprecedented images of and insights into the

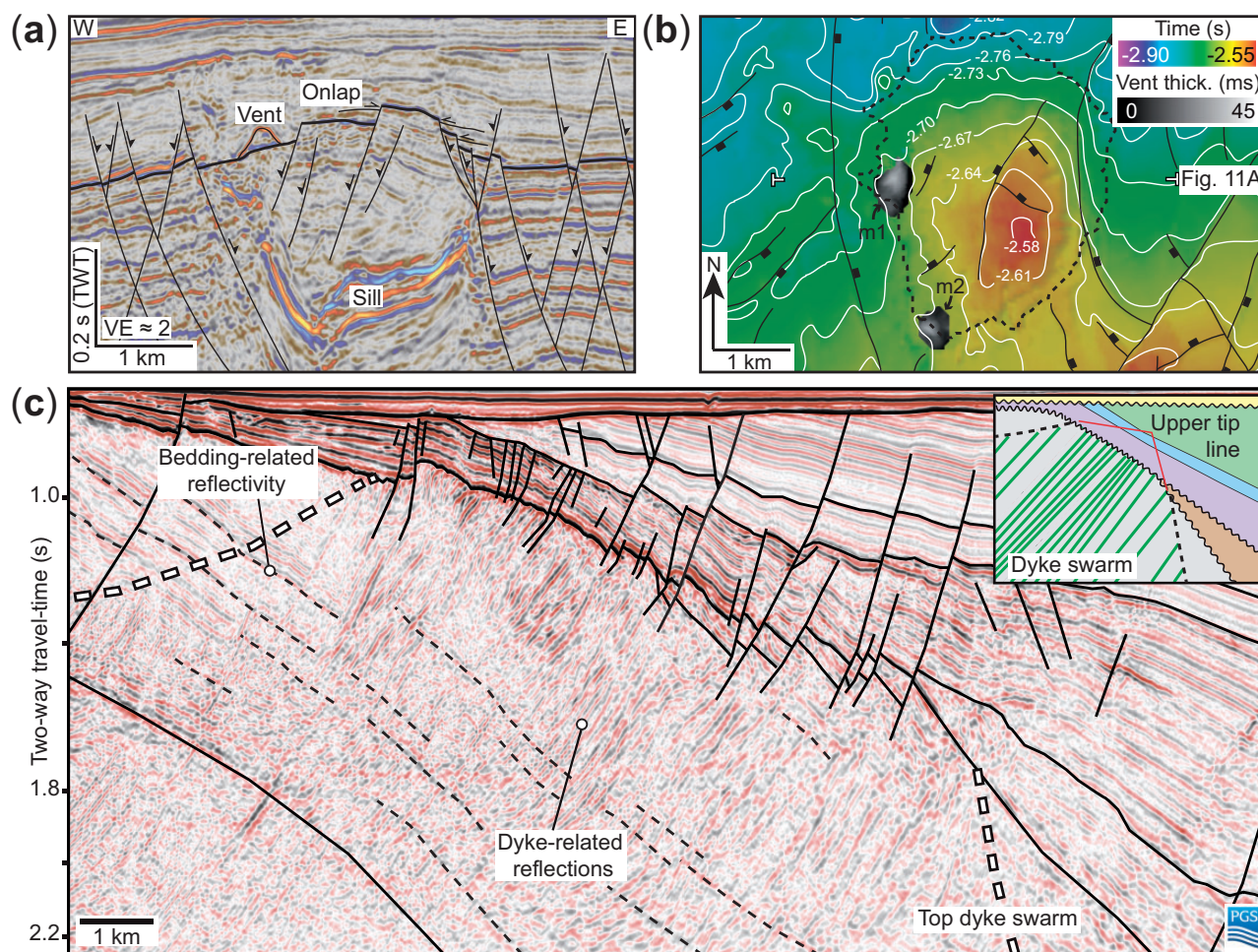


Fig. 11. (a) Interpreted seismic section from the Exmouth Sub-basin offshore NW Australia, which images a saucer-shaped sill that is overlain by a forced fold and feeds a small vent from its inclined limb (modified from Magee *et al.*, 2013a). See Fig. 11b for line location). (b) Time-structure map of the folded horizon (thick black line) in (a), highlighting fault traces and vent locations and thicknesses (modified from Magee *et al.*, 2013a). (c) Seismic section from the Farsund Basin, offshore southern Norway, which images part of a dyke-swarm that has been rotated by basin flexure post-emplacement (modified from Phillips *et al.*, 2017).

geometry and dynamics of shallow-level, crystallised, magma plumbing systems (e.g. Fig. 10) (e.g. Planke *et al.*, 2000; Smallwood & Maresh, 2002; Thomson & Hutton, 2004; Cartwright & Hansen, 2006; Jackson *et al.*, 2013; Magee *et al.*, 2016; Schofield *et al.*, 2017). Whilst seismic reflection data are traditionally used to find and assist in the production of hydrocarbons in sedimentary basins (Cartwright & Huuse, 2005), here we discuss and support its application to volcanological problems.

Acquiring active source seismic reflection data involves firing acoustic energy (i.e. seismic waves) into the subsurface and measuring the surface arrival times (i.e. the travel-time) of reflected energy. Processing of these arrival time data allows reconstruction of the location and geometry of the geological interfaces from which acoustic energy was reflected. Mafic intrusive igneous rocks are generally well-imaged in seismic reflection data because they typically have greater densities ($>2.5\text{ g/cm}^3$) and acoustic velocities (i.e. $>4000\text{ m/s}$) than encasing sedimentary strata; these differences result in a high acoustic impedance contrast, causing more seismic energy to be reflected back to the surface

compared to low acoustic impedance boundaries (Smallwood & Maresh, 2002; Brown, 2004). In contrast, silicic igneous rocks have similar acoustic properties to encasing sedimentary strata, meaning that felsic intrusions are rarely imaged in seismic reflection data (Mark *et al.*, 2018; Rabbel *et al.*, 2018). Furthermore, because reflection seismology relies on the return of acoustic energy to the surface, seismic reflection data favourably image mafic, sub-horizontal-to-moderately inclined intrusions (e.g. sills, inclined sheets, and laccoliths; Smallwood & Maresh, 2002; Jackson *et al.*, 2013; Magee *et al.*, 2016). Sub-vertical dykes reflect only a limited amount of acoustic energy back to the surface and are thus typically poorly imaged in seismic reflection data (e.g. Smallwood & Maresh, 2002; Planke *et al.*, 2005; Thomson, 2007; Wall *et al.*, 2010; Eide *et al.*, 2017b; Phillips *et al.*, 2017).

Observations

Sills and inclined sheets are commonly observed in seismic reflection data as laterally discontinuous, high-

amplitude reflections, which may cross-cut the host rock strata (Fig. 10) (e.g. Symonds *et al.*, 1998, Smallwood & Maresh, 2002; Planke *et al.*, 2005, Magee *et al.*, 2015). Many of the sills and inclined sheets imaged in seismic reflection data are, however, expressed as tuned reflection packages, whereby discrete reflections from the top and base contacts interfere on their return to the surface and cannot be distinguished (e.g. Figs 10 and 11a) (e.g. Smallwood & Maresh, 2002; Peron-Pinvidic *et al.*, 2010; Magee *et al.*, 2015; Eide *et al.*, 2017b; Rabbel *et al.*, 2018). Therefore, it is difficult to assess either intrusion thicknesses, or to detect whether imaged sills are composite bodies made of numerous, stacked, thin sheets. Either way, subtle vertical offsets and corresponding amplitude variations of sill reflections can often be mapped, defining linear structures that radiate out from either the central, deepest portions of sills or areas where underlying intrusions intersect the sill (e.g. Schofield *et al.*, 2012b; Magee *et al.*, 2014, 2016). These structures are interpreted to relate to magma flow indicators such as intrusive steps, broken bridges, and magma fingers (e.g. Schofield *et al.*, 2010, 2012a; Magee *et al.*, 2017b).

A recurring observation from seismic reflection-based studies of extinct and buried intrusive systems is that complexes of interconnected sills and inclined sheets, which may cover $>3 \times 10^6 \text{ km}^2$, can dominate magma plumbing systems (e.g. Fig. 10b) (e.g. Svensen *et al.*, 2012; Magee *et al.*, 2016). Importantly, where buried volcanic edifices are imaged in seismic reflection data, they rarely appear to be underlain by 'magma chambers' (i.e. a spheroidal or ellipsoidal body of now-crystallised magma). Instead, these imaged volcanoes commonly appear laterally offset from genetically related sills and/or laccoliths that are inferred to represent their feeder reservoirs (e.g. Fig. 10b) (Magee *et al.*, 2013b; McLean *et al.*, 2017). The geometry, location and connectivity of these intrusions, which can represent magma storage sites and conduits to the surface, are often heavily influenced by both the host rock structure and lithology (see review by Magee *et al.*, 2016). For example, magma may flow along pronounced discontinuities (e.g. bedding) or within specific stratigraphic units (e.g. coal) for considerable distances, occasionally climbing to higher stratigraphic levels by instigating deformation of the host rock or by exploiting pre-existing faults (e.g. Jackson *et al.*, 2013; Magee *et al.*, 2016; Schofield *et al.*, 2017; Eide *et al.*, 2017a). It is clear from seismic reflection data that shallow-level tabular intrusions are commonly accommodated by roof uplift to form a flat-topped or dome-shaped forced fold (e.g. Fig. 11a and b) (e.g. Trude *et al.*, 2003; Hansen & Cartwright, 2006; Jackson *et al.*, 2013; Magee *et al.*, 2013a). Moreover, if the age of reflections overlapping onto these intrusion-induced forced folds can be ascertained, the timing and to some extent the duration of magmatic activity can be determined (e.g. Trude *et al.*, 2003; Hansen & Cartwright, 2006; Magee *et al.*, 2014; Reeves *et al.*, 2018). Although most seismic-based

studies examine intrusions within sedimentary basins, saucer-shaped sills and laterally extensive sill-complexes emplaced into crystalline basement rock are also imaged (e.g. Ivanic *et al.*, 2013; McBride *et al.*, 2018). Lastly, seismic reflection data can also be used to image the internal structure of layered ultramafic–mafic intrusions (e.g. the Bushveld Layered Intrusion, Malehmir *et al.*, 2012) and, in some instances, identify dykes (e.g. Fig. 11c) (e.g. Wall *et al.*, 2010; Abdelmalak *et al.*, 2015; Bosworth *et al.*, 2015; Phillips *et al.*, 2017).

Implications and integration

Despite being limited in terms of their spatial resolution (typically a few tens of metres) and ability to image steeply dipping features (i.e. dykes), they provide unprecedented snapshots into the final 3D structure of magma plumbing systems. Beyond quantifying the structure and connectivity of magma plumbing systems, seismic-based studies have shown that: (i) magma flow patterns mapped across entire sill-complexes indicate they can transport melt from source to surface over great lateral ($>100 \text{ s km}$) and vertical distances (10s km), potentially without significant input from dykes (Fig. 10a) (e.g. Thomson & Hutton, 2004; Cartwright & Hansen, 2006; Magee *et al.*, 2014, 2016; Schofield *et al.*, 2017); and (ii) a variety of elastic and inelastic mechanisms can accommodate host rock deformation during magma emplacement, meaning that the location and size of ground deformation does not necessarily equal that of the forcing intrusion (e.g. Jackson *et al.*, 2013, Magee *et al.*, 2013a). Importantly, observations from seismic reflection data highlight that the lateral dimension should be considered when modelling the transit of magma in the crust, posing problems for the widely held and simple assumption that magma simply travels vertically from melt source to eruption site.

Seismic-based studies have also shown that direct comparison to active deformation structures can be informative. For example, through comparing mapped lava flows and structures associated with the Alu dome to similar features observed in seismic reflection data, Magee *et al.*, (2017a, 2017b) concluded that the shallow-level sill likely has a saucer-shaped, as opposed to the sill-like tabular morphology inferred from an episode of deformation measured using InSAR (Fig. 3c and d). Despite its benefits, it is important to remember that seismic reflection data typically reveal only the final geometry of the magma plumbing system. Thus there remains a challenge in using these data to understand areas where deformation captures potentially transient, active processes, rather than structures resulting from (multiple) periods of intrusion and cooling (Reeves *et al.*, 2018). One potential and exciting way forward is the development of Virtual Reflection Seismic Profiling, by which microseismicity at active volcanoes may be used to image magma reservoirs and subsurface structure in 4D (Kim *et al.*, 2017). Although challenges exist

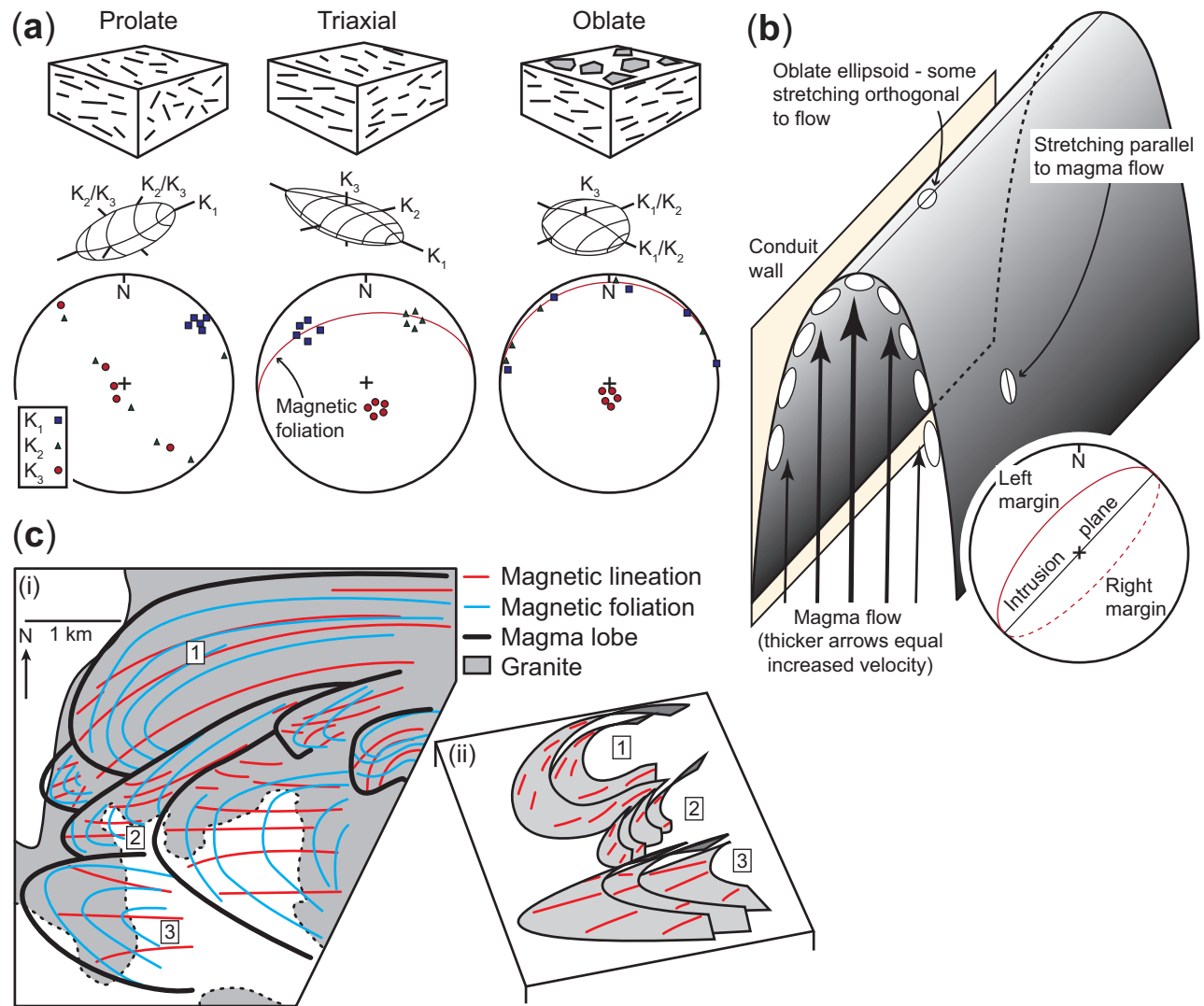


Fig. 12. (a) At the sample scale, all magnetic grains create a magnetic fabric. (i) Dominantly prolate fabric, where K_2 and K_3 are least certain and form a girdle. Only the magnetic lineation (K_1) can be confidently determined. (ii) When $K_1 > K_2 > K_3$, both a foliation (K_1 – K_2) and a lineation (K_1) may be discerned, defining a triaxial fabric. (iii) When K_1 and K_2 are equally uncertain and form a girdle, K_3 is perpendicular to a foliation. (b) Schematic representation of how magma flow within a planar sheet intrusion can produce imbricated magnetic fabrics at its margins, the closure of which define the magma flow direction (after Féménias *et al.*, 2004). (c) AMS data and interpretations from part of the Trawenagh Bay Granite, NW Ireland (adapted from Stevenson *et al.*, 2007a). (i) AMS foliation traces are shown in blue and lineation traces in red. Lobes were defined in this intrusion based on foliations curving around a lineation axis. In some lobes, the magnetic lineation trend was parallel to this axis, whilst in others they tended to splay or converge down flow. (ii) 3D sketch showing the geometry of three of the lobes (numbered in part i).

in dataset integration, the imaging power afforded by modern seismic reflection data thus presents a unique opportunity to further unite field-, petrological-, geochemical- and other geophysical-based analyses within more realistic structural frameworks (e.g. Figs 3, 11a and b). In our view, however, seismic reflection data are under-utilised in igneous research, remaining an unfamiliar technique to many Earth Scientists in the volcanic and magmatic community.

Rock magnetism

Technique

Whilst seismic reflection data provide unique 3D images of ancient magma plumbing systems, which

can be used to infer magma flow patterns across entire intrusion networks, we commonly lack sufficient data (e.g. boreholes) to test seismic-based hypotheses. Therefore, it is critical to compare seismic interpretations to field analogues where magma flow patterns, emplacement mechanics, and intrusion evolution can be investigated via other techniques. In this section, we examine how rock magnetic analyses can be used to systematically study magnetic mineralogy and petrofabrics, thereby illuminating the structure and history of igneous intrusions.

There are two principal types of rock magnetic study: magnetic remanence and magnetic susceptibility, where the total magnetisation (M) of a rock is the sum of the magnetic remanence (M_{rem}) and the induced

magnetisation (M_{ind}), which is a product of the susceptibility (K) and applied field strength (H) (Dunlop & Özdemir, 2001). Remanence carries a geological record of the various magnetisations acquired over time and is central to palaeomagnetic studies. However, we focus on magnetic fabric analysis, which relies on measurements of the anisotropy of magnetic susceptibility (AMS). The AMS signal of a rock carries information from all constituent grains. Although mineral phases that have a paramagnetic behaviour (i.e. they are weakly attracted to externally applied magnetic fields) volumetrically dominate most igneous rocks (e.g. olivine, clinopyroxene, biotite), ferromagnetic mineral phases (e.g. titanomagnetite) are highly susceptible to magnetization and, therefore, tend to dominate K (e.g. Dunlop & Özdemir, 2001; Biedermann *et al.*, 2014). Magnetic fabrics, therefore, typically reflect the preferential orientation of crystallographic axes (i.e. crystalline anisotropy), the shape-preferred orientation of individual crystals (i.e. shape anisotropy) and/or the alignment of closely spaced crystals (i.e. distribution anisotropy) of Fe-bearing silicate and oxide phases (e.g. Voigt & Kinoshita, 1907; Graham, 1954; Hrouda, 1982; Tarling & Hrouda, 1993; Dunlop & Özdemir, 2001). The principal axes of the magnetic fabrics measured by AMS can thus be related to the orientation, shape and distribution of individual grains (i.e. the petrofabric) (e.g. Fig. 12a).

Regardless of whether mineral phases crystallise early or late, whereby their orientation and distribution typically mimics the earlier silicate framework, it is expected that the initial petrofabric developed in intrusive rocks will likely be sensitive to alignment of crystals during primary magma flow. However, it is also critical to recognise that later magmatic processes (e.g. convection and melt extraction) and syn- or post-emplacement tectonic deformation can modify or overprint primary magma flow fabrics during intrusion, solidification (i.e. mush development), or sub-solidus conditions (e.g. Borradaile & Henry, 1997; Bouchez, 1997; O'Driscoll *et al.*, 2015; Kavanagh *et al.*, 2018). Whilst anisotropy of magnetic susceptibility (AMS) can thus rapidly and accurately detect weak or subtle mineral alignments within igneous intrusions, which may be attributable to magmatic and/or tectonic processes, evaluating the origin and evolution of petrofabric development requires additional information (e.g. Borradaile & Henry, 1997; Bouchez, 1997). For example, shape-preferred orientation analyses and comparison to visible flow indicators (e.g. intrusive steps and bridge structures) allow magma flow axes and directions that have been inferred from magnetic fabrics to be verified (e.g. Launeau & Cruden, 1998; Callot *et al.*, 2001; Magee *et al.*, 2012b). For a useful précis of AMS-related magnetic theory in igneous rocks, the reader is referred to early works by Balsley & Buddington (1960) and Khan (1962), and more recent summaries provided by Martín-Hernández *et al.*, (2004), O'Driscoll *et al.*, (2008), and O'Driscoll *et al.*, (2015).

The principle behind AMS relies on the measurement of the bulk susceptibility (K_m) of a single sample in different orientations to determine the susceptibility anisotropy tensor, which relates the induced magnetisation (M_{ind}) to the applied field (H) in three dimensions (Tarling & Hrouda, 1993). The orientation and magnitude of the eigenvectors and eigenvalues of this tensor define an ellipsoid with three principal axes; the long axis of the ellipsoid, K_1 , defines the magnetic lineation and the short axis, K_3 , defines the normal (i.e. the pole) to the magnetic foliation plane (K_1 – K_2 ; Fig. 12a) (Stacey *et al.*, 1960; Khan, 1962; Tarling & Hrouda, 1993). In order to interpret magnetic fabrics, it is important to determine the mineralogy of the phases carrying the magnetic signal because the composition, grain size, and distribution of magnetically dominant minerals (e.g. titanomagnetite) can control fabric orientation (e.g. Hargraves *et al.*, 1991; Stephenson, 1994; Dunlop & Özdemir, 2001). In addition to primary crystallographic and textural controls on magnetic fabrics, subsequent oxidation of remaining melt and secondary hydrothermal alteration can affect the magnetic mineralogy and, thereby, the AMS signal (e.g. Trindade *et al.*, 2001; Stevenson *et al.*, 2007a). A variety of rock magnetic experiments are thus required to determine the magnetic mineralogy. The most widely used method involves measuring susceptibility, and thereby behaviour of magnetic materials, at varying temperatures ranging from -200°C to 700°C (i.e. thermomagnetic analysis *sensu* Orlický, 1990; Hrouda *et al.*, 1997). For example, paramagnetic materials (e.g. biotite) follow the Curie-Weiss law, whereby their susceptibility drops hyperbolically with increasing temperature. In contrast, the thermomagnetic curve of ferromagnetic materials (e.g. titanomagnetite) displays little change in susceptibility with temperature, apart from when characteristic crystallographic transitions occur (e.g. the Curie point for pure magnetite at $\sim 580^\circ\text{C}$, Petrovský & Kapička, 2006). To determine the grain size of the ferromagnetic fraction in the magnetic susceptibility signal, the hysteretic property of the magnetisation is important (Dunlop, 2002). Other rock magnetic experiments (e.g. anisotropy of anhysteretic remanent magnetism (AARM) can be conducted to further isolate the relative importance of different paramagnetic and ferromagnetic phases (e.g. McCabe *et al.*, 1985; Richter & van der Pluijm, 1994; Kelso *et al.*, 2002).

Observations

Having established the magnetic mineralogy, AMS fabrics can be interpreted. Even in weakly anisotropic igneous rocks (i.e. visually isotropic), particularly sheet intrusions, it is now accepted that the magnetic lineation and foliation can provide information on magma migration (e.g. flow direction) or regional and local strain (e.g. Hrouda, 1982; Knight & Walker, 1988; Rochette *et al.*, 1992; Bouchez, 1997; Tauxe, 1998; Callot *et al.*, 2001; Féménias *et al.*, 2004; Magee *et al.*, 2012b).

For example, comparisons to other indicators of magma flow (e.g. intrusive steps and visible mineral alignments) in sheet intrusions have shown that magnetic lineations commonly parallel the magma flow (e.g. Knight & Walker, 1988; Cruden & Launeau, 1994; Callot *et al.*, 2001; Magee *et al.*, 2012b), whilst imbrication of elongate crystals induced by simple shear at intrusion margins define the sense of magma flow (Fig. 12b) (e.g. Knight & Walker, 1988; Hargraves *et al.*, 1991; Stephenson, 1994; Geoffroy *et al.*, 2002; Féménias *et al.*, 2004). Alternatively, contact-parallel magnetic fabrics generated during the formation and inflation of magma lobes can be used to determine flow and emplacement dynamics, even if other evidence for the presence of magma lobes is lacking (e.g. Fig. 12c) (Cruden *et al.*, 1999; Stevenson *et al.*, 2007a; Magee *et al.*, 2012a). Identifying changes in fabric orientation within or between individual sheet intrusions is also important because these variations suggest that deformation, imparted by either the emplacement of adjacent magma bodies or tectonic processes, did not significantly modify magma emplacement fabrics (e.g. Clemente *et al.*, 2007).

Post solidification textural modification and the possibility of overlap in tectonic and magmatic strain fields during protracted emplacement is a particular complication when studying granitoid and gabbroic plutons (e.g. Mamtani *et al.*, 2013; O'Driscoll *et al.*, 2015; Cheadle & Gee *et al.*, 2017). In fact, most early studies of granitoid emplacement using AMS, in conjunction with many other structural analysis tools, concluded that tectonic strain was the main source of subtle fabrics (e.g. Brun *et al.*, 1990; Bouchez, 1997; de Saint Blanquat & Tikoff, 1997; Neves *et al.*, 2003; Mamtani & Greiling, 2005). Although primary magma flow fabrics in granitic and gabbroic plutons may thus be overprinted, the magnetic fabrics characterised by AMS can still provide fundamental insights into emplacement mechanics (e.g. Stevenson *et al.*, 2007a; Petronis *et al.*, 2012) and magma/mush evolution (e.g. formation of layering; O'Driscoll *et al.*, 2015).

Implications and integration

Overall, AMS has provided vital magma flow and evolution information that has helped to understand mafic and silicic magma plumbing systems (e.g. Knight & Walker, 1988; Ernst & Baragar, 1992; Glen *et al.*, 1997; Aubourg *et al.*, 2008; Petronis *et al.*, 2013, 2015). Critical insights emanating from these AMS studies have revealed that: (i) flow trajectories predicted by classic emplacement models (e.g. for ring dykes and cone sheets) are not always consistent with measured AMS fabrics and supporting data, which thereby call into question the application of such models (e.g. Stevenson *et al.*, 2007b; Magee *et al.*, 2012b); (ii) lateral magma flow is recorded in many shallow, planar intrusions associated with volcanic magma plumbing systems (e.g. Ernst & Baragar, 1992; Cruden & Launeau, 1994;

Cruden *et al.*, 1999; Herrero-Bervera *et al.*, 2001; Magee *et al.*, 2012b; Petronis *et al.*, 2013, 2015); and (iii) plutons, particularly those with a granitic composition, commonly consist of incrementally emplaced magma pulses that often develop lobate geometries (e.g. Fig. 12c) (e.g. Stevenson *et al.*, 2007a). Analysing AMS fabrics from layered mafic–ultramafic intrusions can also provide evidence for magma reservoir processes, including crystal settling, or post-cumulus modification of crystal mushes (O'Driscoll *et al.*, 2008, 2015). Importantly, AMS and related analyses provide robust, testable, and repeatable methods to constrain subtle shape and crystallographic orientations of crystals in igneous rocks. Rock magnetic instrumentation technology continues to advance with better automation of measurement protocols, sensitivity of measurements, and a greater ability to unravel contributors to the AMS signal. The direction and scope of these developments are improving the holistic integration of AMS with other structural, microstructural, geophysical, petrological and geochemical techniques, promising to advance our understanding of magmatism and crustal evolution.

Future advances

Our understanding of magma plumbing system structure and evolution has been significantly enhanced by the geophysical techniques described above. We have demonstrated that there is scope for advancement within individual methodologies and through the integration of different techniques, particularly involving the synthesis of geophysical, petrological, and geochemical data. In this section, we discuss two new techniques that will potentially revolutionize our understanding of magma plumbing systems. We also briefly discuss how integration of geophysical data with numerical modelling can enhance our knowledge of reservoir construction and evolution.

Full-waveform inversion

Technique

We have demonstrated that seismic reflection data can provide unique insight into the 3D structure of magma plumbing systems (e.g. see review by Magee *et al.*, 2016). In addition to using seismic reflection data to image the subsurface, we can also invert the measured travel-times of reflected acoustic energy to model subsurface P-wave velocities. Full-waveform inversion (FWI) is a rapidly developing technology using active source seismic data to generate models that reproduce both the travel-times and full waveform of the arriving wavefield, thereby matching observed seismic data (Tarantola, 1984). Because FWI considers the full wavefield, as opposed to conventional techniques that only model travel-times, it is a technique capable of recovering high-resolution models of subsurface P-wave velocities and other physical properties (Warner *et al.*, 2013; Routh *et al.*, 2017). The FWI technique begins with a best-guess starting velocity model for the subsurface

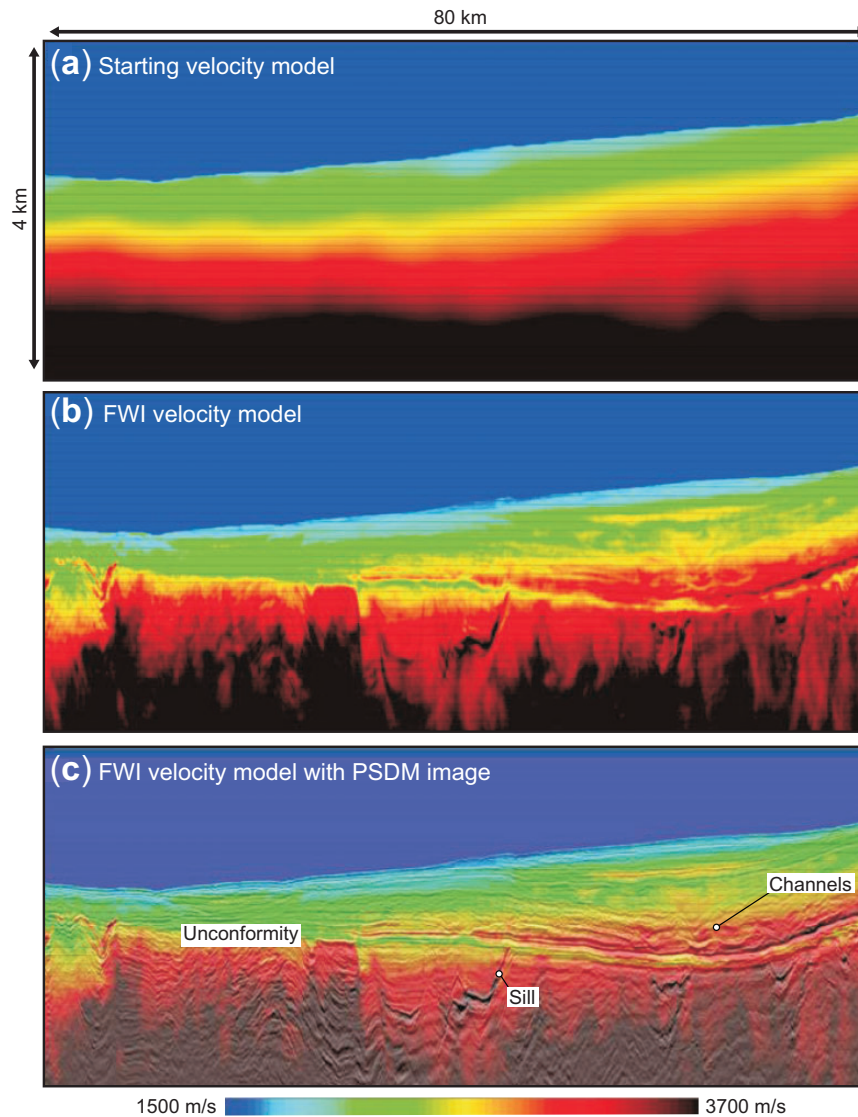


Fig. 13. (a) Starting model derived from smoothed, pre-stack, time-migrated (PSTM) stacking velocities. (b) Final 2D FWI-derived velocity model obtained using 10 km streamer data and inversion frequencies of between 2.5 and 24 Hz. (c) FWI velocity model overlain by the 2D pre-stack, depth-migrated (PSDM) section. Strong irregular reflections in the lower half of the section are from basaltic intrusions, which appear as high-velocity anomalies in the FWI velocity model. Both the FWI velocity model and the PSDM pick out a major unconformity and show shallow channels in the upper parts of the section (redrawn from Kalinicheva *et al.*, 2017).

geology, which is then iteratively updated using a local linearised inversion until the observed seismic data are matched (Virieux & Operto, 2009). FWI is much more computationally expensive than travel-time tomography, as a full-physics implementation of the wave equation is required to generate the predicted seismic data at all energy source and receiver locations for each iteration (Routh *et al.*, 2017). FWI, however, has the advantage of being able to resolve much finer-scale structure than conventional techniques.

Observations

To date, 3D FWI has principally been applied within the petroleum sector to obtain high-resolution velocity models that can be used to improve depth-migrated

(i.e. travel-time is converted to depth in metres) reflection images of petroleum reservoirs and their overburden (Sirgue *et al.*, 2010; Vigh *et al.*, 2010; Kapoor *et al.*, 2013; Warner *et al.*, 2013; Routh *et al.*, 2017). FWI can also produce interpretable, quantitative models of the physical properties of rocks in the subsurface that can be related directly to compaction, permeability, and overpressure as measured in subsurface boreholes (Lazaratos *et al.*, 2011; Mancini *et al.*, 2015). Of relevance here, is that mafic intrusions, which appear as high-amplitude reflections in seismic reflection data (Figs 10 and 11a), are recovered as high-velocity features in FWI velocity models (Fig. 13) (Mancini *et al.*, 2015; Kalinicheva *et al.*, 2017). For example, successful application of 3D FWI to a marine ocean bottom seismometer dataset acquired across the Endeavour

segment of the Juan de Fuca Ridge led to generation of a velocity model that had a resolution up to four times greater than travel-time tomography (Morgan *et al.*, 2016). Within this new, high-resolution velocity model, several velocity anomalies were identified and interpreted to indicate localised magma recharge of the axial reservoir, induced seismogenic cracking, and increased permeability (Arnoux *et al.*, 2017).

Implications and integration

Active magma plumbing systems comprise a complex network of interconnected conduits and reservoirs with variable geometries and sizes, which likely contain magmatic vapour-rich, liquid-rich and mush zones (Christopher *et al.*, 2015). These intrusions will all be associated with reduced P-wave velocities, which could be resolved in high-resolution, 3D FWI datasets as supported by successes in the fine-scale imaging of: (i) low-velocity gas clouds (Warner *et al.*, 2013); (ii) axial reservoirs at an oceanic spreading centre (Arnoux *et al.*, 2017); (iii) relatively narrow, low-velocity fault zones within an antiform (Morgan *et al.*, 2013); and (iv) a subduction zone using 2D FWI (Kamei *et al.*, 2017). A suite of synthetic tests has been performed to investigate whether 3D FWI could be applied to better understand magma plumbing systems (Morgan *et al.*, 2013). These tests indicate that it is possible to recover high-resolution models of P-wave velocity beneath volcanoes, which can then be used to better determine where magma/mush is stored beneath the surface. In particular, these synthetic tests suggest that FWI could be used to: (i) distinguish between continuous zones of mush and individual magma reservoirs; (ii) image sills and conduits of magma and/or fluids that are a few 10s metres across (Fig. 13); and (iii) image the deeper (lower crustal) part of the magma system. Therefore, we consider that 3D FWI affords an unprecedented opportunity to obtain high-resolution images of actual magma plumbing systems beneath active volcanoes. To this end, the ongoing PROTEUS (Plumbing Reservoirs of The Earth Under Santorini) experiment was specifically designed to use 3D FWI to investigate the Santorini magma plumbing system (Hoofst *et al.*, 2016).

Unmanned aerial vehicle photogrammetry

Technique

Despite major advances in satellite-based remote sensing systems and aeromagnetic surveys, very high-resolution (i.e. mm–cm scale ground sampling distance) imagery of dykes and other igneous intrusions has been limited to low altitude aerial photography. This in turn has created a critical scale gap in intrusion studies, which range from <1 mm at thin section scale to the metres to 100s of metres scale provided by outcrop analysis, conventional remote sensing, and geophysical data. Fortunately, the emerging capability of unmanned aerial vehicle (UAV) photogrammetry fills this gap (e.g. Eisenbeiss, 2009; Westoby *et al.*, 2012; Bemis *et al.*,

2014; Eide *et al.*, 2017a). It is also noteworthy that several studies have demonstrated that digital photogrammetry can deliver high quality datasets with accuracies similar to more established laser scanning techniques (e.g. Leberl *et al.*, 2010; Hodgetts, 2013; Thiele *et al.*, 2015).

The basic setup required to carry out UAV (or drone) photogrammetry is commercially available and relatively inexpensive, comprising a fixed wing or rotary wing UAV, a digital camera, and access to a suitable digital photogrammetry software package (e.g. Agisoft Photoscan Pro, Pix4Dmapper Pro, VisualSFM). UAV photogrammetry combines a simple and cost-effective method to acquire geospatially referenced, overlapping digital aerial images, from which structure-from-motion algorithms can generate spatial 3D datasets (Bemis *et al.*, 2014; Vollgger & Cruden, 2016). Such an approach can be used for high spatial resolution mapping of all types of well-exposed igneous intrusions. The resulting data greatly enhance the effectiveness of traditional field mapping, particularly the characterisation of contact relationships and internal and external structure (e.g. fractures, fabrics, and phase distributions) of intrusive rocks, complementing AMS and petrological analyses.

Observations

A photogrammetric workflow was applied to examine a swarm of 5 cm to 1 m wide Palaeogene dolerite and dacite dykes exposed on coastal outcrops at Bingie Bingie Point, SE Australia (Fig. 14). The orthophotograph of the entire wave-cut platform shows the distribution of the Palaeogene dolerite and dacite dykes and their Devonian host rock lithologies, including a prominent moderately NE-dipping aplite dyke (Fig. 14a). Linear ENE–WSW terrain features pick out the traces of dyke-parallel joints (Fig. 14a). The Palaeogene dykes trend 063° parallel to a major set of joints in the country rock that likely formed contemporaneously with syn-dyking extension (Fig. 14b). Subsidiary joint sets trend NNW–SSE, sub-perpendicular to the Palaeogene dykes, N–S and E–W (Fig. 14b). The Palaeogene dykes display considerable structural complexity such as bridge structures, intrusive steps and apophyses (Fig. 14c). Where present, the steps mostly occur where dykes cross country rock contacts (e.g. the aplite–tonalite contact in the NE; Fig. 14c).

Implications and integration

Data such as the orthophotograph collected at Bingie Bingie Point indicate that high-resolution structural and lithological mapping and measurement can be carried out much more rapidly than by traditional survey methods (e.g. plane table or grid mapping). However, the use of conventional RGB cameras restricts the resulting image data to reflected visible light. Future applications will include the deployment of multispectral and hyperspectral sensors (infrared to short wave infrared to thermal infrared) as well as potential field geophysical or

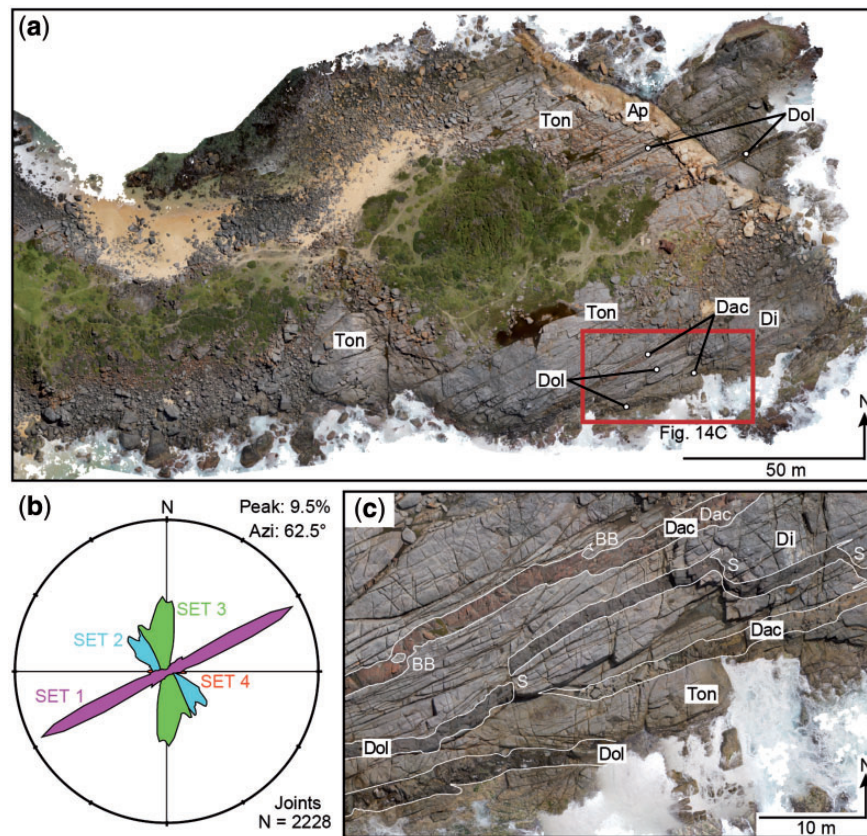


Fig. 14. (a) UAV orthophotograph of the wave cut platform at Bingie Point, NSW, Australia showing the distribution of Palaeogene dolerite (Dol) and dacite (Dac) dykes within Devonian tonalite (Ton), diorite (Di), and aplite (Ap) host rocks. (b) Circular histogram of joint sets measured in the Devonian rocks from the orthophotograph; the dominant (purple) set is parallel to and likely contemporaneous with the Palaeogene dykes. (c) Annotated close-up image highlighting dykes and structural features. The northern dacite dyke shows two broken bridge (BB) structures, whilst the central dolerite dyke displays prominent step structures (S). Narrow apophyses are also associated with the broken bridges and steps.

geodetic instruments (e.g. Sparks *et al.*, 2012). A further challenge for UAV applications in many countries concerns the regulatory framework around the use of drones for research. The global trend is moving to require non-recreational UAV operators to have remotely piloted aircraft licences and for the associated organisation to be certified for UAV operations. Innovations in sensor types and design, attachment of geophysical instruments, machine learning, and integration with complementary techniques such as AMS will open up new avenues for UAV applications in the study of magma plumbing systems.

Numerical modelling of magma reservoir processes constrained by geophysical data

Geophysical imaging of both active and ancient magma plumbing systems is delivering new insights into the 3D geometry of magma reservoirs, the timing and rates of melt and magma transport, the pathways followed by magmas as they ascend through the crust, and typical stored melt fractions in mushes. These data can be used to constrain and calibrate numerical models of reservoir processes. Numerical models are used ubiquitously to understand and predict the behaviour of other

subsurface crustal reservoirs, such as hydrocarbon reservoirs, groundwater resources, and targets for geological CO₂ storage (e.g. Chen *et al.*, 2003; Class *et al.*, 2009; Dean & Chen, 2011). However, there has been relatively little focus to date on developing numerical models for magma/mush reservoirs. Yet such models can integrate across different data sources and types, provide quantitative estimates of rates, volumes and timescales, and provide a framework for data interpretation. For example, numerical modelling of heat transfer within the plumbing system at Okmok Volcano in Alaska, which was informed by analytical models of geodetic data and estimated magma compositions of erupted material, allowed estimation of the role magma injection, crystallisation and degassing processes had on volume changes over time (Caricchi *et al.*, 2014). Numerical thermal modelling has also helped interpret seismic data from the Soufrière Hills Volcano, Montserrat, suggesting a higher melt fraction in the underlying magma reservoir than was inferred from seismic data alone (Paulatto *et al.*, 2012). More recent numerical models focus on crystal mushes, evaluating melt transport and reaction at low melt fractions, and these show that temperature and melt fraction in mushes can be decoupled; i.e. maximum temperature

occurs close to the centre of the reservoir, but maximum melt fraction occurs close to the top (Solano *et al.*, 2012). This decoupling impacts how seismic velocities and electrical conductivities will be modified within the mush (Solano *et al.*, 2012). Other numerical models show the important role played by exsolution, crystallisation, and the viscoelastic response of the crust in driving magma mobilisation in and eruption from shallow reservoirs (e.g. Degruyter & Huber, 2014; Parmigiani *et al.*, 2016), as well as providing insights into the mixing mechanisms of melt and crystals in mushes (Bergantz *et al.*, 2015). However, most models to date have a lower dimensionality (zero dimension box models, or one/two dimensions) and capture only a small subset of the key physical and chemical processes that are likely to occur in crustal magma reservoirs or crystal mushes. Moreover, few studies have integrated modelling with geophysical data (cf. Gutierrez *et al.*, 2013). This is in marked contrast to the 3D modelling routinely undertaken of other crustal reservoirs (e.g. hydrocarbon reservoirs), which is commonly integrated with and delimited by geophysical data. There is thus significant scope for improved, and integrated, numerical modelling of crustal magma reservoirs.

CONCLUSIONS

Determining the structure of magma plumbing systems is critical to understanding where melt and magma are stored in the crust, which can influence the location of volcanic eruptions and economic ore deposits, providing an important framework for interpreting the physical and chemical evolution of magma from petrological and geochemical datasets. Geophysical techniques have revealed unique insights into the architecture of active and ancient magma plumbing systems, which when integrated with traditional structural, petrological and geochemical results has yielded exciting advances in our understanding of magmatic processes. However, divisions between communities applying these methodologies still exist, contributing to diverging views on the nature of magma plumbing systems. To help promote collaboration, we have reviewed a range of geophysical techniques and discussed how they could be integrated with structural, petrological and geochemical datasets to answer outstanding questions in the volcanological community. In particular, we demonstrate how a range of geophysical techniques can be applied to track melt migration in near real-time, map entire intrusion networks in 3D, examine magma emplacement mechanics, and understand the evolution of crystal mushes. For example, Interferometric Synthetic Aperture Radar (InSAR) allows measurement of the development of active magmatic systems by successive intrusion, the vertical and lateral movements of magma, and the relationship between magma plumbing system dynamics and eruption. Seismicity beneath volcanoes can, when the magma interacts dynamically with the host rock, illuminate in high-resolution the time and

spatial scales of the motion of magma and hydrothermal fluids. Seismic imaging of magma plumbing systems allows the spatial distribution of melt and magma to be determined, whilst the inclusion of anisotropy within seismic techniques even allows sub-seismic wavelength features to be identified. Gravimetry can characterise the distribution and redistribution of mass (e.g. magma) in the subsurface over high spatial and temporal resolutions, helping to reveal the structure and composition of magma plumbing systems and the source(s) of volcano deformation. Electromagnetic methods, particularly magnetotellurics, can identify fluids within magmatic systems (e.g. melt, magma, and hydrothermal fluids). Seismic reflection data provide unprecedented 3D images of ancient magma plumbing systems and have revealed that laterally extensive, interconnected networks of sills and inclined sheets can play a pivotal role in transporting magma through the crust to eruption sites potentially located >100 km away from the melt source. Rock magnetics can provide fabric data pertaining to magma flow, deformation or crystallisation. All these methodologies discussed have provided unique insights into the structure of igneous intrusions and, through integration with petrological and geochemical datasets, are beginning to help unravel the entire evolution of magma plumbing systems. In addition to the ongoing application and advancement of these geophysical techniques, emerging methodologies look set to radically improve our understanding of magma plumbing systems. For example, full-waveform inversion can image and characterise physical properties across plumbing systems at an unprecedented resolution, whereas unmanned aerial vehicle photogrammetry provides a tool for high spatial resolution of outcrop scale intrusions that bridges the scale gap between seismic reflection data and traditional mapping of magma plumbing systems. The geophysical techniques discussed also provide critical constraints on input parameters for numerical modelling. Overall, we consider that the future of magma plumbing system studies will benefit greatly from the synthesis of geophysics and more traditional petrological and geochemical approaches.

ACKNOWLEDGEMENTS

We would like to thank Marian Holness for inviting us to put together this review article and for editorial handling. We are very grateful to Juliet Biggs, Martyn Unsworth, John Bartley, and Magnús Gudmundsson for their extensive and constructive reviews.

FUNDING

CM is funded by an Imperial College Research Fellowship at Imperial College London. SKE is funded by an Early Career Fellowship from the Leverhulme Trust. KAW is funded by Natural Environment Research Council grant NE/L013932/1.

REFERENCES

- Abdelmalak, M. M., Andersen, T. B., Planke, S., Faleide, J. I., Corfu, F., Tegner, C., Shephard, G. E., Zastrozhnov, D. & Myklebust, R. (2015). The ocean-continent transition in the mid-Norwegian margin: insight from seismic data and an onshore Caledonian field analogue. *Geology* **43**, 1011–1014.
- Aizawa, K., Kanda, W., Ogawa, Y., Iguchi, M., Yokoo, A., Yakiwara, H. & Sugano, T. (2011). Temporal changes in electrical resistivity at Sakurajima volcano from continuous magnetotelluric observations. *Journal of Volcanology and Geothermal Research* **199**, 165–175.
- Annen, C. (2011). Implications of incremental emplacement of magma bodies for magma differentiation, thermal aureole dimensions and plutonism–volcanism relationships. *Tectonophysics* **500**, 3–10.
- Annen, C., Blundy, J. D. & Sparks, R. S. J. (2006). The genesis of intermediate and silicic magmas in deep crustal hot zones. *Journal of Petrology* **47**, 505–539.
- Annen, C., Blundy, J. D., Leuthold, J. & Sparks, R. S. J. (2015). Construction and evolution of igneous bodies: towards an integrated perspective of crustal magmatism. *Lithos* **230**, 206–221.
- Arnoux, G. M., Toomey, D., Hooft, E., Wilcock, W., Morgan, J., Warner, M. & VanderBeek, B. (2017). Seismic evidence that black smoker heat flux is rate-limited by crustal permeability. *Geophysical Research Letters* **44**, 1687–1695.
- Aubourg, C., Tshoso, G., le Gall, B., Bertrand, H., Tiercelin, J.-J., Kampunzu, A. B., Dyment, J. & Modisi, M. (2008). Magma flow revealed by magnetic fabric in the Okavango giant dyke swarm, Karoo igneous province, northern Botswana. *Journal of Volcanology and Geothermal Research* **170**, 247–261.
- Baba, K., Chave, A. D., Evans, R. L., Hirth, G. & Mackie, R. L. (2006). Mantle dynamics beneath the East Pacific Rise at 17°S: insights from the Mantle Electromagnetic and Tomography (MELT) experiment. *Journal of Geophysical Research: Solid Earth* **111**, B02101.
- Bagnardi, M., Amelung, F. & Poland, M. P. (2013). A new model for the growth of basaltic shields based on deformation of Fernandina volcano, Galápagos Islands. *Earth and Planetary Science Letters* **377–378**, 358–366.
- Bailey, R. C. (1970). Inversion of the geomagnetic induction problem. *Proceedings of the Royal Society* **315**, 185–194.
- Balsley, J. R. & Buddington, A. F. (1960). Magnetic susceptibility anisotropy and fabric of some Adirondack granites and orthogneisses. *American Journal of Science* **A258**, 6–20.
- Bannister, S., Reyners, M., Stuart, G. & Savage, M. (2007). Imaging the Hikurangi subduction zone, New Zealand, using teleseismic receiver functions: crustal fluids above the fore-arc mantle wedge. *Geophysical Journal International* **169**, 602–616.
- Battaglia, M. & Segall, P. (2004). The interpretation of gravity changes and crustal deformation in active volcanic areas. *Pure and Applied Geophysics* **161**, 1453–1467.
- Battaglia, M., Roberts, C. & Segall, P. (1999). Magma intrusion beneath Long Valley caldera confirmed by temporal changes in gravity. *Science* **285**, 2119–2122.
- Battaglia, M., Troise, C., Obrizzo, F., Pingue, F. & De Natale, G. (2006). Evidence for fluid migration as the source of deformation at Campi Flegrei caldera (Italy). *Geophysical Research Letters* **33**, L01307.
- Bemis, S. P., Micklethwaite, S., Turner, D., James, M. R., Akciz, S., Thiele, S. & Bangash, H. A. (2014). Ground-based and UAV-Based photogrammetry: a multi-scale, high-resolution mapping tool for structural geology and paleoseismology. *Journal of Structural Geology* **69**, 163–178.
- Bergantz, G. W., Schleicher, J. M. & Burgisser, A. (2015). Open-system dynamics and mixing in magma mushes. *Nature Geoscience* **8**, 793–796.
- Berryman, J. G. (1980). Long-wavelength propagation in composite elastic media II. Ellipsoidal inclusions. *The Journal of the Acoustical Society of America* **68**, 1820–1831.
- Bersi, M., Saibi, H. & Chabou, M. C. (2016). Aerogravity and remote sensing observations of an iron deposit in Gara Djebilet, southwestern Algeria. *Journal of African Earth Sciences* **116**, 134–150.
- Biedermann, A. R., Pettke, T., Reusser, E. & Hirt, A. M. (2014). Anisotropy of magnetic susceptibility in natural olivine single crystals. *Geochemistry, Geophysics, Geosystems* **15**, 3051–3065.
- Biggs, J. & Pritchard, M. E. (2017). Global volcano monitoring: what does it mean when volcanoes deform? *Elements* **13**, 17–22.
- Biggs, J., Anthony, E. Y. & Ebinger, C. J. (2009). Multiple inflation and deflation events at Kenyan volcanoes, East African Rift. *Geology* **37**, 979–982.
- Biggs, J., Bastow, I. D., Keir, D. & Lewi, E. (2011). Pulses of deformation reveal frequently recurring shallow magmatic activity beneath the Main Ethiopian Rift. *Geochemistry, Geophysics, Geosystems* **12**, Q0AB10.
- Biggs, J., Ebmeier, S. K., Aspinall, W. P., Lu, Z., Pritchard, M. E., Sparks, R. S. J. & Mather, T. A. (2014). Global link between deformation and volcanic eruption quantified by satellite imagery. *Nature Communications* **5**, 3471.
- Bonforte, A., Carbone, D., Greco, F. & Palano, M. (2007). Intrusive mechanism of the 2002 NE-rift eruption at Mt Etna (Italy) modelled using GPS and gravity data. *Geophysical Journal International* **169**, 339–347.
- Borradaile, G. J. & Henry, B. (1997). Tectonic applications of the magnetic susceptibility and its anisotropy. *Earth Science Reviews* **42**, 49–93.
- Bosworth, W., Stockli, D. F. & Helgeson, D. E. (2015). Integrated outcrop, 3D seismic, and geochronologic interpretation of Red Sea dike-related deformation in the Western Desert, Egypt—the role of the 23Ma Cairo “mini-plume”. *Journal of African Earth Sciences* **109**, 107–119.
- Bott, M. H. P. (1953). Negative gravity anomalies over acid “intrusions” and their relation to the structure of the Earth’s crust. *Geological Magazine* **90**, 257–267.
- Bouchez, J. L. (1997). Granite is never isotropic: an introduction to AMS studies of granitic rocks. In: Bouchez, J. L., Hutton, D. H. W. & Stephens, W. E. (eds) *Granite: From Segregation of Melt to Emplacement Fabrics* 8. Dordrecht: Kluwer Academic, pp. 95–112.
- Brown, A. R. (2004). *Interpretation of Three-Dimensional Seismic Data*. Society of Exploration Geophysicists and American Association of Petroleum Geologists, Tulsa.
- Brun, J. P., Gapais, D., Cogne, J. P., Ledru, P. & Vignerresse, J. L. (1990). The Flamanville granite (northwest France): an unequivocal example of a syntectonically expanding pluton. *Geological Journal* **25**, 271–286.
- Bucher, W. H. (1944). Discussion in Romberg, F., and Barnes, V. E. Correlation of gravity observations with the geology of the Smoothingiron granite mass, Llano County, Texas. *Geophysics* **9**, 79–93.
- Callot, J.-P., Geoffroy, L., Aubourg, C., Pozzi, J. & Mege, D. (2001). Magma flow directions of shallow dykes from the East Greenland volcanic margin inferred from magnetic fabric studies. *Tectonophysics* **335**, 313–329.
- Carbone, D., Poland, M. P., Diament, M. & Greco, F. (2017). The added value of time-variable microgravimetry to the understanding of how volcanoes work. *Earth-Science Reviews* **169**, 146–179.

- Carbone, D., Poland, M. P., Patrick, M. R. & Orr, T. R. (2013). Continuous gravity measurements reveal a low-density lava lake at Kilauea Volcano, Hawai'i. *Earth and Planetary Science Letters* **376**, 178–185.
- Caricchi, L., Biggs, J., Annen, C. & Ebmeier, S. (2014). The influence of cooling, crystallisation and re-melting on the interpretation of geodetic signals in volcanic systems. *Earth and Planetary Science Letters* **388**, 166–174.
- Cartwright, J. & Hansen, D. M. (2006). Magma transport through the crust via interconnected sill complexes. *Geology* **34**, 929–932.
- Cartwright, J. & Huuse, M. (2005). 3D seismic technology: the geological 'Hubble'. *Basin Research* **17**, 1–20.
- Cashman, K. V. & Sparks, R. S. J. (2013). How volcanoes work: a 25 year perspective. *Geological Society of America Bulletin* **125**, 664–690.
- Cashman, K. V., Sparks, R. S. J. & Blundy, J. D. (2017). Vertically extensive and unstable magmatic systems: a unified view of igneous processes. *Science* **355**, eaag3055.
- Chaussard, E. & Amelung, F. (2013). Depth of magma storage in volcanic arcs: testing the influence of regional parameters using a global data compilation. In *EGU General Assembly Conference Abstracts (Vol. 15)*, Copernicus, Gottingen.
- Cheadle, M. J. & Gee, J. S. (2017). Quantitative textural insights into the formation of gabbro in mafic intrusions. *Elements* **13**, 409–414.
- Chen, Y., Durlinsky, L. J., Gerritsen, M. & Wen, X. H. (2003). A coupled local-global upscaling approach for simulating flow in highly heterogeneous formations. *Advances in Water Resources* **26**, 1041–1060.
- Chmielowski, J., Zandt, G. & Haberland, C. (1999). The central Andean Altiplano-Puna magma body. *Geophysical Research Letters* **26**, 783–786.
- Chouet, B. & Matoza, R. S. (2013). A Multi-decadal view of seismic methods for detecting precursors of magma movement and eruption. *Journal of Volcanology and Geothermal Research* **252**, 108–175.
- Chouet, B., Dawson, P. & Martini, M. (2008). Shallow-conduit dynamics at Stromboli Volcano, Italy, imaged from waveform inversions. In: Lane, S. J. & Gilbert, J. S. (eds) *Fluid Motions in Volcanic Conduits: A Source of Seismic and Acoustic Signals*. Geological Society of London *Special Publication* **307**, 57–84.
- Christopher, T. E., Blundy, J. D., Cashman, K., Cole, P., Edmonds, M., Smith, P. J., Sparks, R. S. J. & Stinton, A. (2015). Crustal-scale degassing due to magma system destabilization and magma-gas decoupling at Soufrière Hills Volcano, Montserrat. *Geochemistry, Geophysics, Geosystems* **16**, 2797–2811.
- Class, H., Ebigo, A., Helmig, R., Dahle, H. K., Nordbotten, J. M., Celia, M. A., Audigane, P., Darcis, M., Ennis-King, J., Fan, Y., Flemisch, B., Gasda, S. E., Jin, M., Krug, S., Labregere, D., Naderi Beni, A., Pawar, R. J., Sbai, A., Thomas, S. G., Trenty, L. & Wei, L. (2009). A benchmark study on problems related to CO₂ storage in geologic formations. *Computational Geosciences* **13**, 409–434.
- Clemente, C. S., Amorós, E. B. & Crespo, M. G. (2007). Dike intrusion under shear stress: effects on magnetic and vesicle fabrics in dikes from rift zones of Tenerife (Canary Islands). *Journal of Structural Geology* **29**, 1931–1942.
- Comeau, M. J., Unsworth, M. J. & Cordell, D. (2016). New constraints on the magma distribution and composition beneath Volcán Uturuncu and the southern Bolivian Altiplano from magnetotelluric data. *Geosphere* **12**, 1391–1421.
- Comeau, M. J., Unsworth, M. J., Ticona, F. & Sunagua, M. (2015). Magnetotelluric images of magma distribution beneath Volcán Uturuncu, Bolivia: implications for magma dynamics. *Geology* **43**, 243–246.
- Constable, S. C., Parker, R. L. & Constable, C. G. (1987). Occam's inversion: a practical algorithm for generating smooth models from electromagnetic sounding data. *Geophysics* **52**, 289–300.
- Cruden, A. R. & Launeau, P. (1994). Structure, magnetic fabric and emplacement of the Archean Lebel Stock, SW Abitibi greenstone belt. *Journal of Structural Geology* **16**, 677–691.
- Cruden, A. R. & Weinberg, R. F. (2018). Mechanisms of magma transport and storage in the lower and Middle crust—magma segregation, ascent and emplacement. In: Burkhardt, S. (ed.) *Volcanic and Igneous Plumbing Systems*. Amsterdam: Elsevier.
- Cruden, A. R., Tobisch, O. T. & Launeau, P. (1999). Magnetic fabric evidence for conduit fed emplacement of a tabular granite: Dinkey Creek Pluton, central Sierra Nevada Batholith, California. *Journal of Geophysical Research: Solid Earth* **104**, 10511–10531.
- Currenti, G., Del Negro, C. & Ganci, G. (2007). Modelling of ground deformation and gravity fields using finite element method: an application to Etna volcano. *Geophysical Journal International* **169**, 775–786.
- Currenti, G., Napoli, R., Coco, A. & Privitera, E. (2017). Effects of hydrothermal unrest on stress and deformation: insights from numerical modeling and application to Vulcano Island (Italy). *Bulletin of Volcanology* **79**, 28.
- Dean, O. S. & Chen, Y. (2011). Recent progress on reservoir history matching: a review. *Computational Geosciences* **15**, 185–221.
- DeGruyter, W. & Huber, C. (2014). A model for eruption frequency of upper crustal silicic magma chambers. *Earth and Planetary Science Letters* **403**, 117–130.
- Delph, J. R., Ward, K. M., Zandt, G., Ducea, M. N. & Beck, S. L. (2017). Imaging a magma plumbing system from MASH zone to magma reservoir. *Earth and Planetary Science Letters* **457**, 313–324.
- del Potro, R., Diez, M., Blundy, J., Gottsmann, J. & Camacho, A. (2013). Diapiric ascent of silicic magma beneath the Bolivian Altiplano. *Geophysical Research Letters* **40**, 2044–2048.
- de Saint Blanquat, M. & Tikoff, B. (1997). Development of magmatic to solid-state fabrics during syntectonic emplacement of the Mono Creek Granite, Sierra Nevada Batholith. In: Bouchez, J. L., Hutton, D. & Stephens, W. E. (eds) *Granite: From Segregation of Melt to Emplacement Fabrics*. Netherlands: Springer, pp. 231–252.
- Desissa, M., Johnson, N. E., Whaler, K. A., Hautot, S., Fisseha, S. & Dawes, G. (2013). A mantle magma reservoir beneath an incipient mid-ocean ridge in Afar, Ethiopia. *Nature Geoscience* **6**, 861–865.
- Di Maio, R., Mauriello, P., Patella, D., Petrillo, Z., Piscitelli, S. & Siniscalchi, A. (1998). Electric and electromagnetic outline of the Mount Somma-Vesuvius structural setting. *Journal of Volcanology and Geothermal Research* **82**, 219–238.
- Dixon, T. H. (1991). An introduction to the Global Positioning System and some geological applications. *Reviews of Geophysics* **29**, 249–276.
- Drew, J., White, R. S., Tilmann, F. & Tarasewicz, J. (2013). Coalescence microseismic mapping. *Geophysical Journal International* **195**, 1773–1785.
- Dugda, M. T., Nyblade, A. A., Julia, J., Langston, C. A., Ammon, C. J. & Simiyu, S. (2005). Crustal structure in Ethiopia and Kenya from receiver function analysis: implications for rift development in eastern Africa. *Journal of Geophysical Research* **110**, B01303.

- Dunlop, D. J. (2002). Theory and application of the Day plot (Mrs/Ms versus Hcr/Hc) 1. Theoretical curves and tests using titanomagnetite data. *Journal of Geophysical Research* **107**, B3, 2056.
- Dunlop, D. J. & Özdemir, Ö. (2001). *Rock Magnetism: Fundamentals and Frontiers*, Vol. 3. Cambridge University Press, Cambridge.
- Dvorak, J. J. & Dzurisin, D. (1997). Volcano geodesy: the search for magma reservoirs and the formation of eruptive vents. *Reviews of Geophysics* **35**, 343–384.
- Dzurisin, D. (2006). *Volcano Deformation: New Geodetic Monitoring Techniques*. Springer Science & Business Media, Berlin.
- Eaton, G. P., Christiansen, R. L., Iyer, H. M., Pitt, A. D., Mabey, D. R., Blank, H. R., Zietz, I. & Gettings, M. E. (1975). Magma beneath yellowstone national park. *Science* **188**, 787.
- Ebinger, C., Keir, D., Ayele, A., Calais, E., Wright, T. J., Belachew, M., Hammond, J. O. S., Campbell, E. & Buck, W. R. (2008). Capturing magma intrusion and faulting processes during continental rupture: seismicity of the Dabbahu (Afar) rift. *Geophysical Journal International* **174**, 1138–1152.
- Ebinger, C. J., Keir, D., Bastow, I. D., Whaler, K., Hammond, J. O., Ayele, A., Miller, M. S., Tiberi, C. & Hautot, S. (2017). Crustal structure of active deformation zones in Africa: Implications for global crustal processes. *Tectonics* **36**, 3298–3332.
- Ebmeier, S. K., Biggs, J., Mather, T. A. & Amelung, F. (2013). On the lack of InSAR observations of magmatic deformation at Central American volcanoes. *Journal of Geophysical Research: Solid Earth* **118**, 2571–2585.
- Ebmeier, S. K., Elliott, J. R., Nocquet, J. M., Biggs, J., Mothes, P., Jarrín, P., Yépez, M., Aguaiza, S., Lundgren, P. & Samsonov, S. V. (2016). Shallow earthquake inhibits unrest near Chiles–Cerro Negro volcanoes, Ecuador–Colombian border. *Earth and Planetary Science Letters* **450**, 283–291.
- Ebmeier, S. K., Andrews, B. J., Araya, M. C., Arnold, D. W. D., Biggs, J., Cooper, C., Cottrell, E., Furtney, M., Hickey, J., Jay, J., Lloyd, R., Parker, A. L., Pritchard, M. E., Robertson, E., Venzke, E. & Williamson, J. L. (2018). Synthesis of global satellite observations of magmatic and volcanic deformation: implications for volcano monitoring & the lateral extent of magmatic domains. *Journal of Applied Volcanology* **7**, 2.
- Eide, C. H., Schofield, N., Jerram, D. A. & Howell, J. A. (2017a). Basin-scale architecture of deeply emplaced sill complexes: Jameson Land, East Greenland. *Journal of the Geological Society of London* **174**, 23–40.
- Eide, C. H., Schofield, N., Lecomte, I., Buckley, S. J. & Howell, J. A. (2017b). Seismic interpretation of sill complexes in sedimentary basins: implications for the sub-sill imaging problem. *Journal of the Geological Society of London*.
- Eisenbeiss, H. (2009). UAV photogrammetry. Ph.D. thesis, ETH Zurich.
- Ernst, R. E. & Baragar, W. R. A. (1992). Evidence from magnetic fabric for the flow pattern of magma in the Mackenzie giant radiating dyke swarm. *Nature* **356**, 511.
- Féménias, O., Diot, H., Berza, T., Gauffriau, A. & Demaiffe, D. (2004). Asymmetrical to symmetrical magnetic fabric of dikes: paleo-flow orientations and Paleo-stresses recorded on feeder-bodies from the Motru Dike Swarm (Romania). *Journal of Structural Geology* **26**, 1401–1418.
- Ferguson, I. J. (2012). Instrumentation and field procedures. In: Chave, A. D. & Jones, A. G. (ed.) *The Magnetotelluric Method: Theory and Practice*. Cambridge University Press, Cambridge.
- Field, L., Blundy, J. D., Brooker, R. A., Wright, T. & Yirgu, G. (2012). Magma storage conditions beneath Dabbahu volcano (Ethiopia) constrained by petrology, seismicity and satellite geodesy. *Bulletin of Volcanology* **74**, 981–1004.
- Fournier, T. J., Pritchard, M. E. & Riddick, S. N. (2010). Duration, magnitude, and frequency of subaerial volcano deformation events: New results from Latin America using InSAR and a global synthesis. *Geochemistry, Geophysics, Geosystems* **11**, Q01003.
- Gaillard, F. (2004). Laboratory measurements of electrical conductivity of hydrous and dry silicic melts under pressure. *Earth and Planetary Science Letters* **218**, 215–228.
- Galland, O. (2012). Experimental modelling of ground deformation associated with shallow magma intrusions. *Earth and Planetary Science Letters* **317–318**, 145–156.
- Gamble, T. D., Goubau, W. M. & Clarke, J. (1979). Magnetotellurics with a remote magnetic reference. *Geophysics* **44**, 53–68.
- Garapic, G., Faul, U. H. & Brisson, E. (2013). High-resolution imaging of the melt distribution in partially molten upper mantle rocks: evidence for wetted two-grain boundaries. *Geochemistry, Geophysics, Geosystems* **14**, 556–566.
- Geoffroy, L., Callot, J. P., Aubourg, C. & Moreira, M. (2002). Magnetic and plagioclase linear fabric discrepancy in dykes: a new way to define the flow vector using magnetic foliation. *Terra Nova* **14**, 183–190.
- Gerst, A. & Savage, M. K. (2004). Seismic anisotropy beneath Ruapehu volcano: a possible eruption forecasting tool. *Science* **306**, 1543–1547.
- Glazner, A. F., Bartley, J. M. & Coleman, D. S. (2016). We need a new definition for “magma”. *Eos* **97**.
- Glen, J. M., Renne, P. R., Milner, S. C. & Coe, R. S. (1997). Magma flow inferred from anisotropy of magnetic susceptibility in the coastal Parana-Etendeka igneous province: evidence for rifting before flood volcanism. *Geology* **25**, 1131–1134.
- Goes, S., Armitage, J., Harmon, N., Smith, H. & Huisman, R. (2012). Low seismic velocities below mid-ocean ridges: attenuation versus melt retention. *Journal of Geophysical Research: Solid Earth* **117**, B12403.
- Gottsmann, J., Blundy, J. D., Henderson, S., Pritchard, M. E. & Sparks, R. S. J. (2017). Thermomechanical modeling of the Altiplano-Puna deformation anomaly: multiparameter insights into magma mush reorganization. *Geosphere* **13**, 1042–1065.
- Gottsmann, J., Rymer, H. & Wooller, L. K. (2005). On the interpretation of gravity variations in the presence of active hydrothermal systems: insights from the Nisyros Caldera, Greece. *Geophysical Research Letters* **32**, L23310.
- Gottsmann, J., Camacho, A. G., Tiampo, K. F. & Fernández, J. (2006). Spatiotemporal variations in vertical gravity gradients at the Campi Flegrei caldera (Italy): a case for source multiplicity during unrest? *Geophysical Journal International* **167**, 1089–1096.
- Gottsmann, J., Carniel, R., Coppo, N., Wooller, L., Hautmann, S. & Rymer, H. (2007). Oscillations in hydrothermal systems as a source of periodic unrest at caldera volcanoes: multiparameter insights from Nisyros, Greece. *Geophysical Research Letters* **34**, L07307.
- Gottsmann, J., Camacho, A. G., Marti, J., Wooller, L., Fernández, J., Garcia, A. & Rymer, H. (2008). Shallow structure beneath the Central Volcanic Complex of Tenerife from new gravity data: implications for its evolution and recent reactivation. *Physics of the Earth and Planetary Interior* **168**, 212–230.
- Graham, J. W. (1954). Magnetic anisotropy, an unexploited petrofabric element. *Geological Society of America Bulletin* **65**, 1257–1258.

- Gudmundsson, O., Brandsdóttir, B., Menke, W. & Sigvaldason, G. E. (1994). The crustal magma chamber of the Katla volcano in south Iceland revealed by 2-D seismic undershooting. *Geophysical Journal International* **119**, 277–296.
- Guidarelli, M., Stuart, G., Hammond, J. O., Kendall, J. M., Ayele, A. & Belachew, M. (2011). Surface wave tomography across Afar, Ethiopia: crustal structure at a rift triple-junction zone. *Geophysical Research Letters* **38**, L24313.
- Guo, X., Zhang, L., Behrens, H. & Ni, H. (2016). Probing the status of felsic magma reservoirs: Constraints from the P - T - H_2O dependences of electrical conductivity of rhyolitic melt. *Earth and Planetary Science Letters* **433**, 54–62.
- Gutiérrez, F., Payacan, I., Gelman, S. E., Bachmann, O. & Parada, M. A. (2013). Late-stage magma flow in a shallow felsic reservoir: merging the anisotropy of magnetic susceptibility record with numerical simulations in La Gloria Pluton, central Chile. *Journal of Geophysical Research: Solid Earth* **118**, 1984–1998.
- Hamilton, M. P., Jones, A. G., Evans, R. L., Evans, S., Fourie, C. J. S., Garcia, X., Mountford, A., Spratt, J. E. & SAMTEX MT Team. (2006). Electrical anisotropy of South African lithosphere compared with seismic anisotropy from shear-wave splitting analyses. *Physics of the Earth and Planetary Interiors* **158**, 226–239.
- Hamling, I. J., Hreinsdóttir, S. & Fournier, N. (2015). The ups and downs of the TVZ: geodetic observations of deformation around the Taupo Volcanic Zone, New Zealand. *Journal of Geophysical Research: Solid Earth* **120**, 4667–4679.
- Hamling, I. J., Wright, T. J., Calais, E., Bennati, L. & Lewi, E. (2010). Stress transfer between thirteen successive dyke intrusions in Ethiopia. *Nature Geoscience* **3**, 713–717.
- Hammer, S. (1945). Estimating ore masses in gravity prospecting. *Geophysics* **10**, 50–62.
- Hammond, J. O. S. (2014). Constraining melt storage geometries beneath the Afar Depression, Ethiopia from teleseismic receiver functions: the anisotropic H - κ stacking technique. *Geochemistry, Geophysics, Geosystems* **15**, 1316–1332.
- Hammond, J. O. S. & Kendall, J. (2016). Constraints on melt distribution from seismology: a case study in Ethiopia. In: Wright, T. J., Ayele, A., Ferguson, D. J., Kidane, T. & Vye-Brown, C. (eds) *Magmatic Rifting and Active Volcanism*. Geological Society, Special Publication, London **420**, 127–147.
- Hammond, J. O. S., Kendall, J., Stuart, G. W., Keir, D., Ebinger, C. J., Ayele, A. & Belachew, M. (2011). The nature of the crust beneath the Afar triple junction: evidence from receiver functions. *Geochemistry, Geophysics, Geosystems* **12**, Q12004.
- Hammond, W. & Humphreys, E. (2000a). Upper mantle seismic wave velocity: effects of realistic partial melt geometries. *Journal of Geophysical Research: Solid Earth* **105**, 10975–10986.
- Hammond, W. & Humphreys, E. (2000b). Upper mantle seismic wave attenuation: effects of realistic partial melt distribution. *Journal of Geophysical Research: Solid Earth* **105**, 10987–10999.
- Hansen, D. M. & Cartwright, J. (2006). The three-dimensional geometry and growth of forced folds above saucer-shaped igneous sills. *Journal of Structural Geology* **28**, 1520–1535.
- Hargraves, R. B., Chan, C. Y. & Johnson, D. (1991). Distribution anisotropy: the cause of AMS in igneous rocks? *Geophysical Research Letters* **18**, 2193–2196.
- Harmon, N. & Rychert, C. A. (2015). Seismic imaging of deep crustal melt sills beneath Costa Rica suggests a method for the formation of the Archean continental crust. *Earth and Planetary Science Letters* **430**, 140–148.
- Hashin, Z. & Shtrikman, S. (1962). A variational approach to the theory of the effective magnetic permeability of multiphase materials. *Journal of Applied Physics* **33**, 3125–3131.
- Hawkesworth, C. J., Blake, S., Evans, P., Hughes, R., Macdonald, R., Thomas, L. E., Turner, S. P. & Zellmer, G. (2000). Time scales of crystal fractionation in magma chambers—integrating physical, isotopic and geochemical perspectives. *Journal of Petrology* **41**, 991–1006.
- Heinson, G., Constable, S. & White, A. (2000). Episodic melt transport at mid-ocean ridges inferred from magnetotelluric sounding. *Geophysical Research Letters* **27**, 2317–2320.
- Hemmings, B., Coco, A., Gottsmann, J. & Whitaker, F. (2016). Investigating hydrological contributions to volcano monitoring signals. *Geophysical Journal International* **207**, 259–273.
- Herrero-Bervera, E., Walker, G. P. L., Cañon-Tapia, E. & Garcia, M. O. (2001). Magnetic fabric and inferred flow direction of dikes, conesheets and sill swarms, Isle of Skye, Scotland. *Journal of Volcanology and Geothermal Research* **106**, 195–210.
- Hickey, J., Gottsmann, J., Nakamichi, H. & Iguchi, M. (2016). Thermomechanical controls on magma supply and volcanic deformation: application to Aira caldera, Japan. *Scientific Reports* **6**, 32691.
- Hickey, J., Gottsmann, J., Mothes, P., Odbert, H., Prutkin, I. & Vajda, P. (2017). *The Ups and Downs of Volcanic Unrest: Insights from Integrated Geodesy and Numerical Modelling*. In: *Advances in Volcanology*. Springer, Berlin, pp. 1–17.
- Hildreth, W. (2004). Volcanological perspectives on Long Valley, Mammoth Mountain, and Mono Craters: several contiguous but discrete systems. *Journal of Volcanology and Geothermal Research* **136**, 169–198.
- Hodgetts, D. (2013). Laser scanning and digital outcrop geology in the petroleum industry: a review. *Marine and Petroleum Geology* **46**, 335–354.
- Hooft, E. E. E., Morgan, J. V., Nomikou, P., Toomey, D. R., Papazachos, C. V., Warner, M., Heath, B., Christopoulou, M.-E., Lampridou, D. & Kementzetzidou, D. (2016). The PROTEUS experiment: active source seismic imaging of the crustal magma plumbing structure of the Santorini Arc volcano. *AGU Fall Meeting Abstract#* D123B-2619.
- Holohan, E. P., Sudhaus, H., Walter, T. R., Schöpfer, M. P. & Walsh, J. J. (2017). Effects of host-rock fracturing on elastic-deformation source models of volcano deflation. *Scientific Reports* **7**, 10970.
- Hrouda, F. (1982). Magnetic anisotropy of rocks and its application in geology and geophysics. *Geophysical Surveys* **5**, 37–82.
- Hrouda, F., Schulmann, K., Suppes, M., Ullemayer, K., de Wall, H. & Weber, K. (1997). Quantitative relationship between low-field AMS and phyllosilicate fabric: a review. *Physics and Chemistry of the Earth* **22**, 153–156.
- Hübner, J., Whaler, K. A. & Fisseha, S. (2018). Preliminary interpretation of the 2010 Youanmi deep seismic reflection lines and magnetotelluric data for the Windimurra Igneous Complex. *Journal of Geophysical Research*.
- Hunt, T. & Bowyer, D. (2007). Reinjection and gravity changes at Rotokawa geothermal field, New Zealand. *Geothermics* **36**, 421–435.
- Husen, S., Taylor, R., Smith, R. B. & Healsler, H. (2004). Changes in geyser eruption behavior and remotely triggered seismicity in Yellowstone National Park produced by the 2002 M 7.9 Denali fault earthquake, Alaska. *Geology* **32**, 537–540.
- Ivanic, T., Zibra, I., Doublier, M. & Wyche, S. (2013). Preliminary interpretation of the 2010 Youanmi deep seismic reflection lines and magnetotelluric data for the Windimurra Igneous

- Complex. In: Wyche, S., Ivanic, T. & Zibra, I. (eds) *Youanmi and Southern Carnarvon Seismic and Magnetotelluric (MT) Workshop 2013*. Geological Survey of Western Australia, Record 6, 93–107.
- Jachens, R. C. & Roberts, C. W. (1985). Temporal and areal gravity investigations at Long Valley Caldera, California. *Journal of Geophysical Research* **90**, 11210–11218.
- Jackson, C. A.-L., Schofield, N. & Golenkov, B. (2013). Geometry and controls on the development of igneous sill-related forced folds: a 2-D seismic reflection case study from offshore southern Australia. *Geological Society of America Bulletin* **125**, 1874–1890.
- Jackson, I., Fitz Gerald, J. D., Faul, U. H. & Tan, B. H. (2002). Grain-size-sensitive seismic wave attenuation in polycrystalline olivine. *Journal of Geophysical Research: Solid Earth* **107**, 2156–2202.
- Jaxybulatov, K., Shapiro, N. M., Koulakov, I., Mordret, A., Landès, M. & Sens-Schönfelder, C. (2014). A large magmatic sill complex beneath the Toba caldera. *Science* **346**, 617–619.
- Jay, J., Costa, F., Pritchard, M., Lara, L., Singer, B. & Herrin, J. (2014). Locating magma reservoirs using InSAR and petrology before and during the 2011–2012 Cordón Caulle silicic eruption. *Earth and Planetary Science Letters* **395**, 254–266.
- Jay, J. A., Pritchard, M. E., West, M. E., Christensen, D. H., Haney, M., Minaya, E., Sunagua, M., McNutt, S. R. & Zabalá, M. (2012). Shallow seismicity, triggered seismicity, and ambient noise tomography at the long-dormant Uturuncu volcano, Bolivia. *Bulletin of Volcanology* **74**, 817–837.
- Johnson, J. H. & Poland, M. P. (2013). Seismic detection of increased degassing before Kilauea's 2008 summit explosion. *Nature Communications* **4**, 1668.
- Johnson, N. E., Whaler, K. A., Hautot, S., Fisseha, S., Desissa, M. & Dawes, G. J. K. (2016). Magma imaged magnetotellurically beneath an active and an inactive magmatic segment in Afar, Ethiopia. *Geological Society, London, Special Publications* **420**, 105–125.
- Jones, A. G. (2012). Distortion of magnetotelluric data: its identification and removal. In: Chave, A. D. & Jones, A. G. (ed.) *The Magnetotelluric Method: Theory and Practice*. Cambridge University Press.
- Jousset, P., Mori, H. & Okada, H. (2000). Possible magma intrusion revealed by temporal gravity, ground deformation and ground temperature observations at Mount Komagatake (Hokkaido) during the 1996–1998 crisis. *Geophysical Journal International* **143**, 557–574.
- Kalinicheva, T., Warner, M., Ashley, J. & Mancini, F. (2017). Two vs three-dimensional FWI in a 3D world. SEG Technical Program Expanded Abstracts 2017, Society of Exploration Geophysicists, 1383–1387.
- Kamei, R., Jang, U. G., Lumley, D., Mouri, T., Nakatsukasa, M., Kato, A. & Takanashi, M. (2017). Time-lapse full waveform inversion for monitoring near-surface microbubble injection. *79th Conference and Exhibition, EAGE, Extended Abstracts*.
- Kapoor, S., Vigh, D., Wiarda, E. & Alwon, S. (2013). Full waveform inversion around the world. *75th Conference and Exhibition, EAGE, Extended Abstracts*.
- Karato, S. & Jung, H. (1998). Water, partial melting and the origin of the seismic low velocity and high attenuation zone in the upper mantle. *Earth and Planetary Science Letters* **157**, 193–207.
- Kavanagh, J. L., Burns, A. J., Hazim, S. H., Wood, E., Martin, S. A., Hignett, S. & Dennis, D. J. (2018). Challenging dyke ascent models using novel laboratory experiments: implications for reinterpreting evidence of magma ascent and volcanism. *Journal of Volcanology and Geothermal Research* **354**, 87–101.
- Keir, D., Belachew, M., Ebinger, C. J., Kendall, J.-M., Hammond, J. O. S., Stuart, G. W., Ayele, A. & Rowland, J. R. (2011). Mapping the evolving strain field during continental breakup from crustal anisotropy in the Afar Depression. *Nature Communications* **2**, 285–287.
- Keir, D., Hamling, I. J., Ayele, A., Calais, E., Ebinger, C. J., Wright, T. J., Jacques, E., Mohamed, K., Hammond, J. O. S., Belachew, M., Baker, E., Rowland, J. V., Lewi, E. & Bennati, L. (2009). Evidence for focused magmatic accretion at segment centers from lateral dike injection captured beneath the Red Sea rift of Afar. *Geology* **37**, 59–62.
- Kelso, P. R., Tikoff, B., Jackson, M. & Sun, W. (2002). A new method for the separation of paramagnetic and ferromagnetic susceptibility anisotropy using low field and high field methods. *Geophysical Journal International* **151**, 345–359.
- Kent, G. M., Singh, S. C., Harding, A. J., Sinha, M. C., Orcutt, J. A., Barton, P. J., White, R. S., Bazin, S., Hobbs, R. W., Tong, C. H. & Pye, J. W. (2000). Evidence from three-dimensional seismic reflectivity images for enhanced melt supply beneath mid-ocean-ridge discontinuities. *Nature* **406**, 614–618.
- Key, K., Constable, S., Liu, L. & Pommier, A. (2013). Electrical image of passive upwelling beneath the northern East Pacific Rise. *Nature* **495**, 499–502.
- Khan, M. A. (1962). The anisotropy of magnetic susceptibility of some igneous and metamorphic rocks. *Journal of Geophysical Research* **67**, 2873–2885.
- Kim, D., Brown, L. D., Árnason, K., Ágústsson, K. & Blanck, H. (2017). Magma reflection imaging in Krafla, Iceland, using microearthquake sources. *Journal of Geophysical Research: Solid Earth* **122**, 5228–5242.
- Kiser, E., Levander, A., Schmandt, B., Palomeras, I., Harder, S. H., Creager, K. C., Vidale, J. E. & Malone, S. D. (2014). Field report on the iMUSH active source seismic experiment. *AGU Fall Meeting Abstracts* **1**, 2.
- Knight, M. D. & Walker, G. P. (1988). Magma flow directions in dikes of the Koolau Complex, Oahu, determined from magnetic fabric studies. *Journal of Geophysical Research: Solid Earth* **93**, 4301–4319.
- Koulakov, I., Gordeev, E. I., Dobretsov, N. L., Vernikovskiy, V. A., Senyukov, S., Jakovlev, A. & Jaxybulatov, K. (2013). Rapid changes in magma storage beneath the Klyuchevskoy group of volcanoes inferred from time-dependent seismic tomography. *Journal of Volcanology and Geothermal Research* **263**, 75–91.
- Laumonier, M., Gaillard, F. & Sifre, D. (2015). The effect of pressure and water concentration on the electrical conductivity of dacitic melts: Implication for magnetotelluric imaging in subduction areas. *Chemical Geology* **418**, 66–76.
- Launeau, P. & Cruden, A. R. (1998). Magmatic fabric acquisition mechanisms in a syenite: results of a combined anisotropy of magnetic susceptibility and image analysis study. *Journal of Geophysical Research: Solid Earth* **103**, 5067–5089.
- Lazaratos, S., Chikichev, I. & Wang, K. (2011). Improving the convergence rate of full waveform inversion using spectral shaping. SEG Technical Program Expanded Abstracts 2011, Society of Exploration Geophysicists, 2428–2432.
- Leberl, F., Irschara, A., Pock, T., Meixner, P., Gruber, M., Scholz, S. & Wiechert, A. (2010). Point Clouds: Lidar versus 3D Vision. *Photogrammetric Engineering & Remote Sensing* **76**, 1123–1134.
- Lees, J. M. (2007). Seismic tomography of magmatic systems. *Journal of Volcanology and Geothermal Research* **167**, 37–56.

- Le Mével, H., Feigl, K. L., Córdova, L., DeMets, C. & Lundgren, P. (2015). Evolution of unrest at Laguna del Maule volcanic field (Chile) from InSAR and GPS measurements, 2003 to 2014. *Geophysical Research Letters* **42**, 6590–6598.
- Lu, Z. & Dzurisin, D. (2014). *InSAR Imaging of Aleutian Volcanoes*. Berlin, Heidelberg: Springer, pp. 87–345.
- MacGregor, L. M., Constable, S. & Sinha, M. C. (1998). The RAMESSES experiment—III. Controlled-source electromagnetic sounding of the Reykjanes Ridge at 57° 45' N. *Geophysical Journal International* **135**, 773–789.
- Magee, C., Briggs, F. & Jackson, C. A.-L. (2013a). Lithological controls on igneous intrusion-induced ground deformation. *Journal of the Geological Society* **170**, 853–856.
- Magee, C., Hunt-Stewart, E. & Jackson, C. A. L. (2013b). Volcano growth mechanisms and the role of sub-volcanic intrusions: Insights from 2D seismic reflection data. *Earth and Planetary Science Letters* **373**, 41–53.
- Magee, C., Jackson, C. L. & Schofield, N. (2014). Diachronous sub-volcanic intrusion along deep-water margins: insights from the Irish Rockall Basin. *Basin Research* **26**, 85–105.
- Magee, C., Maharaj, S. M., Wrona, T. & Jackson, C. A.-L. (2015). Controls on the expression of igneous intrusions in seismic reflection data. *Geosphere* **11**, 1024. GES01150.01151.
- Magee, C., Stevenson, C. T. E., O'Driscoll, B. & Petronis, M. S. (2012a). Local and regional controls on the lateral emplacement of the Ben Hiant Dolerite intrusion, Ardnamurchan (NW Scotland). *Journal of Structural Geology* **39**, 66–82.
- Magee, C., Stevenson, C. T. E., O'Driscoll, B., Schofield, N. & McDermott, K. (2012b). An alternative emplacement model for the classic Ardnamurchan cone sheet swarm, NW Scotland, involving lateral magma supply via regional dykes. *Journal of Structural Geology* **43**, 73–91.
- Magee, C., Bastow, I. D., van Wyk de Vries, B., Jackson, C. A. L., Hetherington, R., Hagos, M. & Hoggett, M. (2017a). Structure and dynamics of surface uplift induced by incremental sill emplacement. *Geology* **45**, 431–434.
- Magee, C., Muirhead, J., Schofield, N., Walker, R., Galland, O., Holford, S., Spacapan, J., Jackson, C., A.-L. & McCarthy, W. (2017b). Structural signatures of igneous sheet intrusion propagation. *EarthArXiv* doi:10.17605/OSF.IO/PDN42.
- Magee, C., Muirhead, J. D., Karvelas, A., Holford, S. P., Jackson, C. A. L., Bastow, I. D., Schofield, N., Stevenson, C. T. E., McLean, C., McCarthy, W. & Shtukert, O. (2016). Lateral magma flow in mafic sill complexes. *Geosphere* **12**, 809.
- Malehmir, A., Durrheim, R., Bellefleur, G., Urosevic, M., Juhlin, C., White, D. J., Milkereit, B. & Campbell, G. (2012). Seismic methods in mineral exploration and mine planning: a general overview of past and present case histories and a look into the future. *Geophysics* **77**, WC173–WC190.
- Mamtani, M. A. & Greiling, R. O. (2005). Granite emplacement and its relation with regional deformation in the Aravalli Mountain Belt (India) –inferences from magnetic fabric. *Journal of Structural Geology* **27**, 2008–2029.
- Mamtani, M. A., Pal, T. & Greiling, R. O. (2013). Kinematic analysis using AMS data from a deformed granitoid. *Journal of Structural Geology* **50**, 119–132.
- Mancini, F., Moss, J., Prindle, K. & Ridsdill-Smith, T. (2015). Where can full waveform inversion have the biggest impact in the exploration and production cycle? *77th International Conference and Exhibition, EAGE, Extended Abstracts*.
- Manzella, A., Volpi, G., Zaja, A. & Meju, M. (2004). Combined TEM-MT investigation of shallow-depth resistivity structure of Mt Somma-Vesuvius. *Journal of Volcanology and Geothermal Research* **131**, 19–32.
- Marjanovic, M., Carbotte, S. M., Carton, H., Nedimovic, M. R., Mutter, J. C. & Canales, J. P. (2014). A multi-sill magma plumbing system beneath the axis of the East Pacific Rise. *Nature Geoscience* **7**, 825–829.
- Mark, N. J., Schofield, N., Pugliese, S., Watson, D., Holford, S., Muirhead, D., Brown, R. & Healy, D. (2017). Igneous intrusions in the Faroe Shetland basin and their implications for hydrocarbon exploration; new insights from well and seismic data. *Marine and Petroleum Geology* **92**, 733–753.
- Martín-Hernández, F., Lüneburg, C. M., Aubourg, C. & Jackson, M. (2004). Magnetic fabric: methods and applications—an introduction. In: Martín-Hernández, F., Lüneburg, C. M., Aubourg, C. & Jackson, M. (eds) *Magnetic Fabric: Methods and Applications*. Geological Society, London, Special Publications **238**, 1–7.
- Masterlark, T. (2007). Magma intrusion and deformation predictions: sensitivities to the Mogi assumptions. *Journal of Geophysical Research* **112**, B06419.
- Masturyono, McCaffrey, R., Wark, D. A., Roecker, S. W., Fauzi Ibrahim, G. & Sukhyar. (2001). Distribution of magma beneath Toba caldera complex, north Sumatra, Indonesia, constrained by three-dimensional P wave velocities, seismicity, and gravity. *Geochemistry Geophysics Geosystems* **2**, 1014.
- Matsushima, N., Oshima, H., Ogawa, Y., Takakura, S., Satoh, H., Utsugi, M. & Nishida, Y. (2001). Magma prospecting in Usu volcano, Hokkaido, Japan, using magnetotelluric soundings. *Journal of Volcanology and Geothermal Research* **109**, 263–277.
- McBride, J. H., William Keach, R., Leetaru, H. E. & Smith, K. M. (2018). Visualizing Precambrian basement tectonics beneath a carbon capture and storage site, Illinois Basin. *Interpretation* **6**, T257–T270.
- McCabe, C., Jackson, M. & Ellwood, B. B. (1985). Magnetic anisotropy in the Trenton limestone: results of a new technique, anisotropy of anhysteretic susceptibility. *Geophysical Research Letters* **12**, 333–336.
- McCormick Kilbride, B., Edmonds, M. & Biggs, J. (2016). Observing eruptions of gas-rich compressible magmas from space. *Nature Communications* **7**, 13744.
- McKenzie, D. A. N. & O'Nions, R. K. (1991). Partial melt distributions from inversion of rare earth element concentrations. *Journal of Petrology* **32**, 1021–1091.
- McLean, C. E., Schofield, N., Brown, D. J., Jolley, D. W. & Reid, A. (2017). 3D seismic imaging of the shallow plumbing system beneath the Ben Nevis Monogenetic Volcanic Field: Faroe-Shetland Basin. *Journal of the Geological Society* **174**, 468–485.
- Miller, C. A., Le Mével, H., Currenti, G., Williams-Jones, G. & Tikoff, B. (2017). Microgravity changes at the Laguna del Maule volcanic field: Magma-induced stress changes facilitate mass addition. *Journal of Geophysical Research: Solid Earth* **122**, 3179–3196.
- Miller, C. F., Furbish, D. J., Walker, B. A., Claiborne, L. L., Koteas, G. C., Bleick, H. A. & Miller, J. S. (2011). Growth of plutons by incremental emplacement of sheets in crystal-rich host: evidence from Miocene intrusions of the Colorado River region, Nevada, USA. *Tectonophysics* **500**, 65–77.
- Miller, K. J., Zhu, W., Montesi, L. G. J. & Gaetani, G. A. (2014). Experimental quantification of permeability of partially molten mantle rock. *Earth and Planetary Science Letters* **388**, 273–282.
- Miller, V. & Savage, M. (2001). Changes in seismic anisotropy after volcanic eruptions: evidence from Mount Ruapehu. *Science* **293**, 2231–2233.
- Mitchell, M. A., White, R. S., Roecker, S. & Greenfield, T. (2013). Tomographic image of melt storage beneath Askja Volcano,

- Iceland using local microseismicity. *Geophysical Research Letters* **40**, 5040–5046.
- Morgan, J. V., Warner, M., Arnoux, G., Hooft, E., Toomey, D., VanderBeek, B. & Wilcock, W. (2016). Next-generation seismic experiments—II: wide-angle, multi-azimuth, 3-D, full-waveform inversion of sparse field data. *Geophysical Journal International* **204**, 1342–1363.
- Morgan, J. V., Warner, M., Bell, R. E., Ashley, J., Barnes, D., Little, R., Roele, K. & Jones, C. (2013). Next-generation seismic experiments: wide-angle, multi-azimuth, three-dimensional, full-waveform inversion. *Geophysical Journal International* **195**, 1657–1678.
- Muirhead, J. D., Airolidi, G., White, J. D. & Rowland, J. V. (2014). Cracking the lid: sill-fed dikes are the likely feeders of flood basalt eruptions. *Earth and Planetary Science Letters* **406**, 187–197.
- Neuberg, J., Baptie, B., Luckett, R. & Stewart, R. (1998). Results from the broadband seismic network on Montserrat. *Geophysical Research Letters* **25**, 3661–3664.
- Neuberg, J., Tuffen, H., Collier, L., Green, D., Powell, T. & Dingwell, D. (2006). The trigger mechanism of low-frequency earthquakes on Montserrat. *Journal of Volcanology and Geothermal Research* **153**, 37–50.
- Neves, S. P., Araújo, A. M., Correia, P. B. & Mariano, G. (2003). Magnetic fabrics in the Cabanas Granite (NE Brazil): interplay between emplacement and regional fabrics in a dextral transpressive regime. *Journal of Structural Geology* **25**, 441–453.
- Newman, A. V., Dixon, T. H. & Gourmelen, N. (2006). A four-dimensional viscoelastic deformation model for Long Valley Caldera, California, between 1995 and 2000. *Journal of Volcanology and Geothermal Research* **150**, 244–269.
- O'Driscoll, B., Stevenson, C. T. E. & Troll, V. R. (2008). Mineral lamination development in layered gabbros of the British Palaeogene Igneous Province: A combined anisotropy of magnetic susceptibility, textural and mineral chemistry study. *Journal of Petrology* **49**, 1187–1221.
- O'Driscoll, B., Ferré, E. C., Stevenson, C. T. E. & Magee, C. (2015). The significance of magnetic fabrics in layered mafic-ultramafic intrusions. In: Charlier, B., Latypov, R., Namur, O. & Tegner, C. (eds) *Layered Intrusions*. Springer, Berlin, pp. 295–329.
- Okubo, P. G., Benz, H. M. & Chouet, B. A. (1997). Imaging the crustal magma sources beneath Mauna Loa and Kilauea volcanoes, Hawaii. *Geology* **25**, 867–870.
- Orlický, O. (1990). Detection of magnetic carriers in rocks: results of susceptibility changes in powdered rock samples induced by temperature. *Physics of the Earth and Planetary Interiors* **63**, 66–70.
- Padilha, A. L., Vitorello, Í., Pádua, M. B. & Bologna, M. S. (2006). Lithospheric and sublithospheric anisotropy beneath central-southeastern Brazil constrained by long period magnetotelluric data. *Physics of the Earth and Planetary Interiors* **158**, 190–209.
- Pagli, C., Wright, T. J., Ebinger, C. J., Yun, S. H., Cann, J. R., Barnie, T. & Ayele, A. (2012). Shallow axial magma chamber at the slow-spreading Erta Ale Ridge. *Nature Geoscience* **5**, 284–288.
- Parker, A. L. (2016). *InSAR Observations of Ground Deformation: Application to the Cascades Volcanic Arc*. Springer Theses, Cham, Switzerland.
- Parker, R. L. (1980). The inverse problem of electromagnetic induction: Existence and construction of solutions based on incomplete data. *Journal of Geophysical Research: Solid Earth* **85**, 4421–4428.
- Parker, A. L., Biggs, J. & Lu, Z. (2016). Time-scale and mechanism of subsidence at Lassen Volcanic Center, CA, from InSAR. *Journal of Volcanology and Geothermal Research* **320**, 117–127.
- Parks, M. M., Biggs, J., England, P., Mather, T. A., Nomikou, P., Palamartchouk, K., Papanikolaou, X., Paradissis, D., Parsons, B., Pyle, D. M., Raptakis, C. & Zacharis, V. (2012). Evolution of Santorini Volcano dominated by episodic and rapid fluxes of melt from depth. *Nature Geoscience* **5**, 749–754.
- Parmigiani, A., Faroughi, S. A., Huber, C., Bachmann, O. & Su, Y. (2016). Bubble accumulation and its role on the evolution of upper crustal magma reservoirs. *Nature* **532**, 492–495.
- Paulatto, M., Annen, C., Henstock, T. J., Kiddle, E., Minshull, T. A., Sparks, R. S. J. & Voight, B. (2012). Magma chamber properties from integrated seismic tomography and thermal modeling at Montserrat. *Geochemistry, Geophysics, Geosystems* **13**, Q01014.
- Paulatto, M., Minshull, T. A., Baptie, B., Dean, S., Hammond, J. O. S., Henstock, T., Kenedi, C. L., Kiddle, E. J., Malin, P., Peirce, C., Ryan, G., Shalev, E., Sparks, R. S. J. & Voight, B. (2010). Upper crustal structure of an active volcano from refraction/reflection tomography, Montserrat, Lesser Antilles. *Geophysical Journal International* **180**, 685–696.
- Pedersen, R. & Sigmundsson, F. (2006). Temporal development of the 1999 intrusive episode in the Eyjafjallajökull volcano, Iceland, derived from InSAR images. *Bulletin of Volcanology* **68**, 377–393.
- Peron-Pinvidic, G., Shillington, D. J. & Tucholke, B. E. (2010). Characterization of sills associated with the U reflection on the Newfoundland margin: evidence for widespread early post-rift magmatism on a magma-poor rifted margin. *Geophysical Journal International* **182**, 113–136.
- Petford, N., Cruden, A. R., McCaffrey, K. J. W. & Vigneresse, J. L. (2000). Granite magma formation, transport and emplacement in the Earth's crust. *Nature* **408**, 669–673.
- Petronis, M. S., O'Driscoll, B., Stevenson, C. T. E. & Reavy, R. J. (2012). Controls on emplacement of the Caledonian Ross of Mull Granite, NW Scotland: Anisotropy of magnetic susceptibility and magmatic and regional structures. *Geological Society of America Bulletin* **124**, 906–927.
- Petronis, M. S., Delcamp, A. & de Vries, B. V. W. (2013). Magma emplacement into the Lemptégy scoria cone (Chaîne Des Puys, France) explored with structural, anisotropy of magnetic susceptibility, and Paleomagnetic data. *Bulletin of Volcanology* **75**, 753.
- Petronis, M. S., Brister, A. R., Rapprich, V., de Vries, B. V. W., Lindline, J. & Misurec, J. (2015). Emplacement history of the Trosky basaltic volcano (Czech Republic): paleomagnetic, rock magnetic, petrologic, and anisotropy of magnetic susceptibility evidence for lingering growth of a monogenetic volcano. *Journal of Geosciences* **60**, 129–147.
- Petrovský, E. & Kapička, A. (2006). On determination of the Curie point from thermomagnetic curves. *Journal of Geophysical Research: Solid Earth* **111**, B12S27.
- Phillips, T. B., Magee, C., Jackson, C. A. L. & Bell, R. E. (2017). Determining the three-dimensional geometry of a dike swarm and its impact on later rift geometry using seismic reflection data. *Geology* **46**, 119–122.
- Pinel, V., Poland, M. P. & Hooper, A. (2014). Volcanology: lessons learned from synthetic aperture radar imagery. *Journal of Volcanology and Geothermal Research* **289**, 81–113.
- Planke, S., Rasmussen, T., Rey, S. S. & Myklebust, R. (2005). Seismic characteristics and distribution of volcanic intrusions and hydrothermal vent complexes in the Vøring and Møre basins. In: Doré, A. G. (ed.) *Petroleum Geology: North-West Europe and Global Perspectives—Proceedings of the 6th Petroleum Geology Conference: Geological Society* **6**, London 833–844.

- Planke, S., Symonds, P. A., Alvestad, E. & Skogseid, J. (2000). Seismic volcanostratigraphy of large-volume basaltic extrusive complexes on rifted margins. *Journal of Geophysical Research: Solid Earth* **105**, 19335–19351.
- Poland, M. P. & Carbone, D. (2016). Insights into shallow magmatic processes at Kilauea Volcano, Hawai'i, from a multi-year continuous gravity time series. *Journal of Geophysical Research: Solid Earth* **121**, 5477–5492.
- Poland, M. P., Miklius, A., Sutton, A. J. & Thornber, C. R. (2012). A mantle-driven surge in magma supply to Kilauea Volcano during 2003–2007. *Nature Geoscience* **5**, 295–300.
- Pommier, A. (2014). Interpretation of magnetotelluric results using laboratory measurements. *Surveys in Geophysics* **35**, 41–84.
- Pommier, A. & Le Trong, E. (2011). SIGMELTS: a web portal for electrical conductivity calculations in geosciences. *Computational Geoscience* **37**, 1450–1459.
- Pommier, A., Tarits, P., Hautot, S., Pichavant, M., Scaillet, B. & Gaillard, F. (2010). A new petrological and geophysical investigation of the present-day plumbing system of Mount Vesuvius. *Geochemistry, Geophysics, Geosystems* **11**, Q07013.
- Pritchard, M. E. & Simons, M. (2004). An InSAR-based survey of volcanic deformation in the central Andes. *Geochemistry, Geophysics, Geosystems* **5**, Q02002.
- Prutkin, I., Vajda, P. & Gottsmann, J. (2014). The gravimetric picture of magmatic and hydrothermal sources driving hybrid unrest on Tenerife in 2004/5. *Journal of Volcanology and Geothermal Research* **282**, 9–18.
- Rabbel, O., Galland, O., Mair, K., Lecomte, I., Senger, K., Spacapan, J. B. & Manceda, R. (2018). From field analogues to realistic seismic modelling: a case study of an oil-producing andesitic sill complex in the Neuquén Basin, Argentina. *Journal of the Geological Society* **175**, 580–593.
- Reeves, J., Magee, C. & Jackson, C. A. L. (2018). Unravelling intrusion-induced forced fold kinematics and ground deformation using 3D seismic reflection data. *Volcanica* **1**, 1–17.
- Reich, H. (1932). Die Bedeutung der finnischen Schweremessungen für die angewandte Geophysik. *Ergänz.-Hefte für die angewandte Geophysik* **2**, 1–13.
- Richter, C. & van der Pluijm, B. A. (1994). Separation of paramagnetic and ferrimagnetic susceptibilities using low temperature magnetic susceptibilities and comparison with high field methods. *Physics of the Earth and Planetary Interiors* **82**, 113–123.
- Rivalta, E. & Segall, P. (2008). Magma compressibility and the missing source for some dike intrusions. *Geophysical Research Letters* **35**, L04306.
- Roberts, J. J. & Tyburczy, J. A. (1999). Partial-melt electrical conductivity: Influence of melt composition. *Journal of Geophysical Research: Solid Earth* **104**, 7055–7065.
- Rocchi, S., Mazzotti, A., Marroni, M., Pandolfi, L., Costantini, P., Giuseppe, B., Biase, D. D., Federici, F. & Lo, P. G. (2007). Detection of Miocene saucer-shaped sills (offshore Senegal) via integrated interpretation of seismic, magnetic and gravity data. *Terra Nova* **19**, 232–239.
- Rochette, P., Jackson, M. & Aubourg, C. (1992). Rock magnetism and the interpretation of anisotropy of magnetic susceptibility. *Reviews of Geophysics* **30**, 209–226.
- Roman, D. C. & Cashman, K. V. (2006). The origin of volcano-tectonic earthquake swarms. *Geology* **34**, 457–460.
- Roman, D. C., Savage, M. K., Arnold, R., Latchman, J. L. & De Angelis, S. (2011). Analysis and forward modeling of seismic anisotropy during the ongoing eruption of the Soufrière Hills Volcano, Montserrat, 1996–2007. *Journal of Geophysical Research* **116**, B03201.
- Ronchin, E., Masterlark, T., Dawson, J., Saunders, S. & Marti Molist, J. (2017). Imaging the complex geometry of a magma reservoir using FEM-based linear inverse modeling of InSAR data: application to Rabaul Caldera, Papua New Guinea. *Geophysical Journal International* **209**, 1746–1760.
- Routh, P., Neelamani, R., Lu, R., Lazaratos, S., Braaksma, H., Hughes, S., Saltzer, R., Stewart, J., Naidu, K., Averill, H., Gottumukkula, V., Homonko, P., Reilly, J. & Leslie, D. (2017). Impact of high-resolution FWI in the western black sea: revealing overburden and reservoir complexity. *The Leading Edge* **36**, 60–66.
- Rubin, A. & Gillard, D. (1998). Dike-induced earthquakes: theoretical considerations. *Journal of Geophysical Research: Solid Earth* **103**, 10017–10030.
- Rymer, H. & Brown, G. C. (1986). Gravity fields and the interpretation of volcanic structures: Geological discrimination and temporal evolution. *Journal of Volcanology and Geothermal Research* **27**, 229–254.
- Rymer, H., Locke, C. A., Brenes, J. & Williams-Jones, G. (2005). Magma plumbing processes for persistent activity at Poas volcano, Costa Rica. *Geophysical Research Letters* **32**, L08307.
- Salzer, J. T., Nikkhoo, M., Walter, T. R., Sudhaus, H., Reyes-Dávila, G., Bretón, M. & Arámbula, R. (2014). Satellite radar data reveal short-term pre-explosive displacements and a complex conduit system at Volcán de Colima, Mexico. *Frontiers in Earth Science* **2**, 12.
- Samrock, F., Kuvshinov, A., Bakker, J., Jackson, A. & Fisseha, S. (2015). 3D analysis and interpretation of Magnetotelluric data from the Aluto-Langano geothermal field, Ethiopia. *Geophysical Journal International* **202**, 1923–1948.
- Saunders, K., Blundy, J. D., Dohmen, R. & Cashman, K. (2012). Linking Petrology and Seismology at an active volcano. *Science* **336**, 1023–1027.
- Saxby, J., Gottsmann, J., Cashman, K. & Gutiérrez, E. (2016). Magma storage in a strike-slip caldera. *Nature Communications* **7**, 12295.
- Schaefer, L. N., Lu, Z. & Oommen, T. (2015). Dramatic volcanic instability revealed by InSAR. *Geology* **43**, 743–746.
- Schmeling, H. (1986). Numerical models on the influence of partial melt on elastic, anelastic and electrical properties of rocks. Part II: electrical conductivity. *Physics of Earth and Planetary Interiors* **43**, 123–136.
- Schofield, N. J., Brown, D. J., Magee, C. & Stevenson, C. T. E. (2012a). Sill morphology and comparison of brittle and non-brittle emplacement mechanisms. *Journal of the Geological Society of London* **169**, 127–141.
- Schofield, N., Heaton, L., Holford, S. P., Archer, S. G., Jackson, C. A. L. & Jolley, D. W. (2012b). Seismic imaging of 'broken bridges': linking seismic to outcrop-scale investigations of intrusive magma lobes. *Journal of the Geological Society of London* **169**, 421–426.
- Schofield, N. J., Alsop, I., Warren, J., Underhill, J. R., Lehné, R., Beer, W. & Lukas, V. (2014). Mobilizing salt: Magma-salt interactions. *Geology* **42**, 599–602.
- Schofield, N., Holford, S., Millett, J., Brown, D., Jolley, D., Passet, S., Muirhead, D., Grove, C., Magee, C., Murray, J., Hole, M., Jackson, C. & Stevenson, C. (2017). Regional Magma Plumbing and emplacement mechanisms of the Faroe-Shetland Sill Complex: implications for magma transport and petroleum systems within sedimentary basins. *Basin Research* **29**, 41–63.
- Schofield, N., Stevenson, C. T. E. & Reston, T. (2010). Magma fingers and host rock fluidization in the emplacement of sills. *Geology* **38**, 63–66.

- Segall, P. (2010). *Earthquake and Volcano Deformation*. Princeton University Press, Princeton.
- Shalev, E., Kenedi, C. L., Malin, P., Voight, V., Miller, V., Hidayat, D., Sparks, R. S. J., Minshull, T., Paulatto, M., Brown, L. & Mattioli, G. (2010). Three-dimensional seismic velocity tomography of Montserrat from the SEA-CALIPSO offshore/onshore experiment. *Geophysical Research Letters* **37**, L00E17.
- Sigmundsson, F. (2016). New insights into magma plumbing along rift systems from detailed observations of eruptive behavior at Axial volcano. *Geophysical Research Letters* **43**, 12423–12427.
- Sigmundsson, F., Hooper, A., Hreinsdóttir, S., Vogfjörð, K. S., Ófeigsson, B. G., Heimisson, E. R., Dumont, S., Parks, M., Spaans, K., Gudmundsson, G. B., Drouin, V., Árnadóttir, T., Jónsdóttir, K., Gudmundsson, M. T., Högnadóttir, T., Fridriksdóttir, H. M., Hensch, M., Einarsson, P., Magnússon, E., Samsonov, S., Brandsdóttir, B., White, R. S., Ágústsdóttir, T., Greenfield, T., Green, R. G., Hjartardóttir, Á. R., Pedersen, R., Bennett, R. A., Geirsson, H., La Femina, P. C., Björnsson, H., Pálsson, F., Sturkell, E., Bean, C. J., Möllhoff, M., Braiden, A. K. & Eibl, E. P. S. (2015). Segmented lateral dyke growth in a rifting event at Bardabunga volcanic system, Iceland. *Nature* **517**, 191–195.
- Sigmundsson, F., Hreinsdóttir, S., Hooper, A., Arnadóttir, T., Pedersen, R., Roberts, M. J., Oskarsson, N., Auriac, A., Decriem, J., Einarsson, P., Geirsson, H., Hensch, M., Ófeigsson, B. G., Sturkell, E., Sveinbjörnsson, H. & Feigl, K. L. (2010). Intrusion triggering of the 2010 Eyjafjallajökull explosive eruption. *Nature* **468**, 426–430.
- Simons, M. & Rosen, P. A. (2007). Interferometric synthetic aperture radar Geodesy. In: Schubert, G. (ed.) *Treatise on Geophysics—Geodesy*, Vol. 3, Amsterdam: Elsevier, pp. 391–446.
- Simpson, F. & Bahr, K. (2005). *Practical Magnetotellurics*. Cambridge: Cambridge University Press.
- Singer, B. S., Andersen, N. L., Le Mével, H., Feigl, K. L., DeMets, C., Tikoff, B., Thurber, C. H., Jicha, B. R., Cardona, C., Córdova, L., Gil, F., Unsworth, M. J., Williams-Jones, G., Miller, C., Fierstein, J., Hildreth, W. & Vazquez, J. (2014). Dynamics of a large, restless, rhyolitic magma system at Laguna del Maule, southern Andes, Chile. *GSA Today* **24**, 4–10.
- Sirgue, L., Barkved, O. I., Dellinger, J., Etgen, J., Albertin, U. & Kommedal, J. H. (2010). Full waveform inversion: the next leap forward in imaging at Valhall. *First Break* **28**, 65–70.
- Smallwood, J. R. & Maresh, J. (2002). The properties, morphology and distribution of igneous sills: modelling, borehole data and 3D seismic from the Faroe-Shetland area. In: Jolley, D. W. & Bell, B. R. (eds) *The North Atlantic Igneous Province: Stratigraphy, Tectonic, Volcanic and Magmatic Processes*. Geological Society, London, *Special Publications* **197**, 271–306.
- Sofyan, Y., Kamah, Y., Nishijima, J., Fujimitsu, Y., Ehara, S., Fukuda, Y. & Taniguchi, M. (2011). Mass variation in outcome to high production activity in Kamojang Geothermal Field, Indonesia: a reservoir monitoring with relative and absolute gravimetry. *Earth, Planets and Space* **63**, 1157–1167.
- Solano, J. M. S., Jackson, M. D., Sparks, R. S. J., Blundy, J. D. & Annen, C. (2012). Melt segregation in deep crustal hot zones: a mechanism for chemical differentiation, crustal assimilation and the formation of evolved magmas. *Journal of Petrology* **53**, 1999–2026.
- Sparks, R., Biggs, J. & Neuberg, J. (2012). Monitoring volcanoes. *Science* **335**, 1310–1311.
- Stacey, F. D., Joplin, G. & Lindsay, J. (1960). Magnetic anisotropy and fabric of some foliated rocks from S.E. Australia. *Pure Applied Geophysics* **47**, 30–40.
- Stankiewicz, J., Ryberg, T., Haberland, C. & Natawidjaja, D. (2010). Lake Toba volcano magma chamber imaged by ambient seismic noise tomography. *Geophysical Research Letters* **37**, L17306.
- Stephens, T. L., Walker, R. J., Healy, D., Bubeck, A., England, R. W. & McCaffrey, K. J. W. (2017). Igneous sills record far-field and near-field stress interaction during volcano construction: Isle of Mull, Scotland. *Earth and Planetary Science Letters* **478**, 159–174.
- Stephenson, A. (1994). Distribution anisotropy: two simple models for magnetic lineation and foliation. *Physics of the Earth and Planetary Interiors* **82**, 49–53.
- Sternberg, B., Washburne, J. C. & Pellerin, L. (1988). Correction for the static shift in magnetotellurics using transient electromagnetic soundings. *Geophysics* **53**, 1459–1468.
- Stevenson, C. T. E., Owens, W. H. & Hutton, D. H. W. (2007a). Flow lobes in granite: the determination of magma flow direction in the Travenagh Bay Granite, N.W. Ireland, using anisotropy of magnetic susceptibility. *Geological Society of America Bulletin* **119**, 1368–1386.
- Stevenson, C. T. E., Owens, W. H., Hutton, D. H. W., Hood, D. N. & Meighan, I. G. (2007b). Laccolithic, as opposed to cauldron subsidence, emplacement of the Eastern Mourne pluton, N. Ireland: evidence from anisotropy of magnetic susceptibility. *Journal of the Geological Society of London* **164**, 99–110.
- Stork, A., Stuart, G. W., Henderson, C. M., Keir, D. & Hammond, J. O. S. (2013). Uppermost mantle (Pn) velocity model for the Afar region, Ethiopia: an insight into rifting processes. *Geophysical Journal International* **193**, 321–328.
- Stuart, G. W., Bastow, I. D. & Ebinger, C. J. (2006). Crustal structure of the Northern Main Ethiopian rift from receiver function studies. In: Yirgu, G., Ebinger, C. J. & Maguire, P. K. H. (eds) *The Afar Volcanic Province within the East African Rift System*. Geological Society, London, *Special Publications* **259**, 253–267.
- Sturkell, E., Einarsson, P., Sigmundsson, F., Geirsson, H., Ólafsson, H., Pedersen, R., de Zeeuw-van Dalfsen, E., Linde, A. T., Sacks, S. I. & Stefánsson, R. (2006). Volcano geodesy and magma dynamics in Iceland. *Journal of Volcanology and Geothermal Research* **150**, 14–34.
- Svensen, H., Corfu, F., Polteau, S., Hammer, Ø. & Planke, S. (2012). Rapid magma emplacement in the Karoo Large Igneous Province. *Earth and Planetary Science Letters* **325–326**, 1–9.
- Symonds, P., A., Planke, S., Frey, O. & Skogseid, J. (1998). Volcanic evolution of the Western Australian Continental Margin and its implications for basin development. In: Purcell, P. G. & Purcell, R. R. (eds). *The Sedimentary Basins of Western Australia 2: Proc. of Petroleum Society Australia Symposium, Perth, WA*.
- Takei, Y. (2002). Effect of pore geometry on V-P/V-S: from equilibrium geometry to crack. *Journal of Geophysical Research* **107**, 2043.
- Tarantola, A. (1984). Inversion of seismic reflection data in the acoustic approximation. *Geophysics* **49**, 1259–1266.
- Tarling, D. H. & Hrouda, F. (1993). *The Magnetic Anisotropy of Rocks*. New York: Chapman and Hall, pp. 1–232.
- Tauxe, L. (1998). *Paleomagnetic principles and practice. Modern Approaches in Geophysics*, Vol. 17. Dordrecht, Boston, London: Kluwer Academic Publishers.
- Thiele, S., Micklethwaite, S., Bourke, P., Verrall, M. & Kovsi, P. (2015). Insights into the mechanics of en-echelon sigmoidal vein formation using ultra-high resolution photogrammetry

- and computed tomography. *Journal of Structural Geology* **77**, 27–54.
- Thomas, M. E. & Neuberg, J. (2012). What makes a volcano tick—a first explanation of deep multiple seismic sources in ascending magma. *Geology* **40**, 351–354.
- Thomson, K. (2007). Determining magma flow in sills, dykes and laccoliths and their implications for sill emplacement mechanisms. *Bulletin of Volcanology* **70**, 183–201.
- Thomson, K. & Hutton, D. (2004). Geometry and growth of sill complexes: insights using 3D seismic from the North Rockall Trough. *Bulletin of Volcanology* **66**, 364–375.
- Tizzani, P., Battaglia, M., Zeni, G., Atzori, S., Bernardino, P. & Lanari, R. (2009). Uplift and magma intrusion at Long Valley caldera from InSAR and gravity measurements. *Geology* **37**, 63–66.
- Tolstoy, M., Waldhauser, F., Bohnenstiehl, D. R., Weekly, R. T. & Kim, W.-Y. (2008). Seismic identification of along-axis hydrothermal flow on the East Pacific Rise. *Nature* **451**, 181–184.
- Trasatti, E., Giunchi, C. & Agostinetti, N. P. (2008). Numerical inversion of deformation caused by pressure sources: application to Mount Etna (Italy). *Geophysical Journal International* **172**, 873–884.
- Trindade, R. I. F., Nguema, T. M. M. & Bouchez, J. L. (2001). Thermally enhanced mimetic fabric of magnetite in a biotite granite. *Geophysical Research Letters* **28**, 2687–2690.
- Trude, J., Cartwright, J., Davies, R. J. & Smallwood, J. (2003). New technique for dating igneous sills. *Geology* **31**, 813–816.
- Tuffen, H., Smith, R. & Sammonds, P. R. (2008). Evidence for seismogenic fracture of silicic magma. *Nature* **453**, 511–514.
- Van Camp, M., de, V., Watlet, O., Meurers, A., Francis, B. & Caudron, O., C. (2017). Geophysics from terrestrial time-variable gravity measurements. *Reviews of Geophysics* **55**, 938–992.
- Vargas-Bracamontes, D. M. & Neuberg, J. W. (2012). Interaction between regional and magma-induced stresses and their impact on volcano-tectonic seismicity. *Journal of Volcanology and Geothermal Research* **243–244**, 91–96.
- Vigh, D., Starr, B., Kapoor, J. & Li, H. (2010). 3D full waveform inversion on a Gulf of Mexico WAZ data set. SEG Technical Program Expanded Abstracts 2010, Society of Exploration Geophysicists, 957–961.
- Vigneresse, J. L. (1995). Crustal regime of deformation and ascent of granitic magma. *Tectonophysics* **249**, 187–202.
- Vigneresse, J. L., Tikoff, B. & Améglio, L. (1999). Modification of the regional stress field by magma intrusion and formation of tabular granitic plutons. *Tectonophysics* **302**, 203–224.
- Virieux, J. & Operto, S. (2009). An overview of full-waveform inversion in exploration geophysics. *Geophysics* **74**, WCC1–WCC26.
- Voigt, W. & Kinoshita, S. (1907). Bestimmung absoluter Werte von Magnetisierungszahlen, insbesondere für Kristalle. *Annalen der Physik* **329**, 492–514.
- Vollgger, S. A. & Cruden, A. R. (2016). Mapping folds and fractures in basement and cover rocks using UAV photogrammetry, Cape Liptrap and Cape Paterson, Victoria, Australia. *Journal of Structural Geology* **85**, 168–187.
- Waite, G. P. & Moran, S. C. (2009). VP Structure of Mount St. Helens, Washington, USA, imaged with local earthquake tomography. *Journal of Volcanology and Geothermal Research* **182**, 113–122.
- Wall, M., Cartwright, J., Davies, R. & McGrandle, A. (2010). 3D seismic imaging of a Tertiary Dyke Swarm in the Southern North Sea, UK. *Basin Research* **22**, 181–194.
- Wannamaker, P. E., Hasterok, D. P., Johnston, J. M., Stodt, J. A., Hall, D. B., Sodergren, T. L., Pellerin, L., Maris, V., Doerner, W. M., Groenewold, K. A. & Unsworth, M. J. (2008). Lithospheric dismemberment and magmatic processes of the Great Basin–Colorado Plateau transition, Utah, implied from magnetotellurics. *Geochemistry, Geophysics, Geosystems* **9**, Q05019.
- Ward, K. M., Zandt, G., Beck, S. L., Christensen, D. H. & McFarlin, H. (2014). Seismic imaging of the magmatic underpinnings beneath the Altiplano-Puna volcanic complex from the joint inversion of surface wave dispersion and receiver functions. *Earth and Planetary Science Letters* **404**, 43–53.
- Warner, M., Ratcliffe, A., Nangoo, T., Morgan, J., Umpleby, A., Shah, N., Vinje, V., Štekl, I., Guasch, L., Win, C., Conroy, G. & Bertrand, A. (2013). Anisotropic 3D full-waveform inversion. *Geophysics* **78**, R59–R80.
- Wauthier, C., Roman, D. C. & Poland, M. P. (2013). Moderate-magnitude earthquakes induced by magma reservoir inflation at Kilauea Volcano, Hawaii. *Geophysical Research Letters* **40**, 5366–5370.
- Wawrzyniak, P., Zlotnicki, J., Sailhac, P. & Marquis, G. (2017). Resistivity variations related to the large March 9, 1998 eruption at La Fournaise volcano inferred by continuous MT monitoring. *Journal of Volcanology and Geothermal Research* **347**, 185–206.
- Weaver, J. (1994). *Mathematical Methods for Geoelectromagnetic Induction*. Research Studies Press, Taunton.
- Westoby, M. J., Brasington, J., Glasser, N. F., Hambrey, M. J. & Reynolds, J. M. (2012). “Structure-from-Motion” photogrammetry: A low-cost, effective tool for geoscience applications. *Geomorphology* **179**, 300–314.
- Whaler, K. A. & Hautot, S. (2006). The electrical resistivity structure of the crust beneath the northern Main Ethiopian Rift. In: Yirgu, G., Ebinger, C. J. & Maguire, P. K. H. (eds) *The Afar Volcanic Province within the East African Rift System*. Geological Society, London, *Special Publications* **259**, 293–305.
- White, R. & McCausland, W. (2016). Volcano-tectonic earthquakes: a new tool for estimating intrusive volumes and forecasting eruptions. *Journal of Volcanology and Geothermal Research* **309**, 139–155.
- Wicks, C. W., Thatcher, W., Dzurisin, D. & Svarc, J. (2006). Uplift, thermal unrest and magma intrusion at Yellowstone caldera. *Nature* **440**, 72–75.
- Yamasaki, T., Kobayashi, T., Wright, T. J. & Fukahata, Y. (2018). Viscoelastic crustal deformation by magmatic intrusion: a case study in the Kutcharo caldera, eastern Hokkaido, Japan. *Journal of Volcanology and Geothermal Research* **349**, 128–145.
- Zandomenighi, D., Aster, R., Kyle, P., Barclay, A., Chaput, J. & Knox, H. (2013). Internal structure of Erebus volcano, Antarctica imaged by high-resolution active-source seismic tomography and coda interferometry. *Journal of Geophysical Research: Solid Earth* **118**, 1067–1078.